DESIGN AND CONSTRUCTION OF A DELTA MODULATION SYSTEM

O. BELLOTTI

A DISSERTATION

IN THE

FACULTY OF ENGINEERING

Presented In Partial Fulfilment Of The Requirements For

The Degree Of MASTER OF ENGINEERING At

SIR GEORGE WILLIAMS UNIVERSITY

MONTREAL, CANADA.

APRIL, 1974.

TABLE OF CONTENTS

LIST OF ABBREVIATIONS & SYMBOLS

DIDM	Double Integration Delta Modulation.
DM	Delta Modulation.
Dr	Dynamic Range of the input signal.
e	Error Signal.
E_o	Quantizer Output Level.
f	Frequency.
f_{a1}	Lower limit of the audio bandwidth.
f_{a2}	Higher limit of the audio bandwidth.
f_b	Audio bandwidth of the input filter.
f_s	Sampling frequency.
f_1	RC integrator cut-off frequency.
f_2	Pole frequency of the lead-lag network.
f_3	Zero frequency of the lead-lag network.
G,H	Transfer function.
HIDM	High Information Delta Modulation.
L(t)	Output binary sequence or code.
N_e	Noise introduced by transmission error.
n(t)	Noise component.
PCM	Pulse Code Modulation.

$q(t)$	Output binary code.
$R(\tau)$	Correlation function.
$s(t)$	Signal component.
SIDM	Single Integration Delta Modulation.
$S_x(f)$	Power spectrum of the input signal.
t	Time.
T_c	Threshold of coding.
T_f	Syllabicus low pass filter time constant.
T_i	$\frac{1}{2\pi f_i}$ $\quad i = 1, 2, 3.$
$u(t)$	Random Pulse.
$U(f)$	Fourier transform of $u(t)$.
$U(s)$	Laplace transform of a unit step.
$W(f)$	Noise power spectrum of transmission errors.
x	Input signal.
$\hat{x}$	Decoding network output (Encoder).
X_m	Input level at slope overload.
$\frac{x}{N_q}$	Signal to quantization noise ratio.
$\frac{X_m}{N_q}$	Maximum signal to quantization noise ratio.
$\frac{X_c}{N_c}$	Signal-to-quantization-noise ratio at coding threshold.

y	Filtered decoded output.
$\hat{y}$	Decoder output.
α	DeJager constant.
ϵ	Quantizing error range.
ν	Error rate (bit/sec)
Δ	Step Size
$\hat{\Delta}$	Fundamental Frequency of Δ

ACKNOWLEDGEMENT

The author wishes to express his thanks to Mr. D.F. Lee for his help and encouragement in conducting the investigation, results of which are shown in this report.

Appreciation is also extended to Dr. V. Ramachandran for his many helpful suggestions during the course of the work and the preparation of the manuscript.

Thanks are also due to Mr. W. Martens for many useful discussions and to Mrs. E. Cherrier for her efficiency in typing the manuscript.

ABSTRACT

Q. BELLOTTI

DESIGN AND CONSTRUCTION OF A DELTA MODULATION SYSTEM

This work considers the encoding and decoding of speech into and from a binary sequence by means of Delta Modulation techniques.

Single integration and double integration Delta Modulation system performance are described. Overload characteristics, signal/quantization-noise ratio, threshold of coding, idle noise, effect of transmission error and system stability are calculated.

Theoretical results have been verified by computer simulation and also by laboratory measurements of experimental models.

High Information Delta Modulation techniques, which overcome some of the limitations of simple Delta Modulation are presented.

A Digitally Companded High Information Delta Modulation system for speech transmission at a bit rate of 20k bit/sec is designed and evaluated.

CHAPTER 1

INTRODUCTION

1.1. Why Digital Communications?

During the last decade, more and more Analog signals have been encoded into digital pulses for transmission and processing. This is true for both commercial and military systems. The shift to digital communication system has been motivated by the following important factors:

i) From information theory, we know that there is an almost complete elimination of noise interference, when the pulse signal exceeds the noise level by 20 dB or more, since only the presence or absence of each pulse is needed to reconstruct the original transmitted signal.

ii) The transmitted signal can be relayed as many times as desired without introducing the progressive signal distortions and deteriorations which are typical of analog communication systems.

iii) Digital information can be easily encrypted to provide privacy or secrecy (military applications).

iv) The use of time division multiplexed systems is becoming widespread in digital communication systems using either radio links or cables. Furthermore, multiplexing of digital signals can be achieved with inexpensive integrated logic circuits.

v) Digital data can be processed by computers.

vi) No crosstalk exists.

vii) No mechanical switches are required which results in an increased system reliability.

viii) There has been a tremendous increase in computer-to-computer communications. Examples could be airline reservation systems and the widespread use of teletypes and computer terminals in industry.

1.2. Pulse Code Modulation & Delta Modulation

Pulse Code Modulation (PCM) and Delta Modulation (DM) are two basic methods for analog to digital conversion. A number of papers [1, 2, 3] compare the performance of DM and PCM, but this comparison is difficult because of the different natures of the two systems. However it can be concluded that Delta Modulation gives better signal-to-noise ratios for sampling frequencies below 40 kHz. (Figure I.1.).

Simple Delta Modulation is not considered of high enough quality for commercial telephone communications. The main reasons are:

i) High clock rate is required to achieve good quality.

ii) A serious limitation of the input amplitudes, which can be reproduced faithfully.

However High Information Delta Modulation (HIDM) techniques introduced by Winkler [4], can overcome some of the deficiency of ordinary Delta Modulation systems and retain most of their advantages. HIDM systems can be used for voice communication with excellent results at 20 kHz sampling frequency.

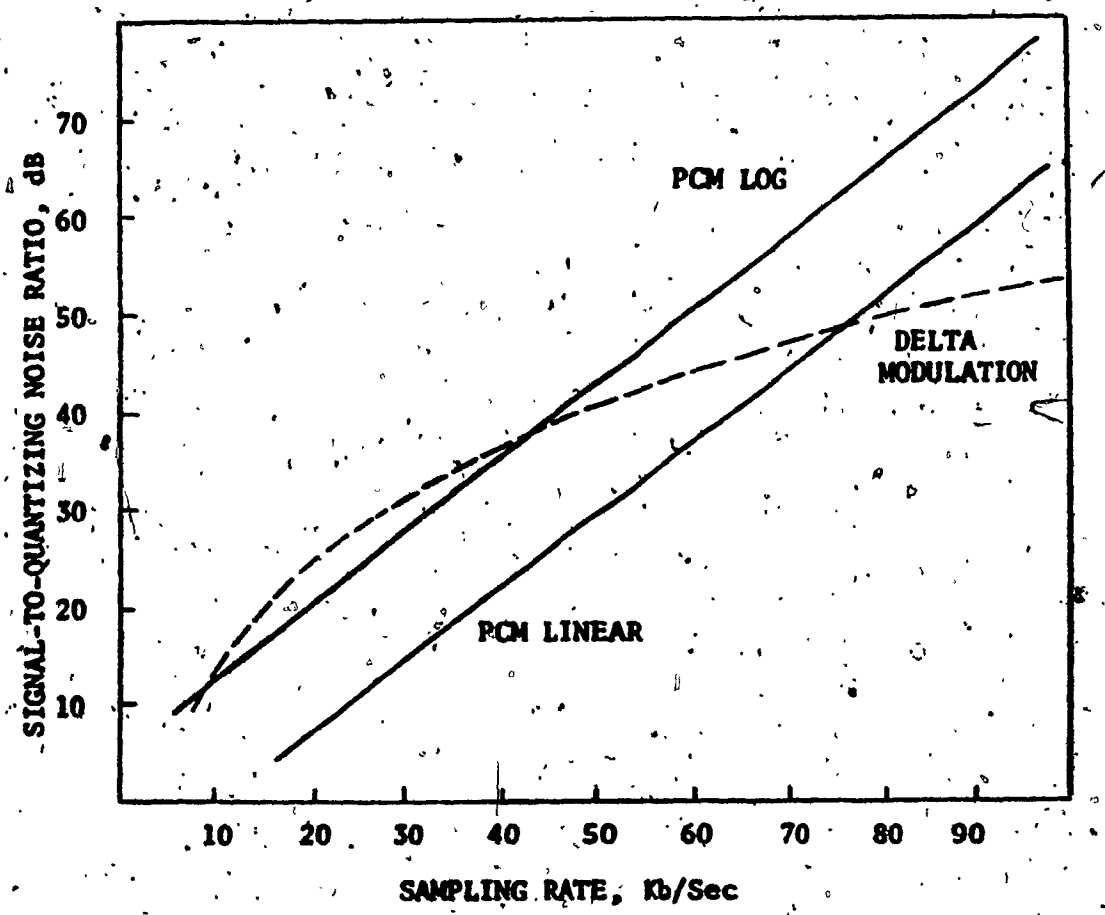

FIGURE 1.1.

SIGNAL-TO-NOISE RATIO OF PCM & DM

1.3. History Of Delta Modulation

Delta Modulation was invented in the ITT French Laboratories by E.M. Deloraine, S. Van Miero and B. Derjavitch [5] in 1946. More detailed description is given by F. de Jager [6] (Phillips) 1952 and Libois [7] (CNET) 1952.

Further work was done by Zetterberg [8] (Ericsson Laboratories) 1955 and H. Inose and Y. Yasuda [9] (Tokyo University) 1963.

High Information Delta Modulation was originally introduced by Winkler [4] (RCA) 1963.

Other HIDM techniques are due to A. Tomozawa and H. Kaneko [10] (Nippon Electric) 1968 and S.J. Brolin and J.H. Brown [11] (Bell Telephone Laboratories) 1968. More detailed system performance calculations were presented by J.E. O'Neal [2] (Bell) 1966 and E.N. Protonotarios [12] (Bell) 1967.

Today a broad amount of literature is available on many aspects of Delta Modulation, and several system improvements have been achieved.

1.4. Scope Of Dissertation

In this dissertation, a simple Delta Modulation System will be analyzed in detail, using, whenever possible, the already existing material available in the literature. A system design is also presented which is experimentally verified.

CHAPTER 2

THE DELTA MODULATION SYSTEM

2.1. Introduction

Delta Modulation is a process by which analog signals are encoded into a binary code. The system is basically a non-linear sampled data system using predictive coding technique.

This means that the value of the input signal is predicted at each sampling instant and only the difference between the actual value of the signal to be transmitted and its predictive value is encoded.

For many types of signals, the first order entropy of the difference signal is much smaller than that of the original signal. Thus most of the redundancy present in the input signal is removed, allowing transmission at lower channel capacity with consequent higher coding efficiency.

Furthermore, the characteristics of the Delta Modulation Coder can be choosen to match the power spectrum curve of human speech. This type of encoding also provides almost optimum filtering in the presence of white noise.

2.2. Theory

Consider the Delta Modulation system of Figure 2.1. The analog input signal $x(t)$, band-limited by a filter, is compared with a reconstructed version of itself $\hat{x}(t)$ which is generated by the local decoder.

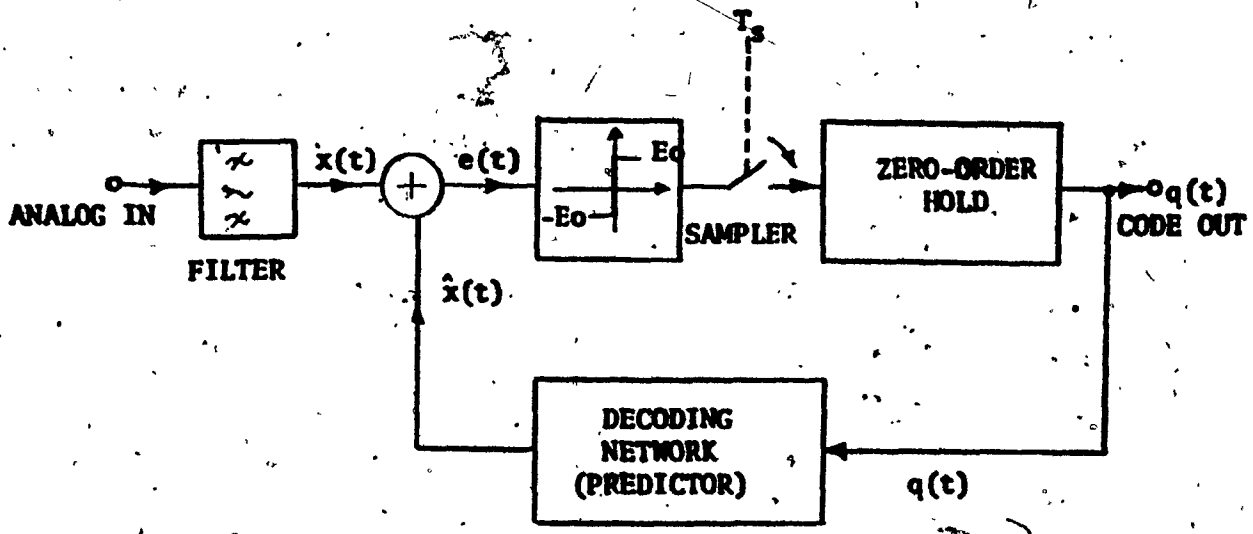

i) DELTA MODULATION ENCODER

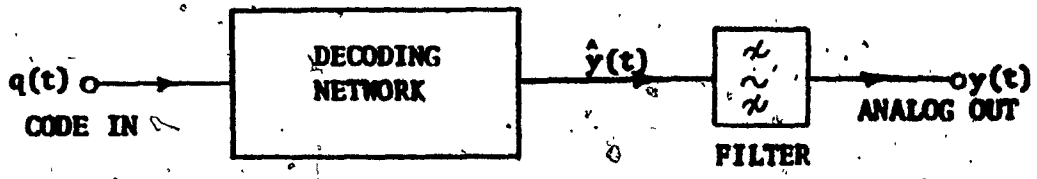

ii) DELTA MODULATION DECODER

FIGURE 2.1.

BASIC DELTA ENCODER - DECODER

The relative difference e(t) is quantized by a comparator whose output is periodically sampled. The zero order hold circuit holds the samples to provide a non-return to zero (NRZ) single bit binary code q(t).

The code controls the local decoder output $\hat{x}(t)$ forcing it to closely track the input signal. This action is that of a servo-system with a negative feedback loop which maintains the signal $\hat{x}(t)$ as close as possible to the input x(t).

If the Delta decoder contains an identical decoding network, a similar track $\hat{y}(t)$ of the input analog signal is recovered.

An output filter with steep cut-off removes all out-of-band signals, (i.e. quantizing noise, sampling frequency components and idle noise) recreating the input signal.

2.3. Single Integration

The simplest Delta Modulation system is obtained by using an integrator as a decoding network. This network consists of a resistance and a capacitance with a very large time constant $T_1 = R_1C_1$. (Figure 2.2.)

The network transfer function is

$$H(s) = \frac{1}{1 + SC_1R_1} \qquad (2.1.)$$

The corner frequency is

$$f_1 = \frac{1}{2\pi R_1C_1} \qquad (2.2.)$$

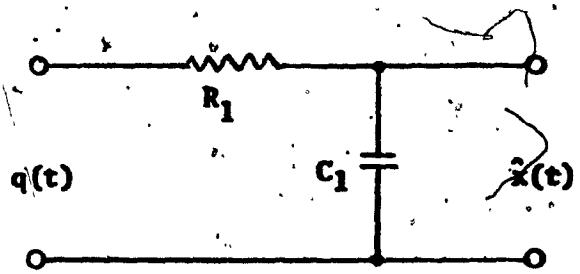

FIGURE 2.2

INTEGRATING NETWORK

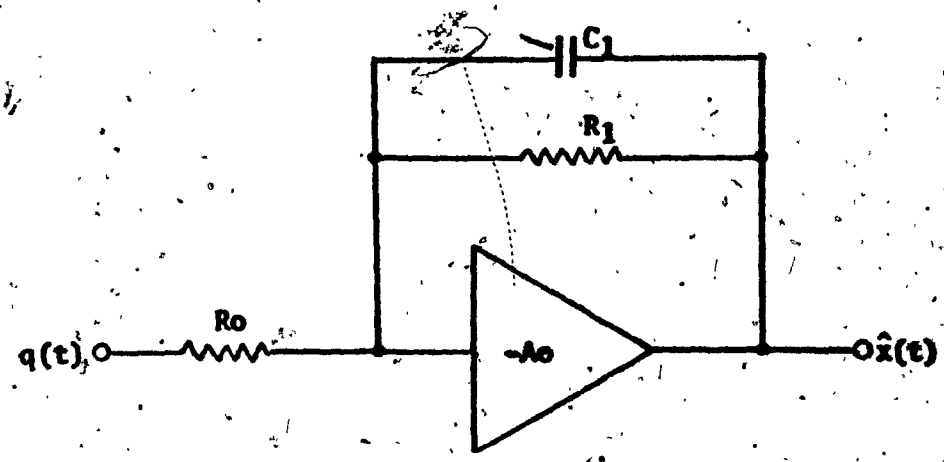

FIGURE 2.3.

ACTIVE INTEGRATING NETWORK

If dc gain K is desired, an active integrating network is required which is as shown in Figure 2.3.

The transfer function is

$$H(s) = -\frac{K}{1 + SC_1R_1} \qquad (2.3.)$$

where

$$K = \frac{R_1}{R_0} = \text{Gain at dc} \qquad (2.4.)$$

The step response is given by:

$$\hat{x}(t) = \mathcal{L}^{-1}\left[H(s)\,U(s)\right] = -K\left(1 - e^{-t/R_1C_1}\right) \qquad (2.5.)$$

If $t \ll R_1C_1$, equation 2.5. simplifies to

$$\hat{x}(t) = -\frac{K}{R_1C_1}\,t \qquad (2.6.)$$

The step response is practically a ramp function.

2.4. Double Integration

If two integrating networks are cascaded, the approximation $\tilde{x}(t)$ of the input signal $x(t)$ is smoother, but the additional delay introduced in the feedback loop of the system may cause instability or a sluggish response to sudden changes in the slope of the input.

A compromise is possible providing the corner frequencies of the network are properly choosen. A typical double integration network is shown in Figure 2.4.

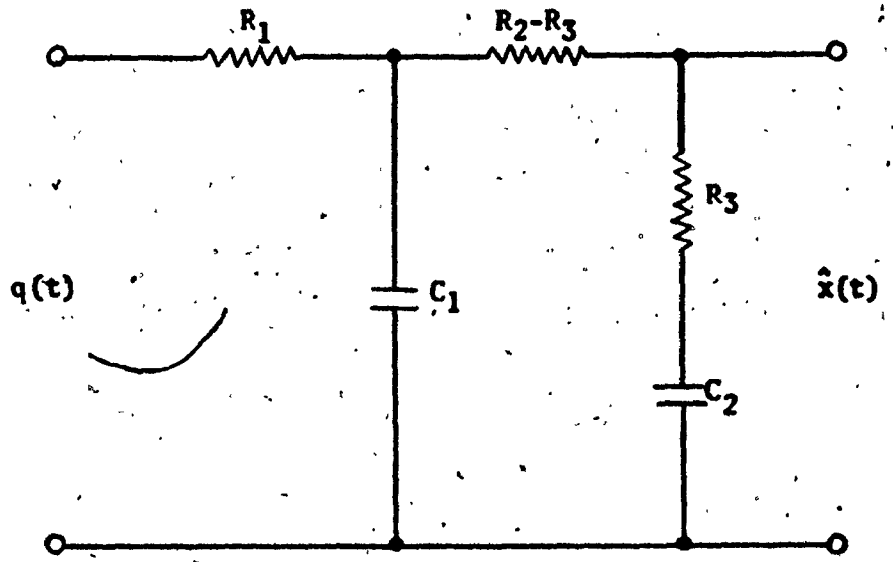

FIGURE 2.4.

DOUBLE INTEGRATING NETWORK

The network transfer function is

$$H(s) = \frac{1 + SC_2R_3}{\left[1+2\pi R_1C_1\left(1+\frac{C_2}{C_1}\right)\right]\left\{1+SC_2R_2\left[1-\frac{1}{4}\left(1+\frac{R_1}{R_2}\right)^2\frac{R_2C_2}{R_1C_1}\right]\right\}} \qquad (2.7.)$$

The corner frequencies are

$$f_1 = \frac{1}{2\pi R_1C_1\left[1+\frac{C_2}{C_1}\right]} \qquad (2.8.)$$

$$f_2 = \frac{1}{2\pi R_2C_2\left[1-\frac{1}{4}\left(1+\frac{R_1}{R_2}\right)^2\frac{R_2C_2}{R_1C_1}\right]} \qquad (2.9.)$$

$$f_3 = \frac{1}{2\pi R_3C_2} \qquad (2.10.)$$

Figure 2.5. shows the network response.

The double integrating network can also be implemented with an active element as shown in Figure 2.6.

The transfer function is

$$H(s) = -K\,\frac{1 + SC_2R_3}{\left(1+SC_1R_1\right)\left[1+SC_2\left(R_2+R_3\right)\right]} \qquad (2.11.)$$

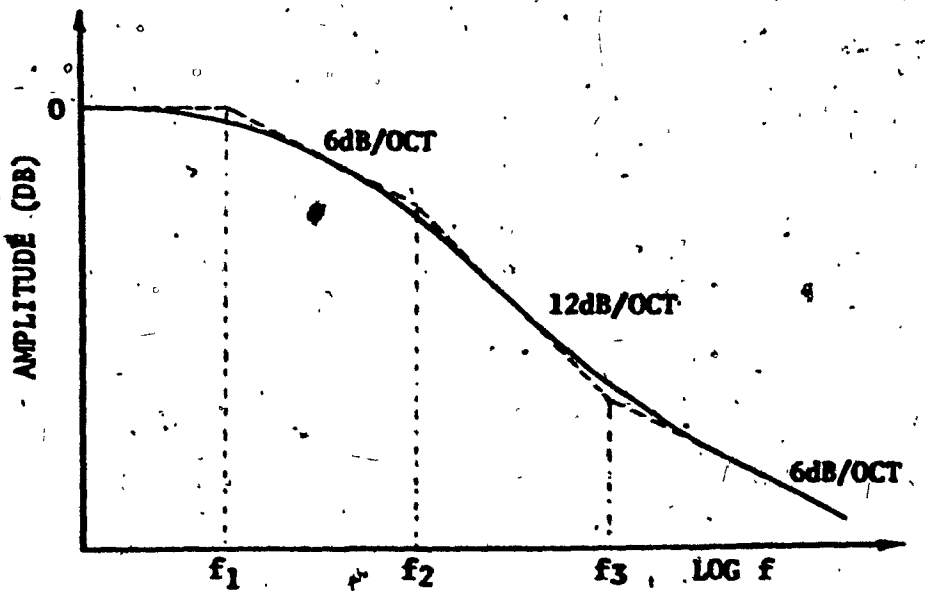

FIGURE 2.5.

AMPLITUDE RESPONSE OF EQUATION (2.7.)

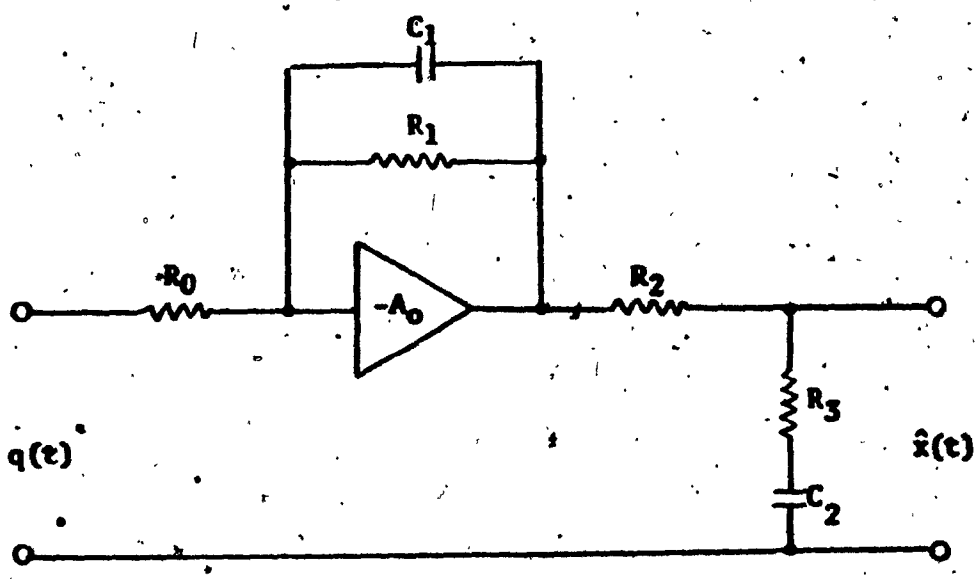

FIGURE 2.6.

ACTIVE DOUBLE INTEGRATING NETWORK

where

$$K = \frac{R_1}{R_o} \tag{2.12.}$$

The corner frequencies are

$$f_1 = \frac{1}{2\pi C_1 R_1} \tag{2.13.}$$

$$f_2 = \frac{1}{2\pi C_2 (R_2+R_3)} \tag{2.14.}$$

$$f_3 = \frac{1}{2\pi C_2 R_3} \tag{2,15.}$$

The step response is given by:

$$\hat{x}(t) = \mathcal{L}^{-1}\left[-K \cdot \frac{1 + sT_3}{(1+sT_1)(1+sT_2)} \cdot U(s)\right] \tag{2.16.}$$

$$\hat{x}(t) = -K\left[\frac{T_1-T_3}{(T_1-T_2)} e^{-t/T_1} - \frac{T_2-T_3}{(T_1-T_2)} e^{-t/T_2} + 1\right] \tag{2.17.}$$

where

$$T_i = \frac{1}{2\pi f_i} \quad i = 1, 2, 3 \tag{2.18.}$$

If $T_3 \ll t \ll T_2$, equation 2.16. simplifies to

$$\hat{x}(t) = \mathcal{L}^{-1}\left[\frac{-K}{S^3T_1T_2}\right] = \frac{-Kt^2}{2T_1T_2} \qquad (2.19.)$$

which is a parabolic response.

If $t \ll T_3$, equation 2.16. becomes

$$\hat{x}(t) = \mathcal{L}^{-1}\left[\frac{-KT_3}{S^2T_1T_2}\right] = -K\frac{T_3}{T_1T_2}t \qquad (2.20)$$

which is a ramp function.

Figures 2.7. and 2.8. show typical waveforms for the Delta Encoder using single and double integration as measured in the laboratory.

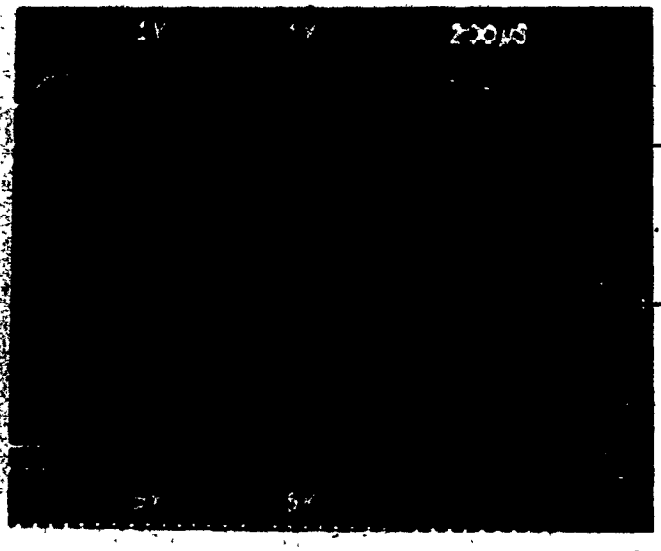

PREDICTOR OUTPUT, $\hat{x}(t)$

INPUT SIGNAL $x(t)$, (800 Hz SINEWAVE)

OUTPUT CODE, $q(t)$

SAMPLING FREQUENCY, f_s

FIGURE 2.7. WAVEFORMS OF SINGLE INTEGRATION DELTA MODULATION SYSTEM (T_1 = 2 msec)

PREDICTOR OUTPUT, $\hat{x}(t)$

INPUT SIGNAL $x(t)$, (800 Hz SINEWAVE)

SAMPLING FREQUENCY, f_s

OUTPUT CODE, $q(t)$

FIGURE 2.8. WAVEFORMS OF A DOUBLE INTEGRATION DELTA MODULATION SYSTEM (f_1 = 79.6 Hz; f_2 = 500 Hz; f_3 = 2500 Hz)

CHAPTER 3

DELTA MODULATION PARAMETERS

3.1. Parameters Definition

The following parameters characterize a Delta Modulation system:

i) Overload Characteristic.

ii) Signal to quantization noise ratio $\left(\frac{x}{N_q}\right)$

iii) Dynamic Range.

iv) Idle code.

v) Threshold of coding.

vi) Idle noise

vii) Effect of transmission errors

viii) System stability.

In what follows, these parameters are discussed in some detail.

3.2. Overload Characteristic

Overload state is defined as the situation where the slope of the input signal x(t) exceeds the slope of the predictor output $\hat{x}(t)$ at a given amplitude.

In a Delta Modulation system, the overload condition produces an output code rich in long chains of either $+E_o$ or $-E_o$ pulses.

Consider the simplified Delta Modulation encoder of Figure 3.1.

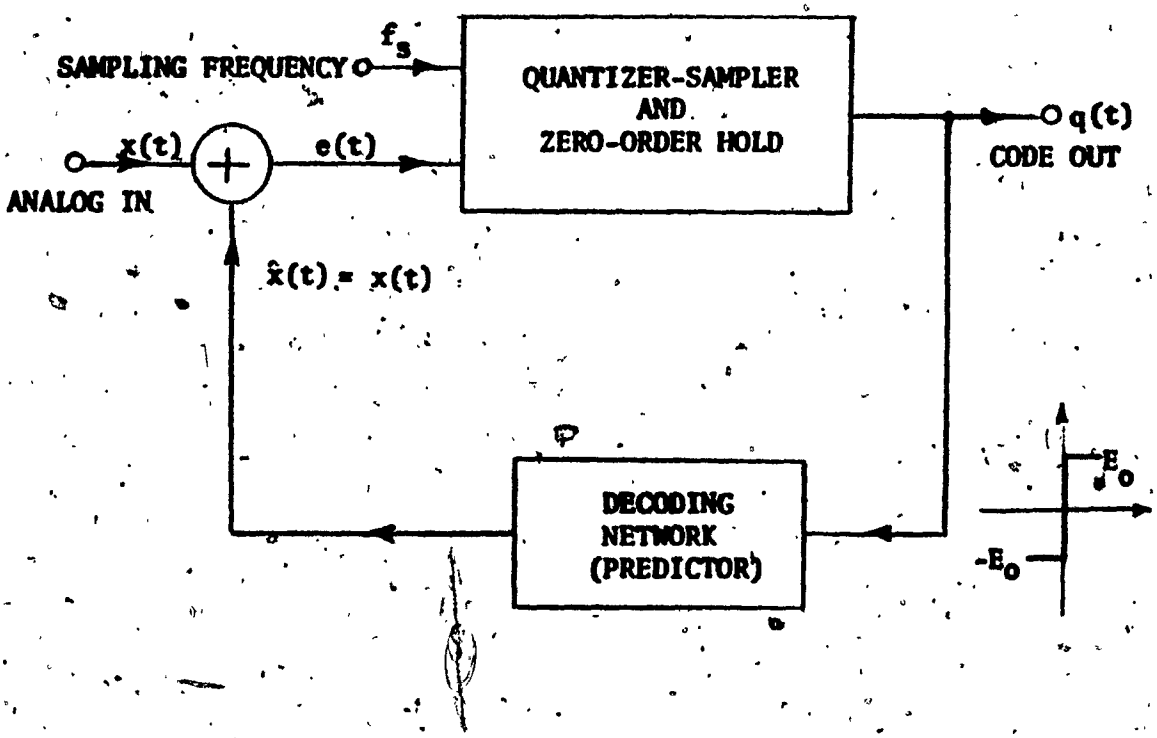

FIGURE 3.1.

SIMPLIFIED DELTA ENCODER BLOCK DIAGRAM

An expression relating the input signal x(t) and the quantizer output ± Eo can be written as: [10]

$$\beta^2 X^2 \cdot \int_{-\infty}^{+\infty} |H^{-1}(f)|^2 S_x(f)df \leq E_o^2 \qquad (3.1.)$$

where

X^2 is the MEAN SQUARE VALUE of the input x(t)

$S_x(f)$ is the normalized power spectral density of the input

β is the input peak factor $\left(\beta = \frac{X_{peak}}{X_{rms}}\right)$

If x(t) is a sinusoidal signal

$$x(t) = \cos \omega_o t \qquad (3.2.)$$

its correlation function is

$$R_{xx}(\tau) = \int x(t)\, x(t+\tau) = \frac{1}{2} \cos \omega_o t \qquad (3.3.)$$

Recalling Wienner-Khintchine relation stating that the power spectral density of a function is the Fourier transform of its auto-correlation function, we have

$$S_{x(\omega_o)} = \mathfrak{F}\left[R_{xx}(\tau)\right] = \int_{-\infty}^{+\infty} e^{-j\omega_o \tau} \frac{1}{2} \cos \omega_o \tau \, d\tau \qquad (3.4.)$$

$$S_x(f) = \frac{1}{2}[\delta(f-f_o) + \delta(f-f_o)] \qquad (3.5.)$$

Substituting equation 3.5. into equation 3.1., we get

$$X_m^2 = \left[\frac{E_o}{2}\right]^2 \frac{1}{\int_{-\infty}^{+\infty} \left|\frac{H^{-1}(f_o)}{2}\right|^2 df} = \frac{E^2_o}{2} |H(f_o)|^2 \qquad (3.6.)$$

Equation 3.6. shows that the overload limit depends only on the quantizer level $\pm E_o$ and the transfer function of the decoding network. For the single integration system of equation 2.3., slope overload point is given by the expression

$$X_m = \frac{E_o}{\sqrt{2}} \frac{K}{\sqrt{1 + \omega^2 T_1^2}} \qquad (3.7.)$$

For the double integration system of equation 2.11., the slope overload expression is

$$X_m = \frac{E_o K}{\sqrt{2}} \left[\frac{1 + \omega^2 T_3^2}{(1+\omega^2 T_1^2)(1+\omega^2 T_2^2)}\right]^{1/2} \qquad (3.8.)$$

where

$$T_i = \frac{1}{2\pi f_i} \qquad i = 1, 2, 3 \qquad (3.9.)$$

K = dc gain of the network

E_o = quantizer output level

Typical overload characteristics of a Delta Modulation System are shown in Figure 3.2.

3.3. Quantizing Noise

3.3.1. General

We define "Quantization Noise" as the error difference between the filtered output signal and the input signal, when correlation between error and desired signal is eliminated.

Thus delay and amplitude equalization of the input - output signal is required to compensate for:

i) encoding - decoding process delay, which is usually one clock period.

ii) delay due to the audio filter, which for a steep response filter is a non-negligible quantity.

iii) delay due to the transmission media which is usually negligible.

iv) amplitude variations due to encoder - decoder mismatch.

In a Delta Modulation system, there are two types of quantization noise [1, 2, 1]], namely:

i) Granular noise is caused by the quantization of the output samples in terms of multiples of the step size Δ. This type of noise is uncorrelated with a random input signal and has a flat power spectrum over the audio band.

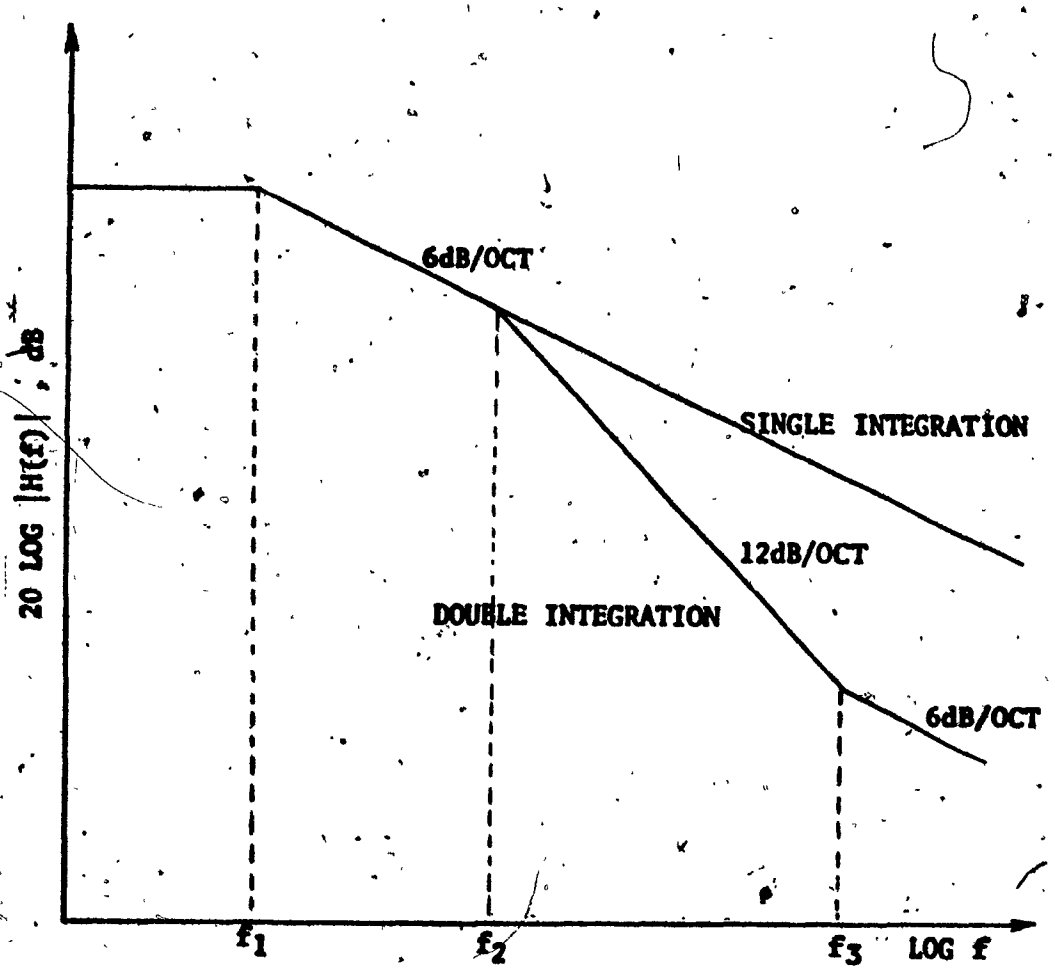

FIGURE 3.2.

DM SYSTEM SLOPE OVERLOAD CHARACTERISTICS

ii) Slope overload noise, which is present when the input signal slope exceeds the one which the integrator is capable of reproducing.

Usually the system operates below the overload point, thus only granular noise will be discussed.

3.3.2. Analysis

The Quantizing Step Size Δ is defined to be the peak-to-peak response of the decoding network when excited by a repetitive pulse of $\pm E_o$ amplitude (idle code) and frequency $f_s/2$ (maximum rate of change of the output code q(t)). (See Figure 3.3.).

Due to the low pass response of the decoding network, only the fundamental frequency of q(t) is considered; thus the step size $\hat{\Delta}$ is given by [10].

$$\hat{\Delta} = \frac{8}{\pi} E_o |H(f_s/2)| \qquad (3.10.)$$

Because of the random nature of granular noise [13] (in PCM system called quantization noise) and its fundamental periodicity f_s, its spectral distribution is assumed to be of the form $\left(\frac{\sin x}{x}\right)^2$.

A property of this distribution is that its total energy is equal to the one of a signal with white spectrum and an equivalent bandwidth $f_s/2$.

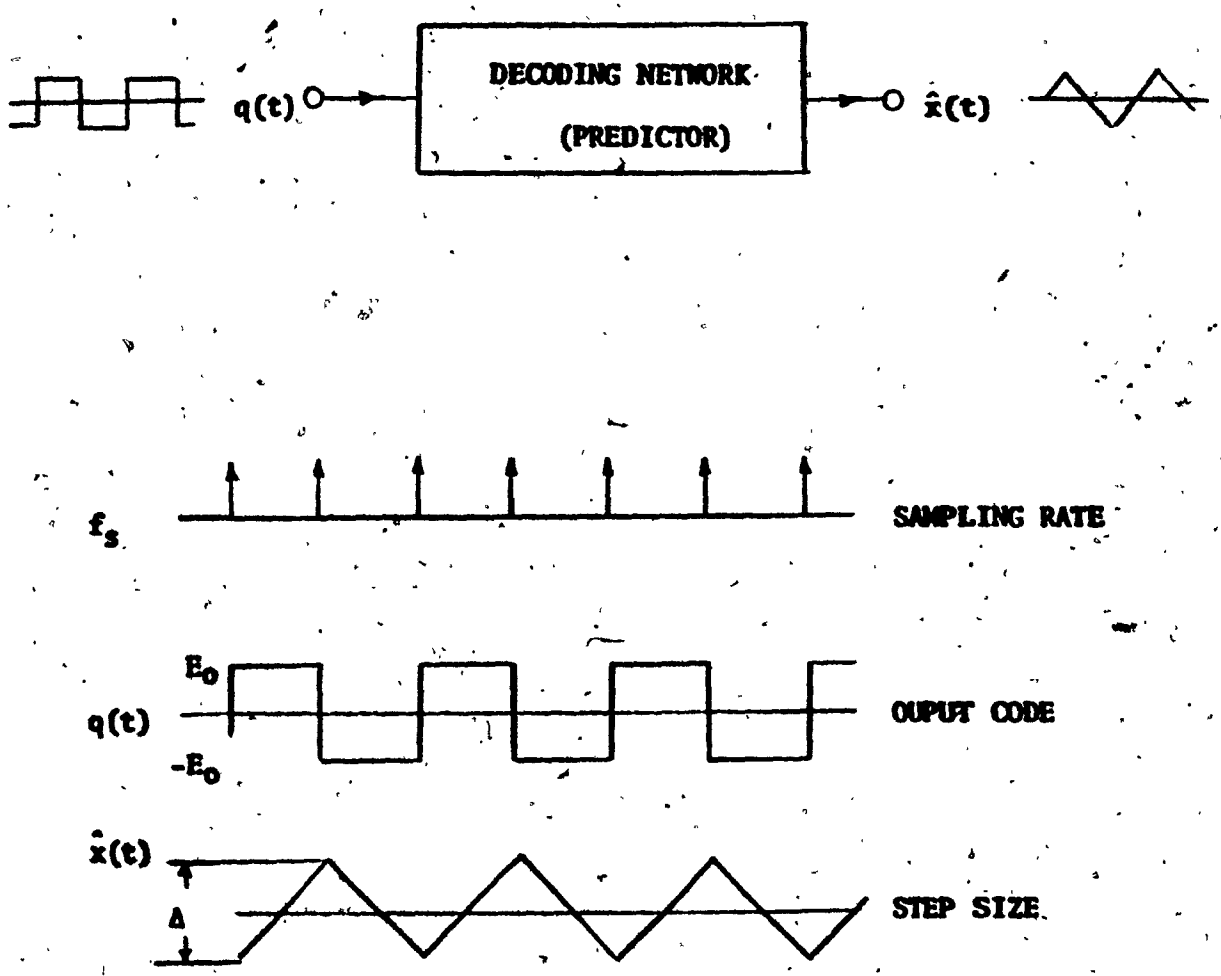

FIGURE 3.3.

SIDM IDLE WAVEFORMS

As shown by Figure 3.4., the spectrum is almost flat in the audio band, therefore the rms quantizing noise is

$$Nq = \alpha \hat{\Delta} \sqrt{\frac{f_b}{f_s/2}} \qquad (3.11.)$$

where α is a constant which describes the rms error range ϵ in terms of $\hat{\Delta}$.

The value of α was originally found by de Jager [6]. A better approximation to its value is given by Tomozawa-Kaneko [10].

$$\alpha = \frac{\epsilon}{\hat{\Delta}} \quad \begin{matrix} .376 \text{ for single integration} \\ .668 \text{ for double integration} \end{matrix} \qquad (3.12.)$$

Figures 3.5. and 3.6. show typical quantization error waveforms for single and double integration systems, as measured in the laboratory.

Replacing equation 3.10. into equation 3.11., we obtain:

$$Nq = \frac{8\sqrt{2}}{\pi} \alpha E_o \sqrt{\frac{f_b}{f_s}} |H(f_s/2)| \qquad (3.13.)$$

From Section 3.2., we know that the maximum input signal is given by the overload formula:

$$X_m = \frac{E_o}{\sqrt{2}} |H(f)| \qquad (3.14.)$$

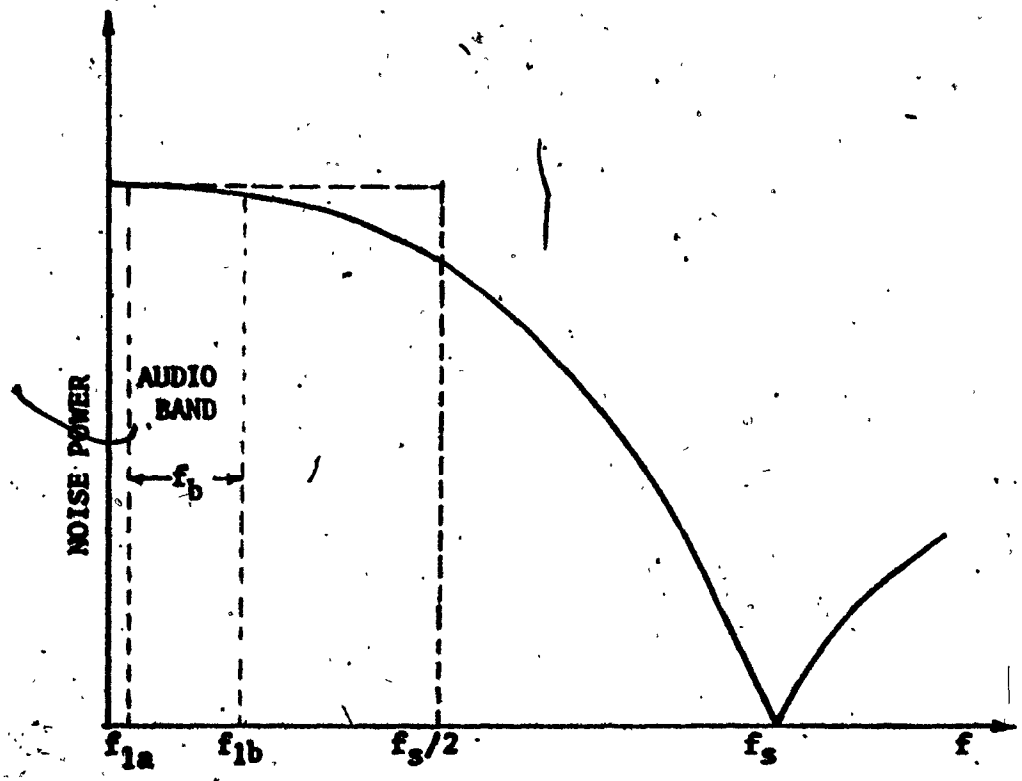

FIGURE 3.4.

SPECTRAL DISTRIBUTION OF QUANTIZING (GRANULAR) NOISE

QUANTIZING ERROR, e(t)

ENCODER INPUT, x(t)
(800 Hz, 0 dBm0)

PREDICTOR OUTPUT, $\hat{x}(t)$

FIGURE 3.5. QUANTIZING ERROR OF A SINGLE INTEGRATION SYSTEM (f_s = 20 kHz)

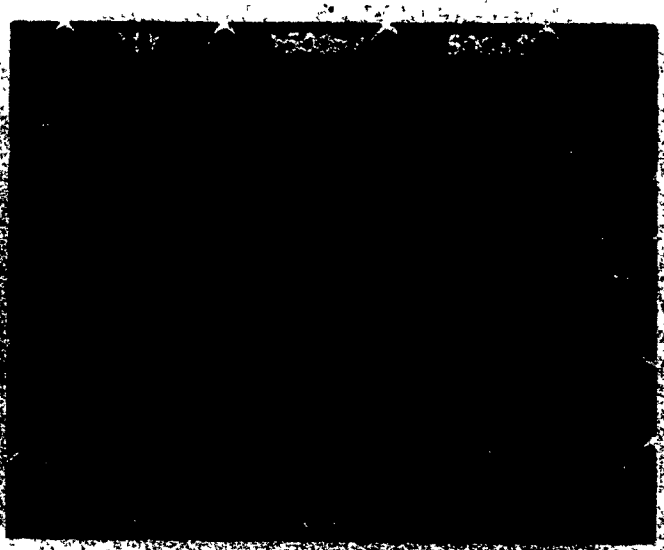

ENCODER INPUT, x(t)
(800 Hz, 0 dBm0)

PREDICTOR OUTPUT, $\hat{x}(t)$

DECODER OUTPUT, y(t)

QUANTIZING ERROR, e(t)

FIGURE 3.6. QUANTIZATION ERROR OF A DOUBLE INTEGRATION SYSTEM (f_s = 20 kHz)

If we define the maximum signal-to-noise ratio $\left(\frac{X_m}{Nq}\right)$ to be the ratio of the maximum rms input level at slope overload point to the rms value of the quantizing noise, it follows that

$$\frac{X_m}{Nq} = \frac{\pi}{16\alpha}\sqrt{\frac{f_s}{f_b}}\left|\frac{H(f)}{H(f_s/2)}\right| \qquad (3.15.)$$

In the case of single integration for $f_1 << f << f_s$ we can write

$$\left|\frac{H(f)}{H(f_s/2)}\right| = \frac{f_s}{2f} \qquad (3.16.)$$

Using equation 3.16., equation 3.10 simplifies to

$$\frac{X_m}{Nq} = .261\ \frac{f_s^{3/2}}{f \cdot f_b^{1/2}} \qquad (3.17.)$$

which is de Jager's formula [10] for single integration system.

Figures 3.7., 3.8., 3.9., 3.10. show theoretical values of maximum signal-to-quantization-noise versus input frequencies for different filter bandwidths and sampling frequency.

3.4. Dynamic Range

The Dynamic Range is defined as the range of the amplitude of the input signal over which the signal-to-quantizing-noise ratio exceeds a minimum threshold value.

Figure 3.11. shows the dynamic range of a Delta Modulator.

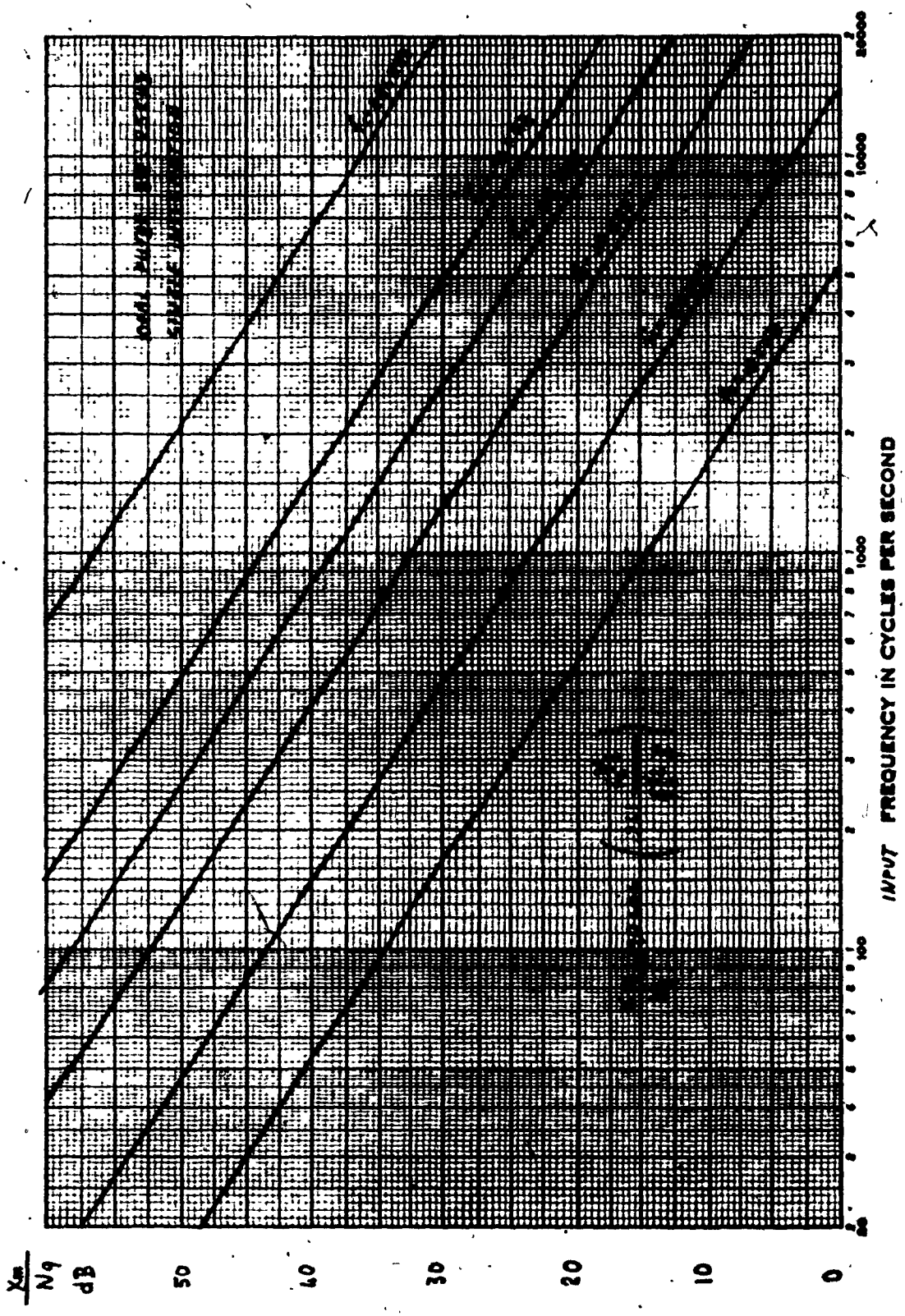

FIGURE 3.7.

MAXIMUM SIGNAL TO QUANTIZING NOISE (f_b = 2.5 kHz)

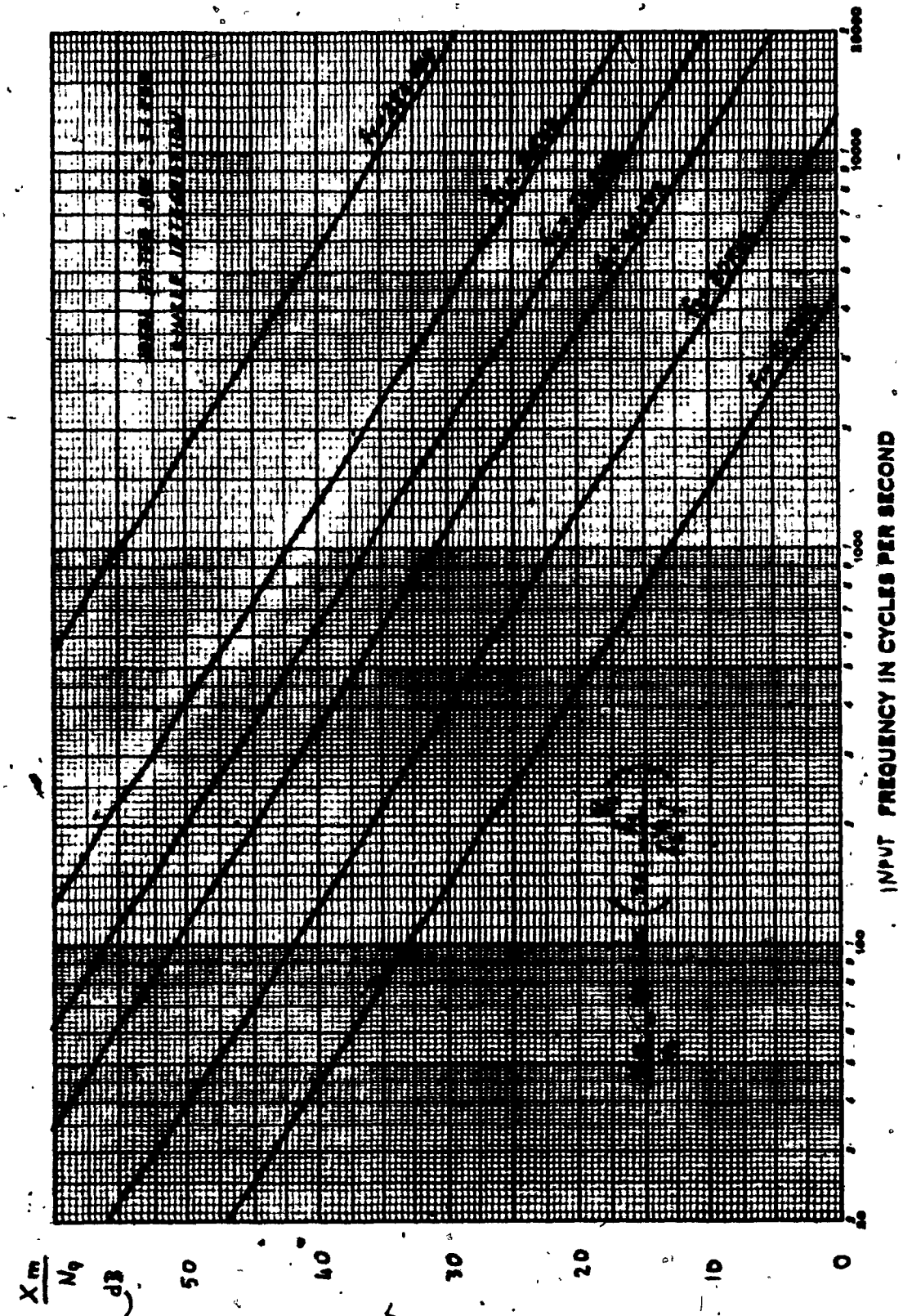

FIGURE 3.8.

MAXIMUM SIGNAL TO QUANTIZING NOISE (f_s = 3.6 kHz)

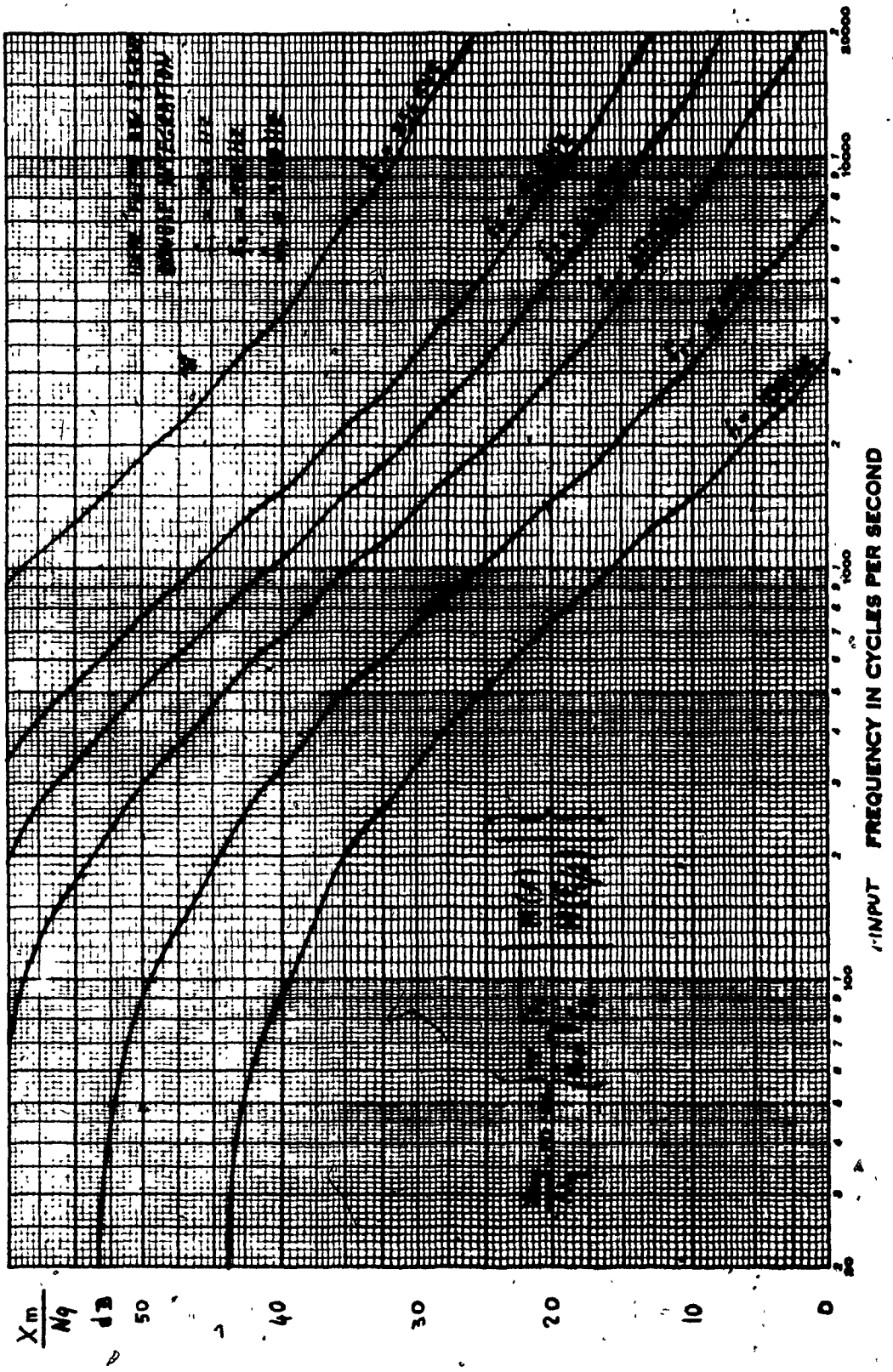

FIGURE 3.9.

MAXIMUM SIGNAL TO QUANTIZING NOISE (f_b = 2.5 kHz)

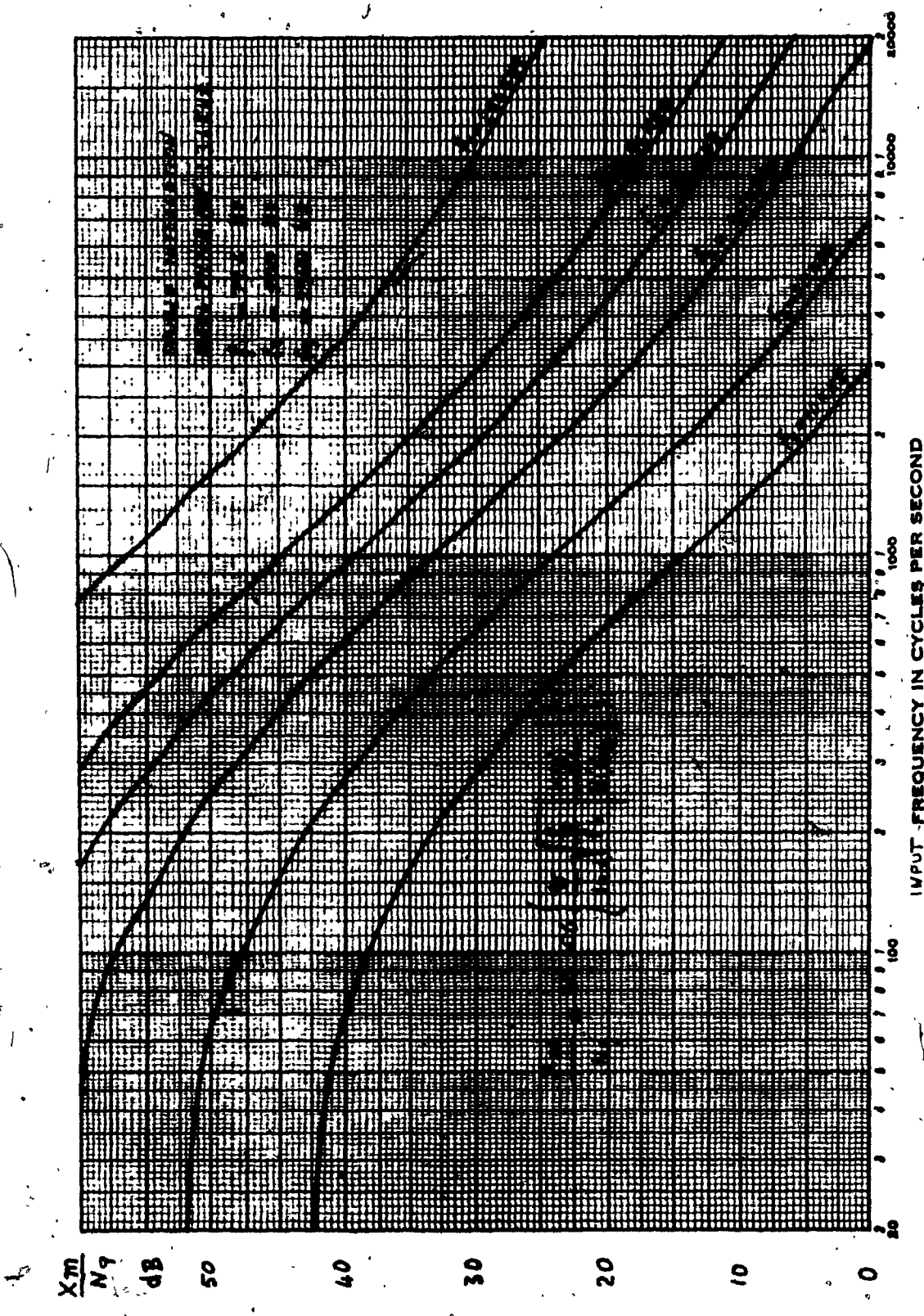

FIGURE 5.10.

MAXIMUM SIGNAL TO QUANTIZING NOISE (f_b = 3.6 kHz).

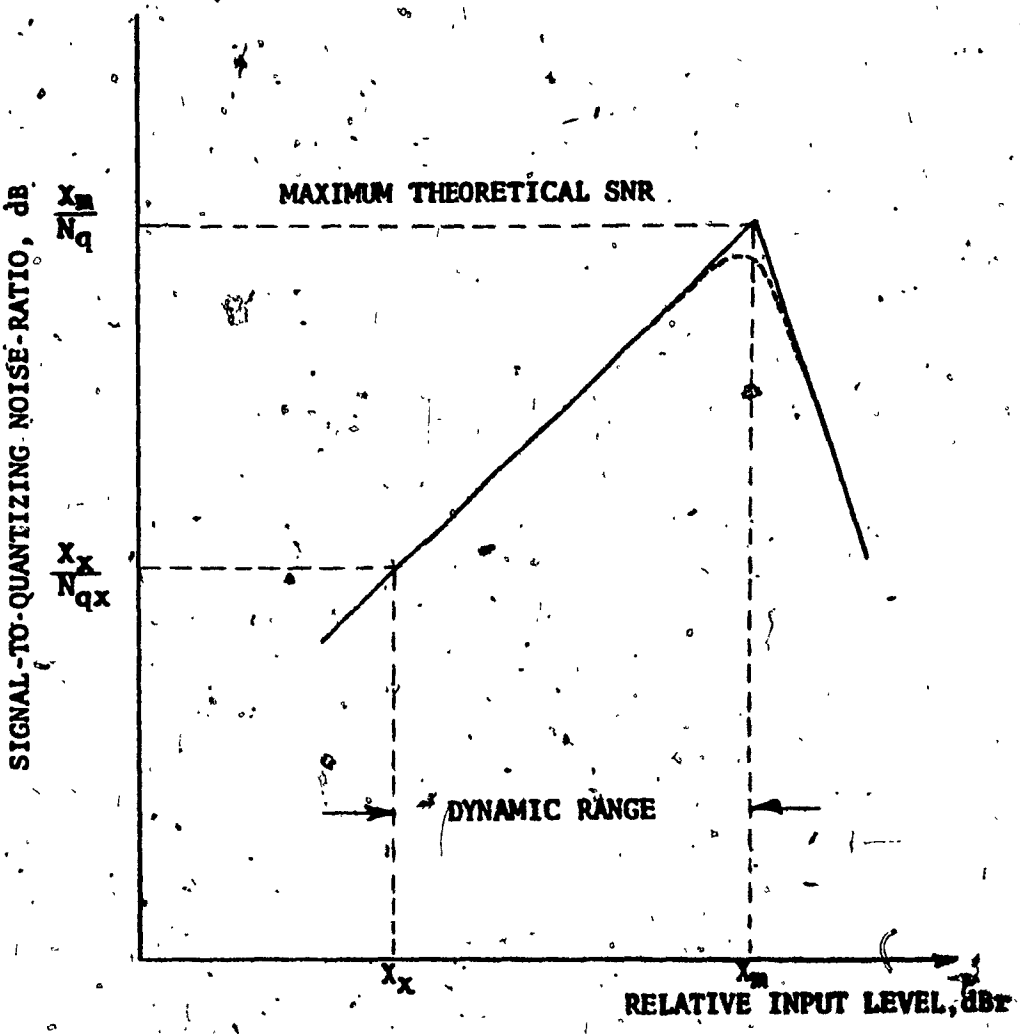

FIGURE 3.11.

DYNAMIC RANGE OF A DELTA MODULATOR

If $\frac{X_x}{N_{qx}}$ denotes the choosen threshold value of signal-to-quantizing-noise ratio, and D_r denotes the dynamic range of the input signal, then equation 3.18. follows:

$$D_r = 20 \log \frac{\frac{X_m}{N_q}}{\frac{X_x}{N_{qx}}} \qquad (3.18.)$$

For uncompanded Delta Modulation system, Nq has a constant value, thus

$$D_r = 20 \log \frac{X_m}{X_x} = 20 \log X_m - 20 \log X_x \qquad (3.19.)$$

3.5. Idle Code

The Idle Code is defined to be the binary code present at the output of the encoder when the input signal is zero.

Idle code exhibits a --1010-- code which is obviously the closest approximation to a zero input.

Thus the integrating network output is a triangular wave of frequency $f_s/2$ and amplitude Δ (Δ is the quantizing step size defined in Section 3.3.2.).

From Figure 3.12. we see that the value of Δ can be calculated by evaluating the decoding network response to a step of value E_0 for a length of time $T_s/2$.

Δ is calculated for both single and double integration cases.

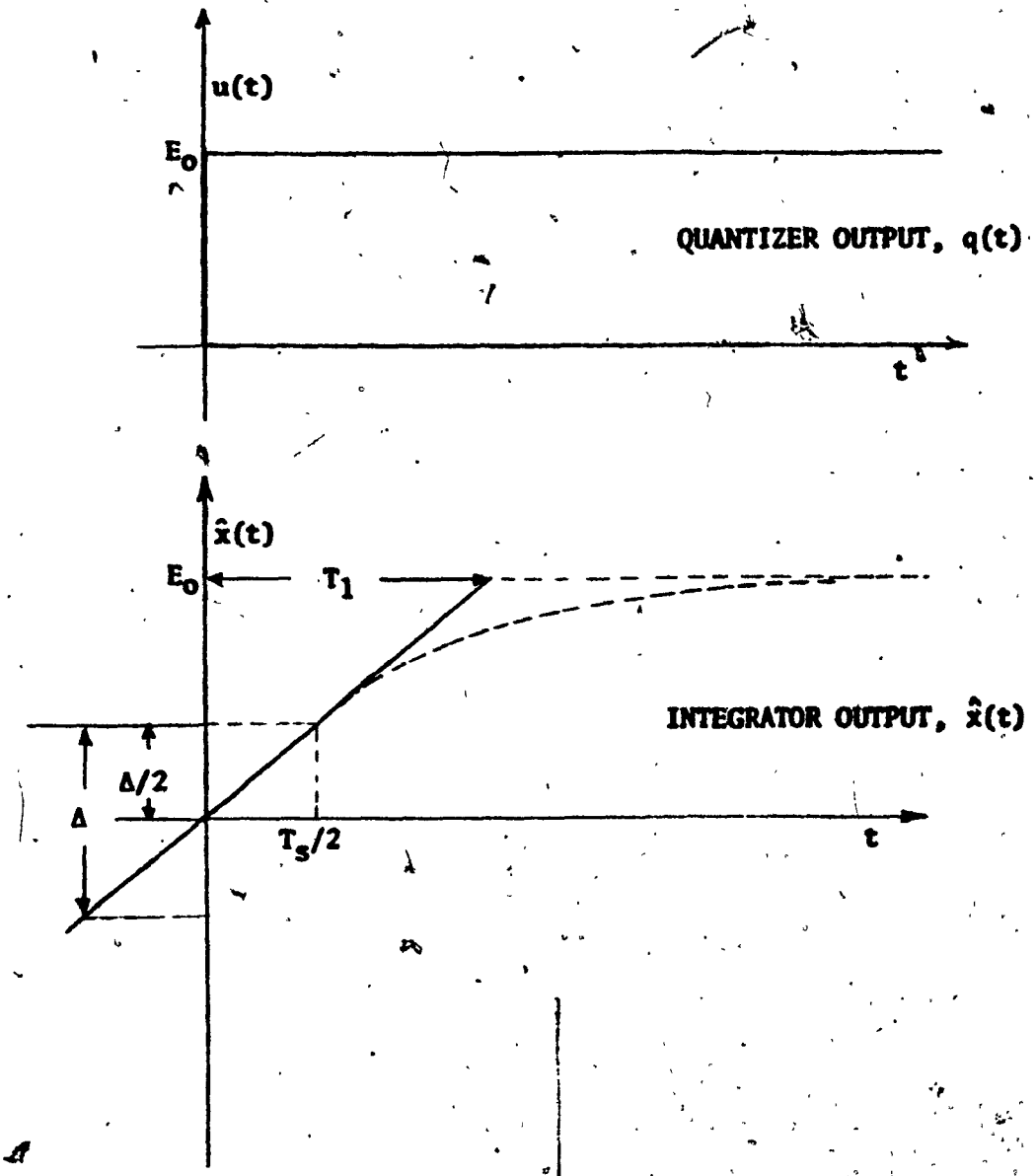

FIGURE 3.12.

IDLE WAVEFORM

i) Single Integration Case:

By using equation 2.5., we have:

$$\Delta = 2 E_0 K \left[1 - e^{\frac{t_s/2}{R_1 C_1}}\right] \qquad (3.20.)$$

If $t_s << RC$, equation 3.20. simplifies to:

$$\Delta = 2\pi E_0 K \frac{f_1}{f_s} \qquad (3.21.)$$

ii) Double Integration Case:

Using equation 2.11., it follows that

$$\Delta = 2E_0K \left[\frac{T_1-T_3}{(T_1-T_2)} e^{\frac{t_s/2}{T_1}} - \frac{T_2-T_3}{(T_1-T_2)} e^{\frac{t_s/2}{T_2}} + 1\right] \qquad (3.22.)$$

If $f >> f_3$ equation 2.16. simplifies to:

$$\Delta = \mathcal{L}^{-1} E_0 K \left[\frac{T_3}{T_1 T_2 S^2}\right]_{t = T_s}$$

$$\Delta = E_0 K \frac{T_3}{T_1 T_2} \cdot T_s$$

OR

$$\Delta = 2\pi E_0 K \frac{f_1 f_2}{f_3 f_s} \qquad (3.23.)$$

Figure 3.13. shows the behavious of a Delta Modulator in idle state as measured in the laboratory; with no analog input, $x(t)$ is

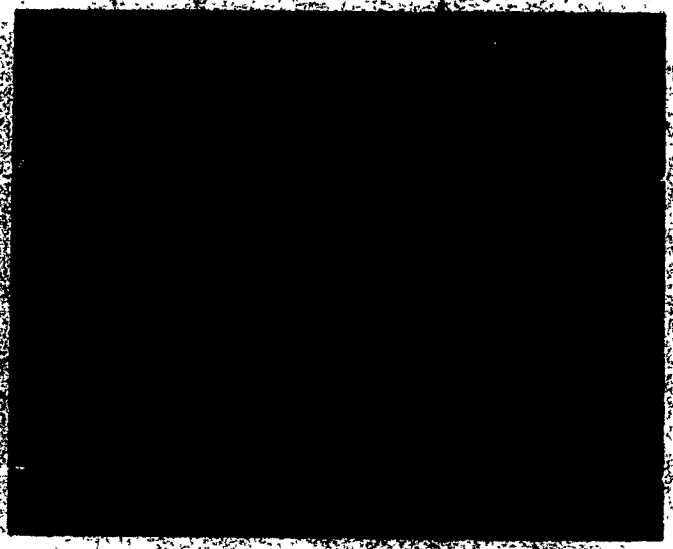

INTEGRATOR OUTPUT, $\hat{x}(t)$

IDLE CODE, $(f_s/2)$

F I G U R E 3.13.

IDLE CODE OF A SINGLE INTEGRATION DELTA MODULATOR

(f_s = 20 kHz)

kept near to zero by a code adopting a --1010-- pattern.

3.6. Threshold Of Coding (Figure 3.14.)

When the peak-to-peak amplitude of the input signal x(t) is smaller than Δ, the idle code will not be disturbed. Only signals exceeding the step size Δ will be encoded.

For a sinusoidal signal, the threshold of coding T_c is given by

$$T_c = \frac{\Delta}{2\sqrt{2}} \text{ (volt rms)} \qquad (3.24.)$$

3.7. Idle Noise

When the encoder idles, the decoding network output is a triangular wave of frequency $f_s/2$ which may be completely removed by the audio filter.

However if the idle code is disturbed, a frequency component falling into the audio band (idle noise) may be generated.

Thus the idle noise is defined as the noise present at the decoder output when the encoder input is zero.

The principle causes for the idle noise are:

i) unsymmetrical quantizer output.

ii) thermal noise present in the system.

iii) offset of active components.

Condition i) is the most important source of idle noise. Therefore our analysis will concern idle noise due to unsymmetrical quantizer

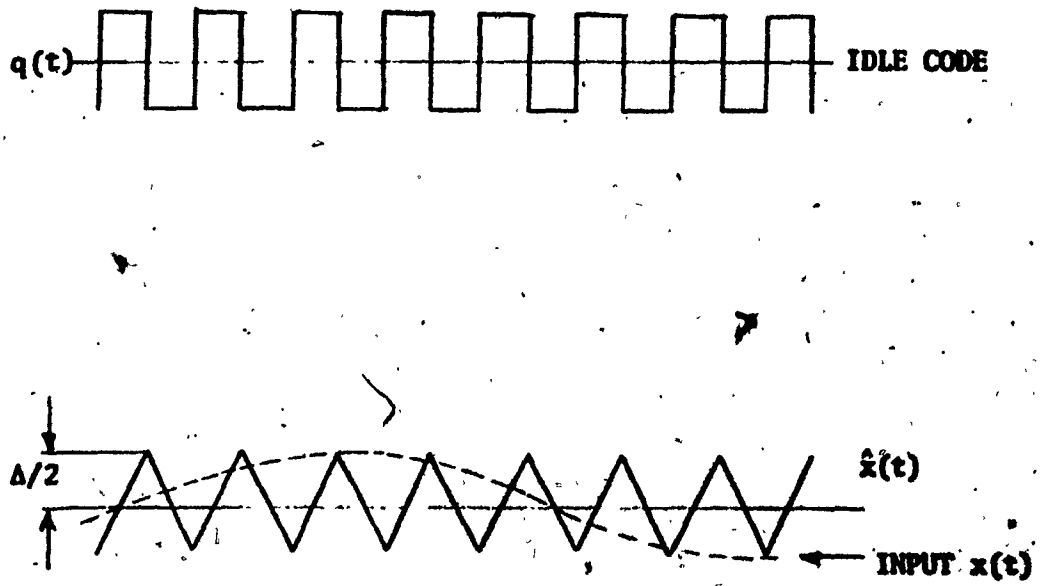

FIGURE 3.14.

THRESHOLD OF CODING FOR A DELTA MODULATOR

output only, for a single integration Delta Modulation system.

Consider the quantizer output q(t) of Figure 3.15.

If an integrator of transfer function H(s) = K/S is driven by the signal of Figure 3.15., a composite response $\hat{x}(t)$ = n(t) + s(t) is obtained (Figure 3.16.)

The idle waveform s(t) is the integrator response to the time varying component of the quantizer output, whereas the envelope n(t) is the response to the quantizer unsymmetry δ.

Thus the integrator output drifts at a rate dependent upon δ until the decision level $\Delta/2$ is reached causing a violation (sequence of two pulses with equal polarity) in the idle code.

This violation will force the integrator output back to a value $-\Delta/2$ and the process is periodically repeated. The equations describing the phenomena are:

$$\frac{\Delta}{2} = KE_o \frac{T_s}{2} \qquad (3.25.)$$

$$\frac{\Delta}{2} = K\delta \frac{T_n}{2} \qquad (3.26.)$$

Equating 3.25. and 3.26.,

$$\frac{T_s}{T_n} = \frac{\delta}{E_o} \qquad (3.27.)$$

or

$$\delta = E_o \frac{f_n}{f_s} \qquad (3.28.)$$

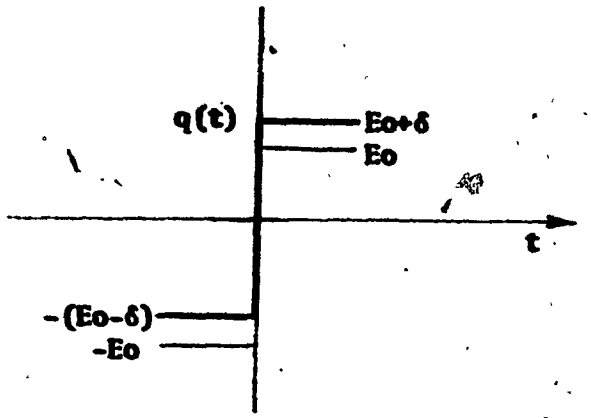

FIGURE 3.15.

QUANTIZER CHARACTERISTIC

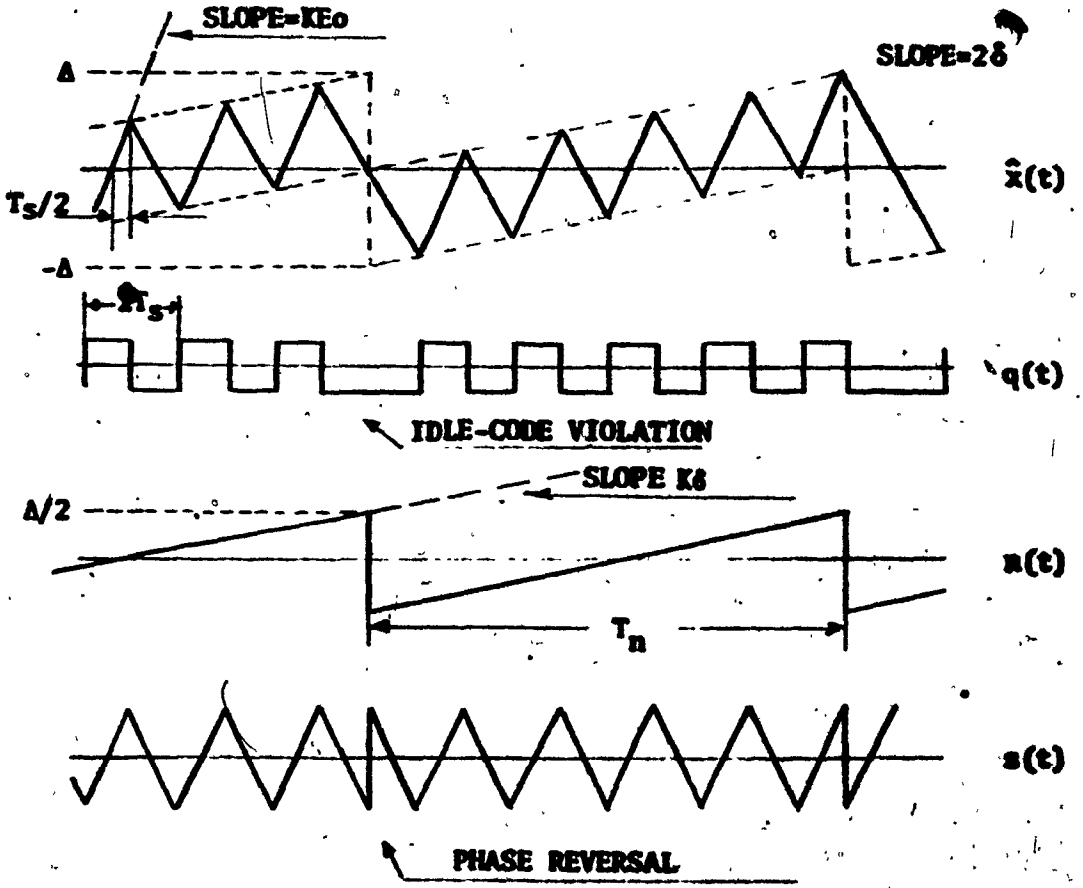

FIGURE 3.16.

IDLE NOISE IN A DELTA MODULATOR

If E_o is a 5 volt step, f_s = 20 kHz, to obtain a 1 kHz tone, a value of δ = 250 mV is required.

3.8. Effect Of Transmission Errors

We have an error when an original bit of the code is replaced by its complement.

That is, a pulse of $\pm E_o$ amplitude is incorrectly received by the decoder as a $\mp E_o$ amplitude. Thus transmission errors are represented by a series of random pulses with amplitude $\pm 2E_o$ and probability p_e. (Figure 3.17.)

The auto-correlation function of a pulse of a certain width with random occurrence in time is given by:

$$R(\tau) = \nu \int_{-\infty}^{\infty} u(t)u(t-\tau)dt = u * u \qquad (3.29.)$$

where ν is the number of occurrences of errors per second and is equal to $f_s \cdot p_e$ (where p_e is the probability of an error)

Recalling the identity

$$u * u \leftrightarrow |U(f)|^2 \qquad (3.30.)$$

where

$$U(f) = \int_{-\infty}^{\infty} e^{-J2\pi ft}\, u(t)dt =$$

$$= 2E_o \frac{\sin \pi f T_s}{\pi f T_s} \qquad (3.31.)$$

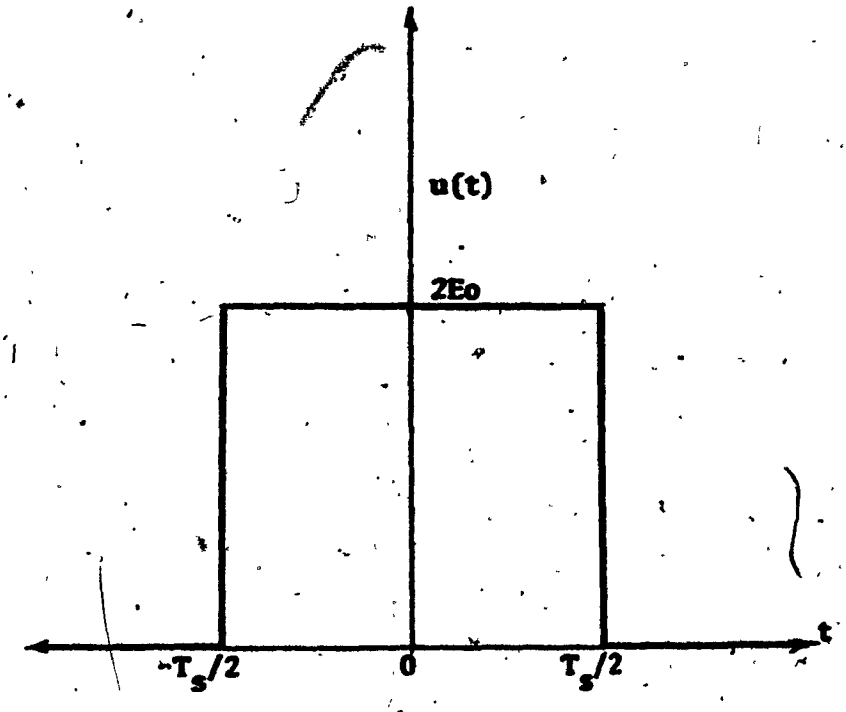

FIGURE 3.17.

REPRESENTATION OF AN ERROR PULSE

The noise spectrum due to the random error pulses is given by:

$$W(f) = \nu|U(f)|^2|H(f)|^2 = 4E_o\nu\left(\frac{\sin\pi fT_s}{\pi fT_s}\right)^2|H(f)|^2 \qquad (3.32.)$$

The amount of noise falling in the voice band is:

$$N_e^2 = 2\int_{f_{1a}}^{f_{2a}} W(f)df = 8E_o\nu\int_{f_{1a}}^{f_{2a}}\left(\frac{\sin\pi fT_s}{\pi fT}\right)^2|H(f)|^2df \qquad (3.33.)$$

We next assume that $f_{2a} << f_s$ so that the expression $\frac{\sin\pi fT_s}{\pi fT_s}$ is essentially unity throughout the audio band.

Thus equation (3.33.) simplifies to

$$N_e^2 = 8E_o^2\nu\int_{f_{1a}}^{f_{2a}}|H(f)|^2df \qquad (3.34.)$$

OR

$$N_e(RMS) = E_o\,2\sqrt{2}\sqrt{\nu\int_{f_{1a}}^{f_{2a}}|H(f)|^2df} \qquad (3.35.$$

Thus, the rms noise is proportional to the square root of the error rate ν.

3.9. System Stability

If the feedback system of Figure 3.18. is opened by braking the loop at the summing point, the transfer function of the open-loop system will be G(s)H(s).

The natural frequencies of the closed loop system are the zeros of 1 + G(s)H(s). It is therefore evident that the stability of

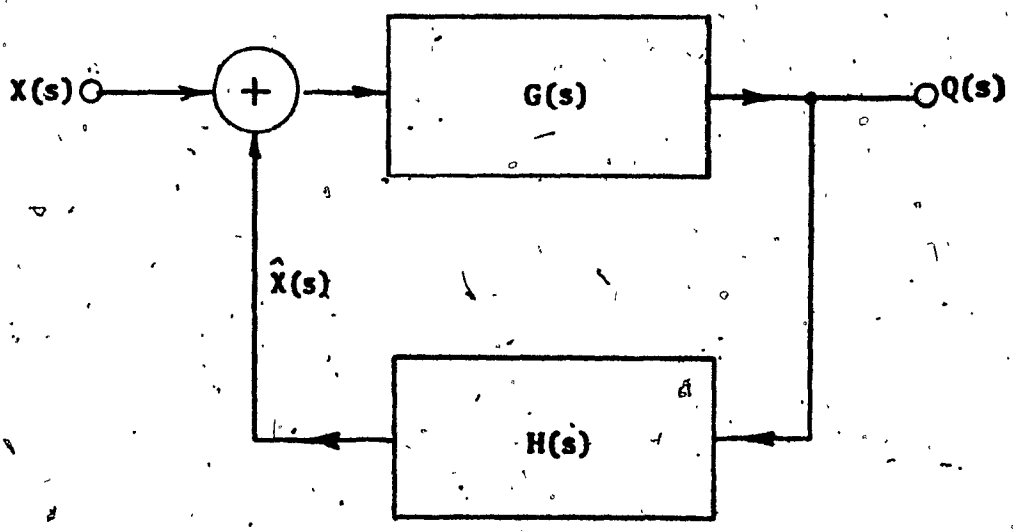

FIGURE 3.18.

LINEAR FEEDBACK SYSTEM

the closed loop system can be determined by the characteristics of its open loop transfer function G(s)H(s).

If the amplitude of G(s) · H(s) is less than unity for the frequency range at which argument [G(s)H(s)] ≥ 180, then the system can be considered stable.

Basically, a Delta Modulation system behaves like a linear system and the above described stability test could be utilized.

However, the contribution of the delay T_s due the sampling process must be included in the feedback loop as shown in Figure 3.19.

Thus the stability condition for a Delta Modulation system can be summarized as:

$$\text{when ARG } [G_1(s) \cdot G_2(s) \cdot H(s)] \geq 180^\circ \qquad (3.36.)$$

$$\text{then} \quad |G_1(s) \cdot G_2(s) \cdot H(s)| < 1 \qquad (3.37.)$$

where

i) $G_1(s)$ depends on the quantizer output level E_o.

$$|G_1(s)| = KE_o \,, \quad \text{ARG}[G_1(s)] = 0$$

ii) $G_2(s)$ is the delay introduced by the sampling process.

$\text{ARG}[G_2(s)]$ is linearly varying with frequency and $|G_2(s)| = 1$.

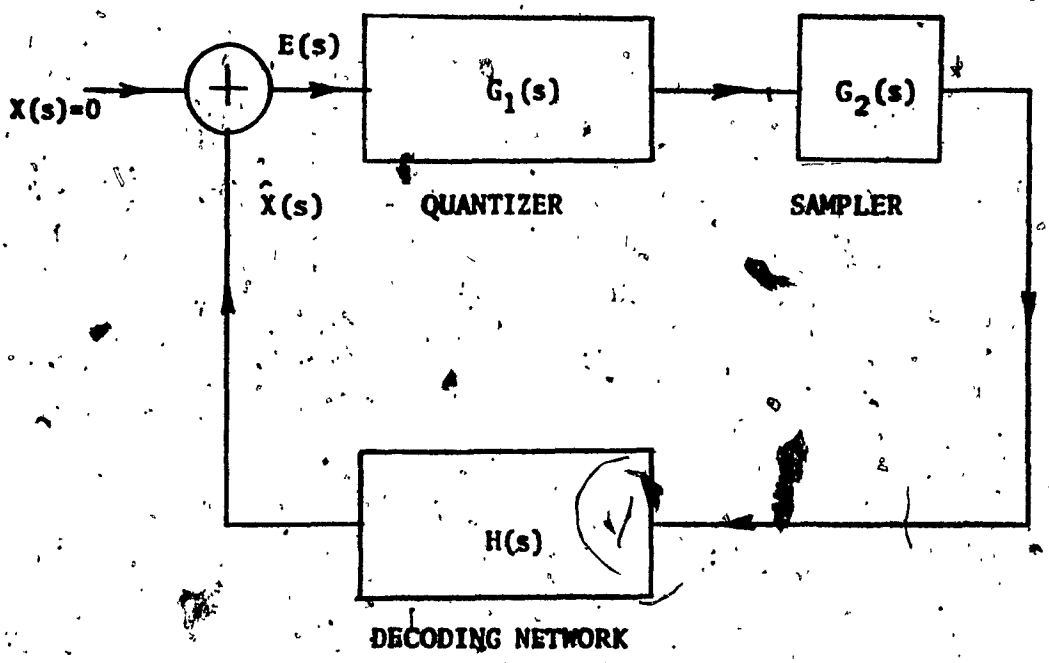

FIGURE 3.19.

FEEDBACK NETWORK UNDER STUDY

iii) H(s) is the decoding network transfer function.

Since single integration Delta Modulator are always stable (ARG H(s) = 90° maximum), the test is only required for double integration systems where the total phase can exceed 180° as shown in Figure 3.20.

The presented method is not believed to be rigorously exact, but still offers useful information in many cases.

This method was used for the stability test of the experimental Delta Modulator of Chapter 4 and was found satisfactory. More rigorous but complex methods are available in the literature [14].

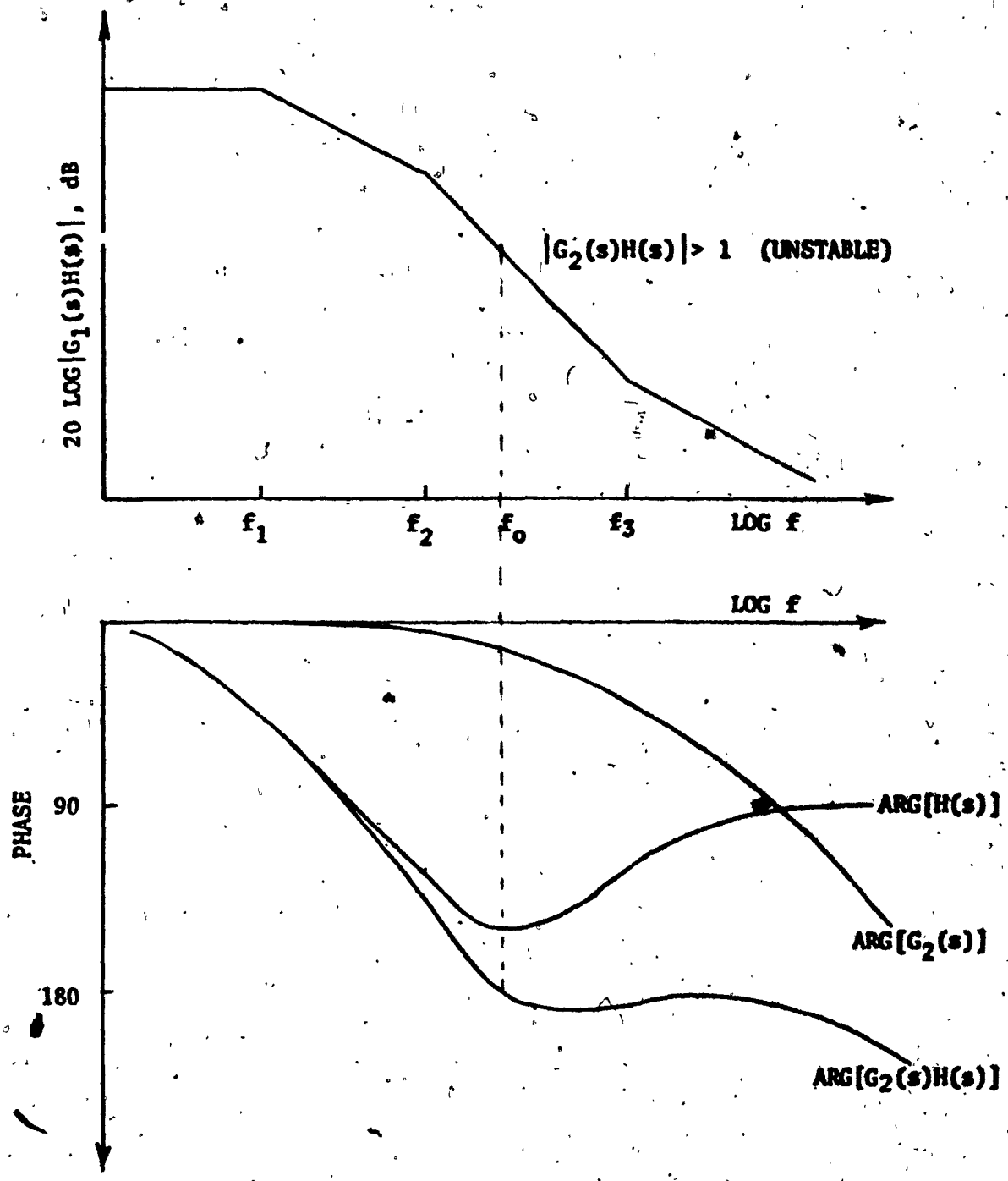

FIGURE 3.20.

AMPLITUDE AND PHASE PLOT OF A DOUBLE INTEGRATION DELTA MODULATOR

CHAPTER 4

DELTA MODULATOR DESIGN

4.1. Design Objective

Our purpose in this Chapter is to describe a Delta Modulator system which was constructed to experimentally verify the theoretical results of Chapter 3. The coder - decoder specifications are:

i) Speech signal of 5 volts peak-to-peak must be encoded without overloading.

ii) The system must be capable of working with a variable sampling frequency (20 kHz and 40 kHz).

iii) A bandwidth of 2.5 kHz is required.

iv) Both single integration and double integration techniques are used.

4.2. Design Procedure

4.2.1. Single Integration

It has been proven [6] that the overload level for a voice signal is almost equivalent to that of an 800 Hz sinewave. Thus the decoding network should not cause slope overload when a 5 volt peak-to-peak 800 Hz sinewave is applied to the input.

If we let:

$$E_0 = 5 \text{ volts}$$

$$T_1 = R_1C_1 = 2 \text{ msec}$$

$$R_0 = 20 \text{ k ohms}$$

Using equation 3.7., the values of K, R_1 and C_1 can be obtained.

$$K = X_m \frac{\sqrt{1+\omega^2 T_1^2}}{2E_o} = 5 \qquad (4.1.)$$

$$R_1 = K R_o = 100k \text{ ohms} \qquad (4.2.)$$

$$C_1 = \frac{T_1}{R_1} = 20{,}000 \text{ pF} \qquad (4.3.)$$

Since K > 1, implementation by active network is necessary. (Figure 4.1.)

The network response is shown in Figure 4.2. The slope overload point (7.068 dBm) is choosen as a system reference level (7.068 dBm* = 0 dBm0*).

4.2.2. Double Integration

To achieve double integration, a lead-lag network is cascaded to the circuit of Figure 4.1.

The stability test described in Section 3.8. will be required since double integrating networks may lead to system instability. For example, the double integrating network of transfer function:

$$H(f) = KE_o \frac{(1 + ST_3)}{(1+ST_1)(1+ST_2)} \qquad (4.4.)$$

NOTE: * By convention, the symbol DBm implies a power reference level of 1 mW. When dBm is used to define relative voltages, the reference voltage is .7746 volt which is the voltage required across a 600 ohm impedance to produce 1 mW of power.

The term dBm0 is used to measure power (or voltage) back to an arbitrary choosen zero level point.

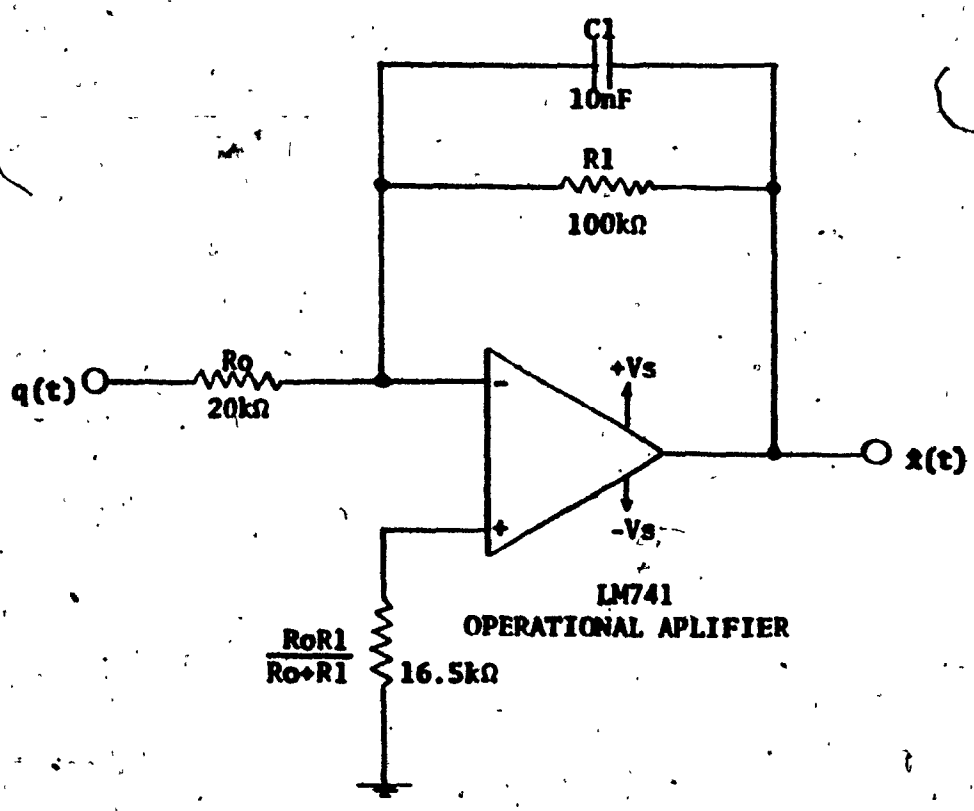

FIGURE 4.1.

ACTIVE INTEGRATING NETWORK

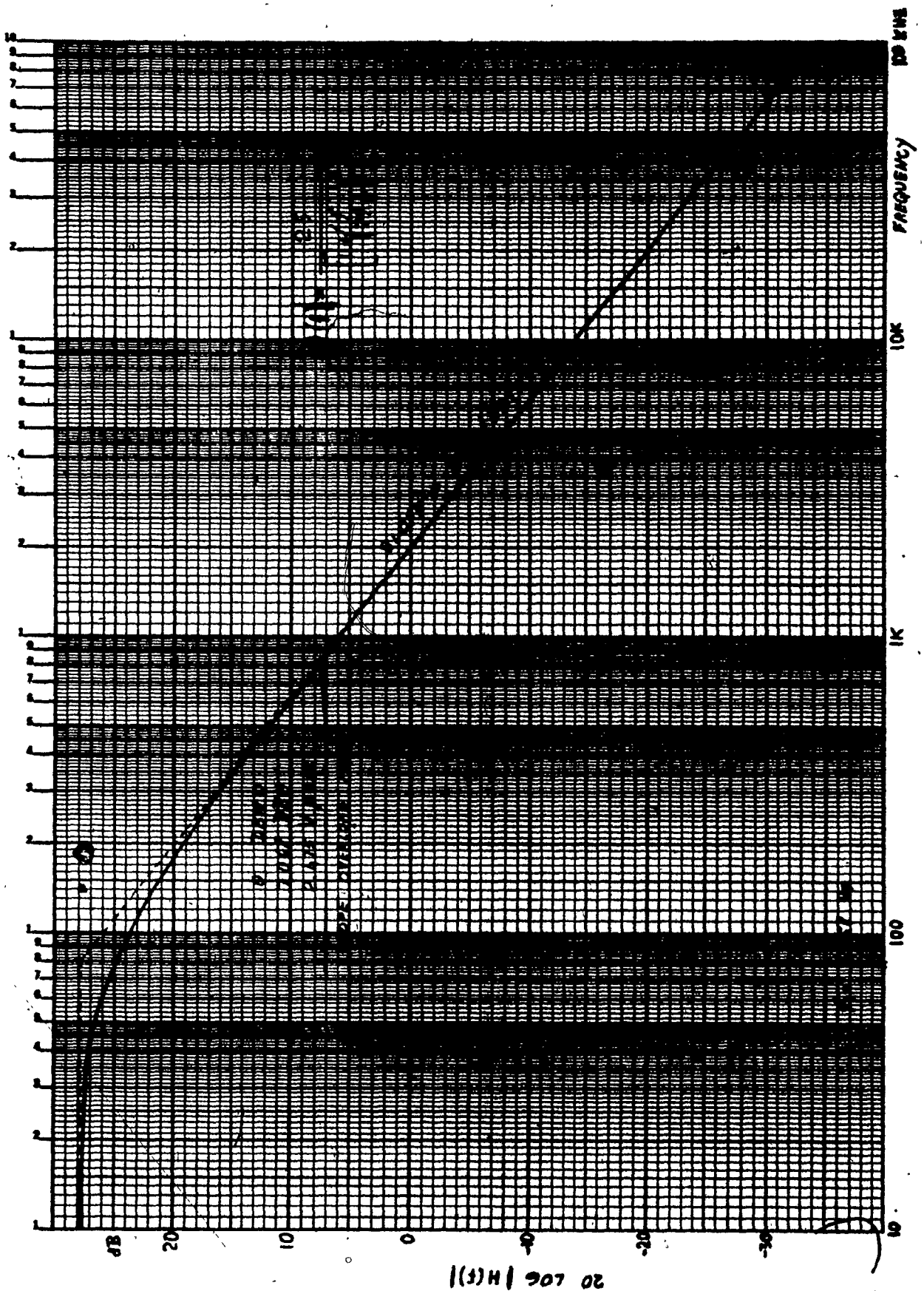

FIGURE 4.2.

SINGLE INTEGRATION NETWORK RESPONSE

where

$$\left.\begin{aligned} K &= 10 \\ E_0 &= 5 \\ T_1 &= 1 \text{ msec} \\ T_2 &= \frac{1}{2\pi f_2} = \frac{1}{2\pi 2500} \\ T_3 &= \frac{1}{2\pi f_3} = \frac{1}{2\pi 10000} \end{aligned}\right\} \quad (4.5.)$$

causes the Delta modulation system to be unstable when operated by a 20 kHz clock (see Figure 4.3.). This was experimentally verified and an oscillation of $f_s/6$ was measured at the decoding network output $\hat{x}(t)$ as shown in Figure 4.4.

It must be noticed that due to the sampling process, only oscillations of frequency f_s/n n=3, 4, --- are possible. Oscillation with n = 2 are referred to as an idle code and they do not constitute a true instability.

A second network characterized by

$$\left.\begin{aligned} K &= 5 \\ E_0 &= 5 \\ T_1 &= 2 \text{ msec} \\ T_2 &= \frac{1}{2\pi f_2} = \frac{1}{2\pi 500} \\ T_3 &= \frac{1}{2\pi f_3} = \frac{1}{2\pi 2500} \end{aligned}\right\} \quad (4.6.)$$

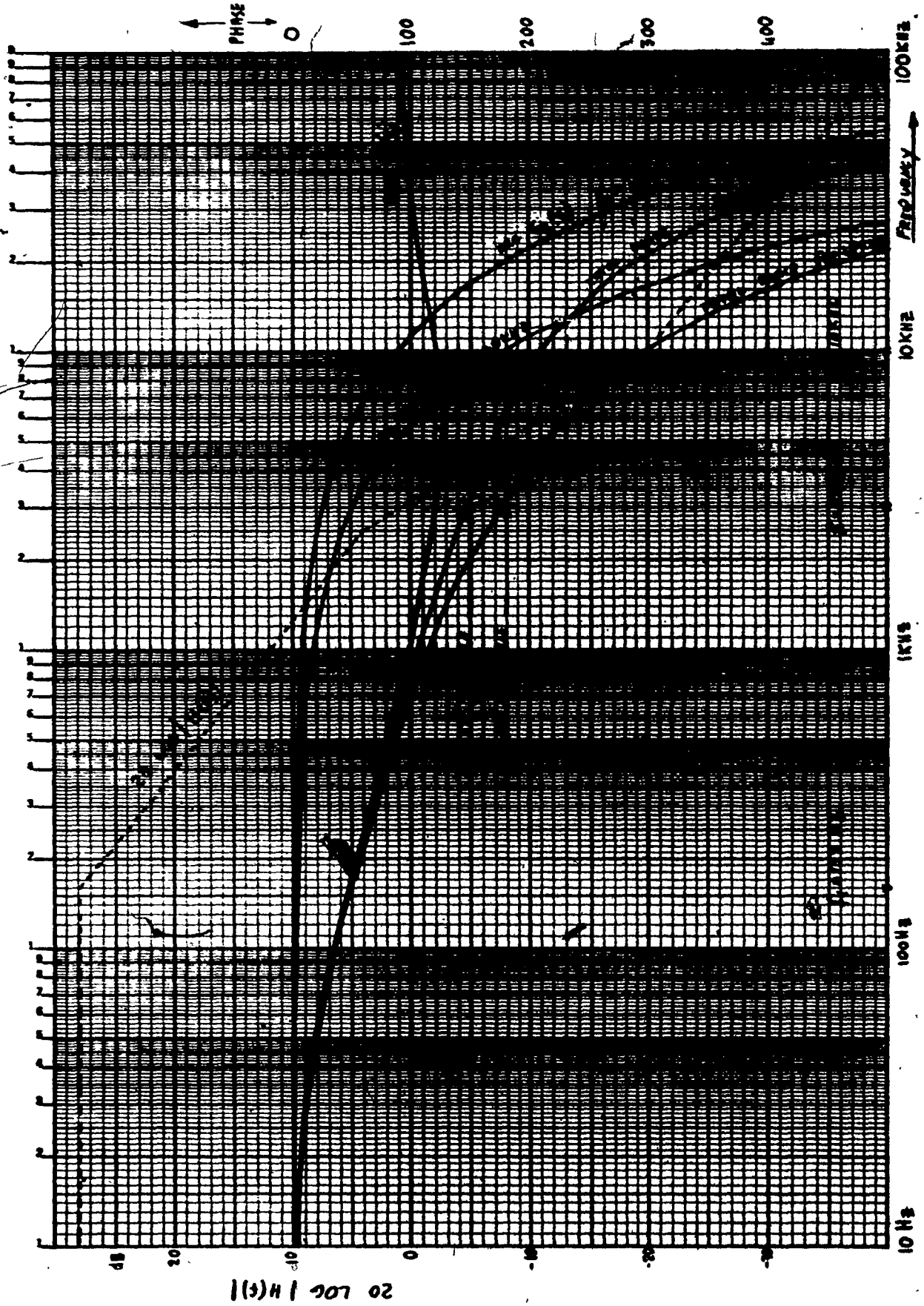

FIGURE 4.3.

SYSTEM STABILITY TEST

SYSTEM OSCILLATION (3.33 kHz), $\hat{x}(t)$

SAMPLING FREQUENCY, f_s

OUTPUT CODE

FIGURE 4.4.

UNSTABLE SYSTEM

did not produce system instability and it was used on the experimental coder-decoder system (Figures 4.5. and 4.6.).

4.3. The Final Circuit Diagram

The overall encoder circuit is shown in Figure 4.7. The functions of the most important components are:

i) A_1 = comparator - limiter

ii) A_2 = sampler - zero order hold

iii) A_3 = integrating network active element

iv) Q_1 = quantizer ($\pm E_o$)

v) S_1 = single or double integration selector switch.

vi) F_1 = audio filter with the following specifications:

a) 3 dB frequency response: 140 Hz to 1640 Hz

b) Bandwidth: 2.5 kHz

c) Insertion Loss: 0 dB

d) Steep low pass cut-off: Elliptic function 5th. order

e) High Pass Section: 3rd. order Butterworth

The filter response is shown in Figure 4.8.

The decoder circuit, which is a duplication of the feedback path of the encoder is shown in Figure 4.9.

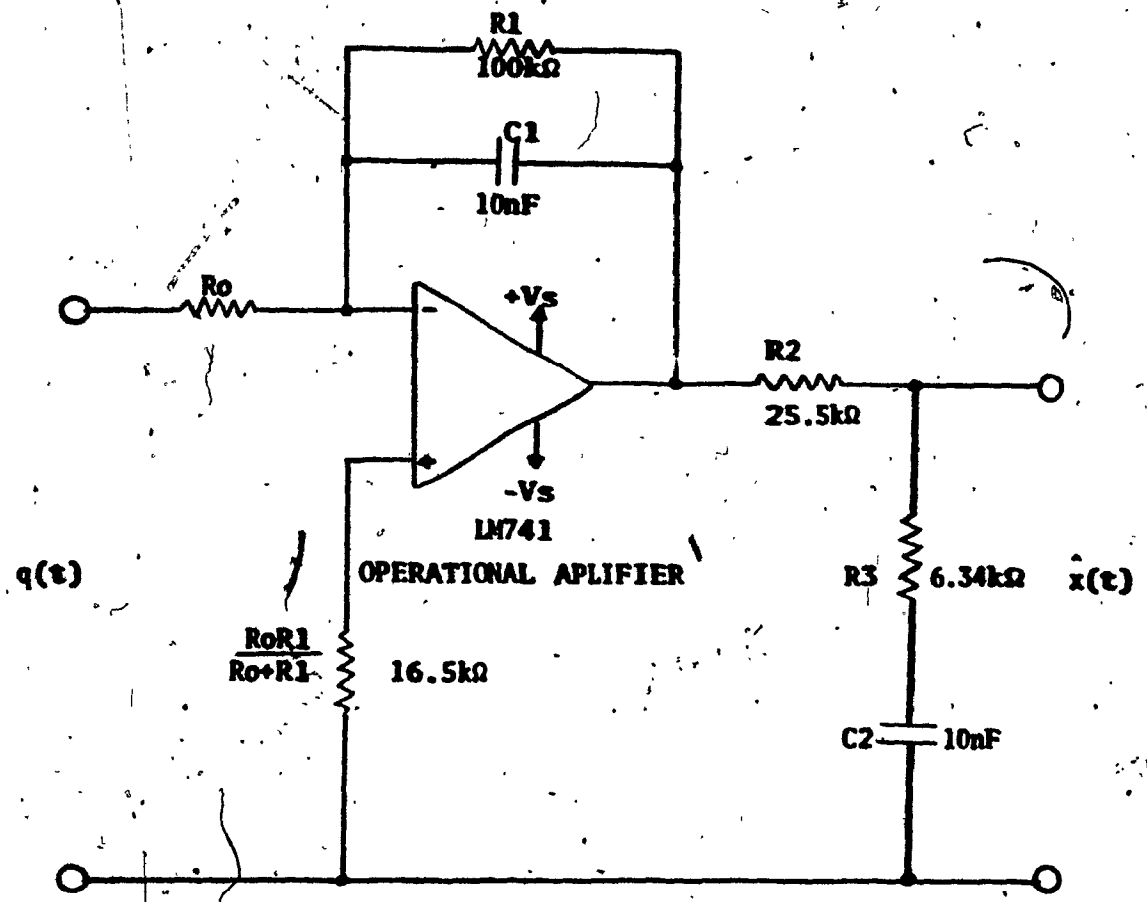

FIGURE 4.5

STABLE DOUBLE INTEGRATION NETWORK

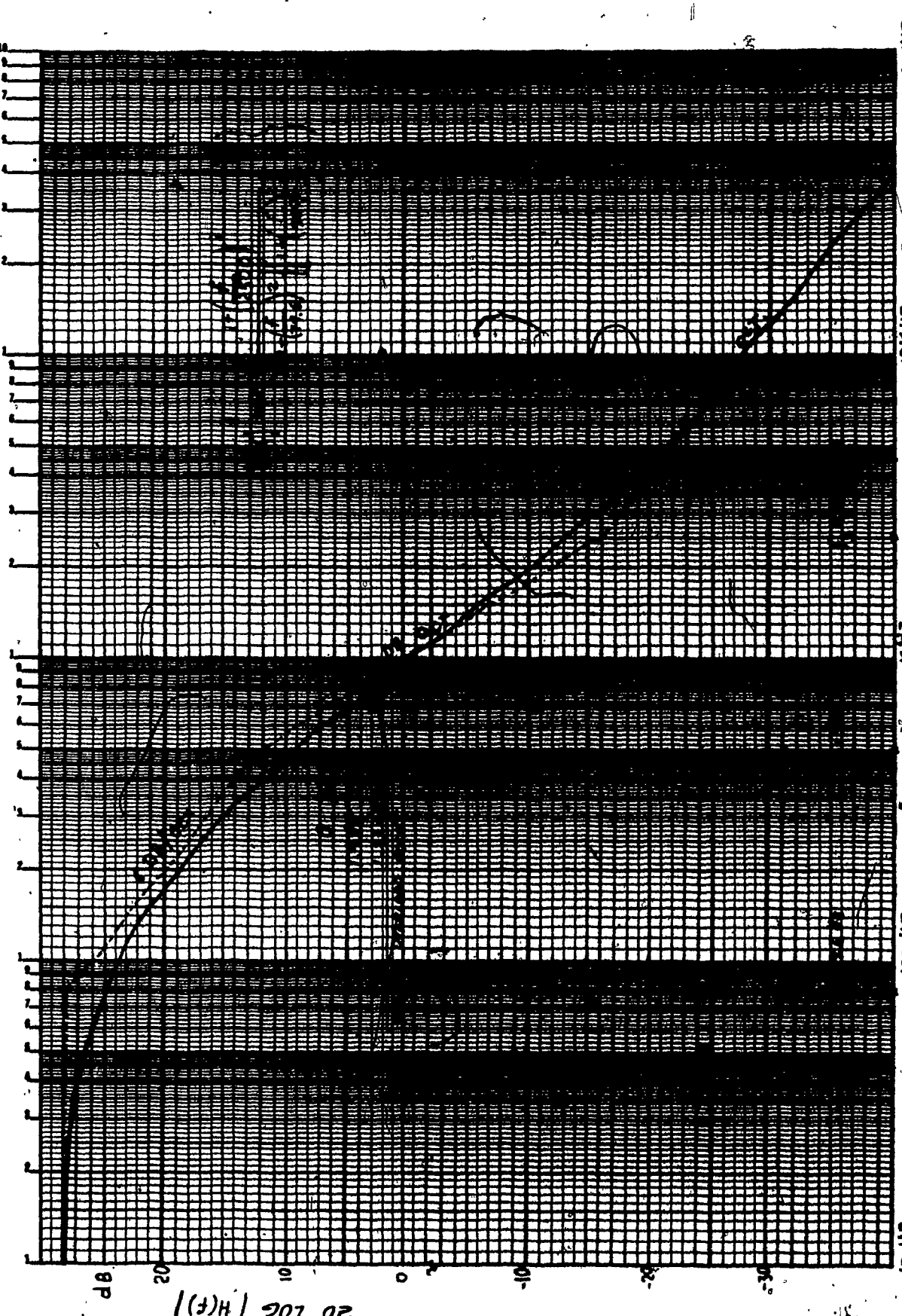

FIGURE 4.6.

DOUBLE INTEGRATION NETWORK RESPONSE

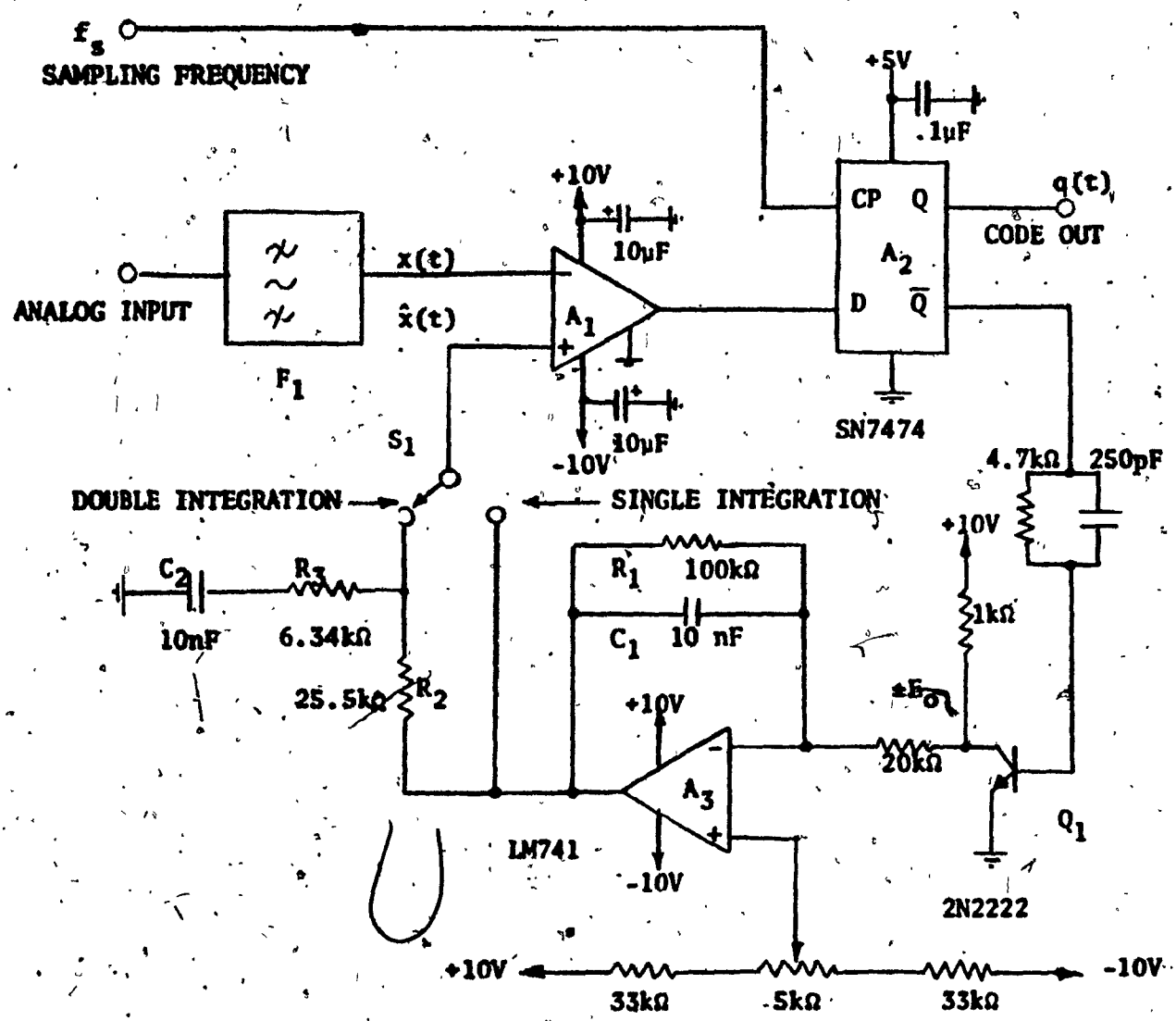

F I G U R E 4.7.

DELTA ENCODER SCHEMATIC DIAGRAM

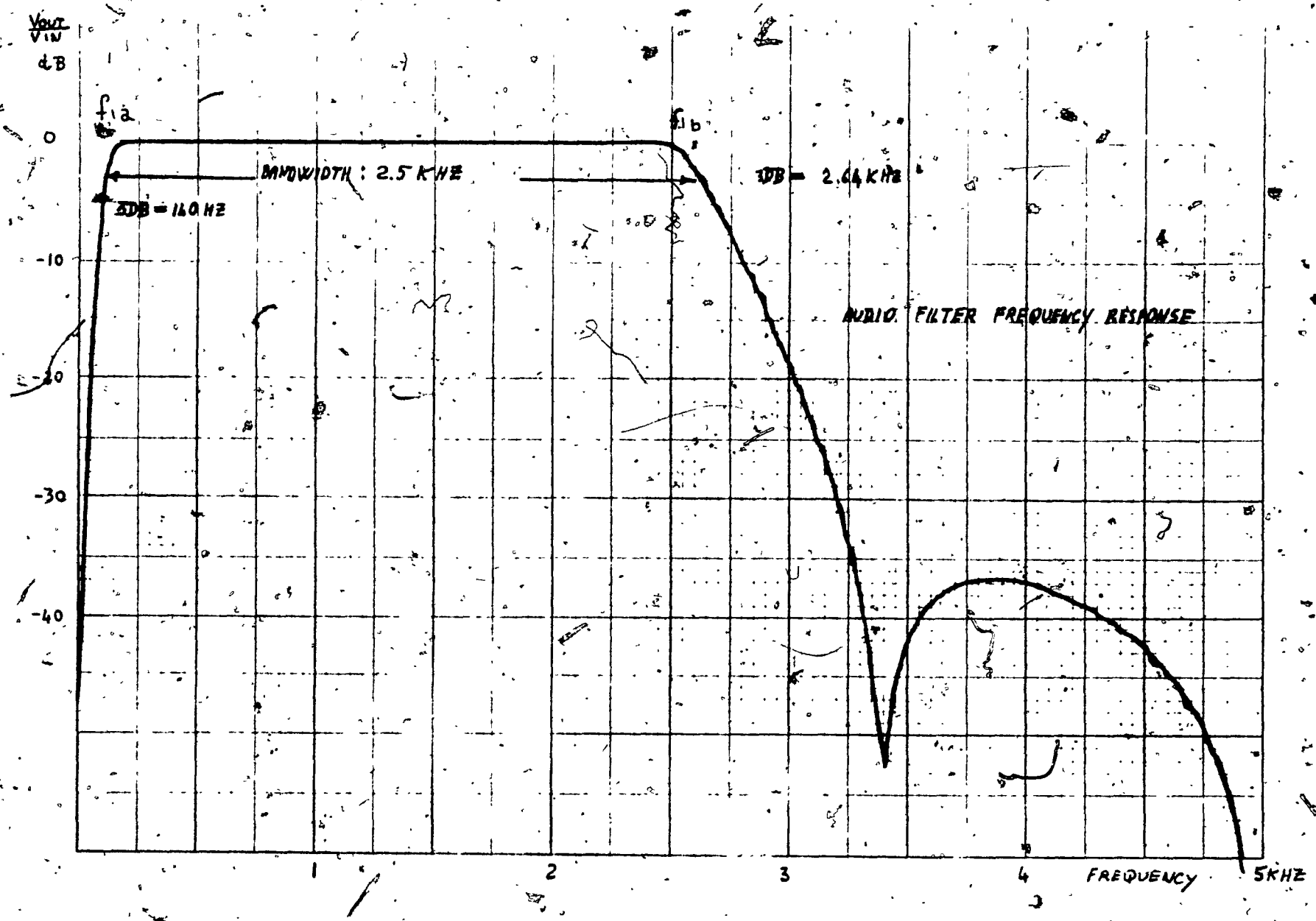

FIGURE 4.8.

AUDIO FILTER FREQUENCY RESPONSE

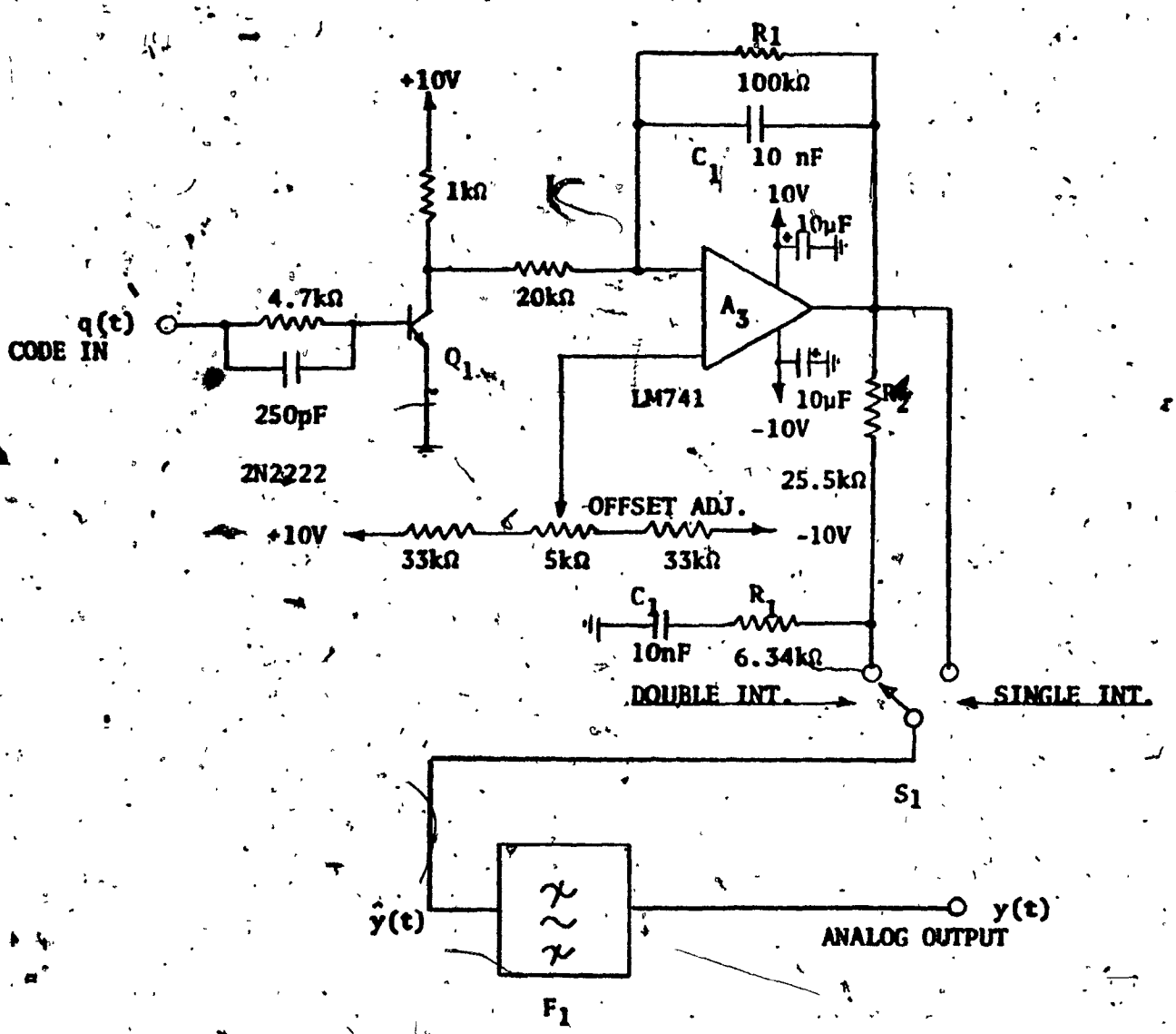

FIGURE 4.9.

DELTA DECODER SCHEMATIC DIAGRAM

4.4 Delta Modulator Parameter Summary

Tables 4.1. and 4.2. summarize the calculated circuit parameters for single and double integration systems.

PARAMETER DESCRIPTION	PARAMETER VALUE		UNIT	EQUATION UTILIZED
	f_s = 20 kHz	f_s = 40 kHz		
Overload Point X_m (800 Hz)	1.75	1.75	V_{RMS}	3.7.
Maximum Signal To Quantizing Noise X_m/N_q	25.32	34.32	dB	3.17.
Coding Threshold T_c	221	110.5	mV_{RMS}	3.24.
Quantizing Noise N_q	94.6	47.3	mV_{RMS}	3.13.
Step Size Δ	.625	.312	V_{pp}	3.21.

TABLE 4.1.

SINGLE INTEGRATION SYSTEM PARAMETER LIST

PARAMETER DESCRIPTION	PARAMETER VALUE		UNIT	EQUATION UTILIZED
	f_s = 20 kHz	f_s = 40 kHz		
Overload Point X_m (800 Hz)	.973	.973	V_{RMS}	3.8.
Maximum Signal To Quantizing Noise X_m/N_q	28.7	37.8	dB	3.15.
Coding Threshold T_c	44.2	22.1	mV_{RMS}	3.24.
Quantizing Noise N_q	35.7	12.5	mV_{RMS}	3.13.
Step Size Δ	125	62.5	mV_{RMS}	3.23.

T A B L E 4.2.

DOUBLE INTEGRATION SYSTEM PARAMETER LIST

CHAPTER 5

EXPERIMENTAL RESULTS

The Delta Modulation encoder and decoder shown in Figures 4.6. and 4.7. were assembled and tested in the laboratory. Figure 5.1. shows the response of a Single Integration Delta Modulation (SIDM) to a sinusoidal input at slope overload level (5V peak-to-peak).

The output code is random in time. Figure 5.2. shows the response of a Dual Integration Delta Modulation (DIDM) system. The smoother response typical of double integration systems is evident.

Figure 5.3. shows a SIDM system at gross overload point. The output code contains a strong component of the input signal.

Figure 5.4. shows a SIDM system behaviour to low level inputs.

Small signal encoding suffers from excessive quantizing distortion due to the coarse approximation of the input signal.

Figures 5.5. and 5.6. show the SIDM system performance when the sampling frequency is increased from 20 kHz to 40 kHz.

The increase of the signal-to-quantizing-noise ratio with the increase of the sampling frequency is evident (Figure 5.6.).

Figures 5.7. and 5.8. show the quantizing error introduced by the SIDM encoder. If the sampling frequency is increased to 40 kHz, the amplitude of the error signal is considerably reduced (Figure 5.8.).

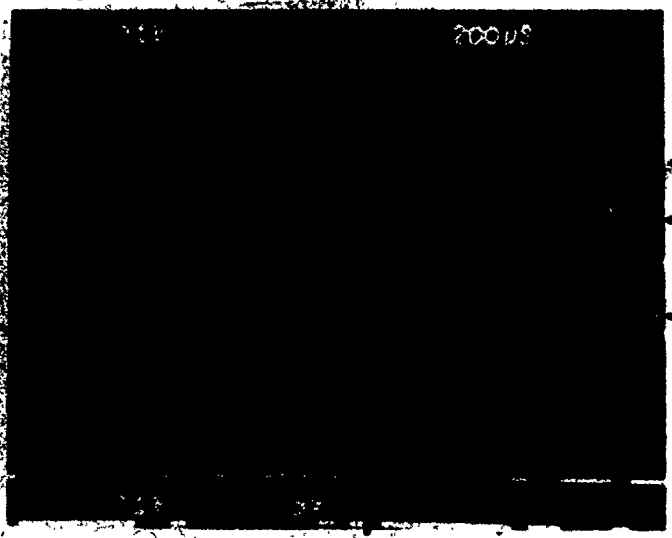

INTEGRATOR OUTPUT, $\hat{x}(t)$

ENCODER INPUT, X(t)
(800 Hz, 0 dBm0)

OUTPUT CODE q(t)

FIGURE 5.1. SIDM SYSTEM AT SLOPE OVERLOAD
(f_s = 20 kHz)

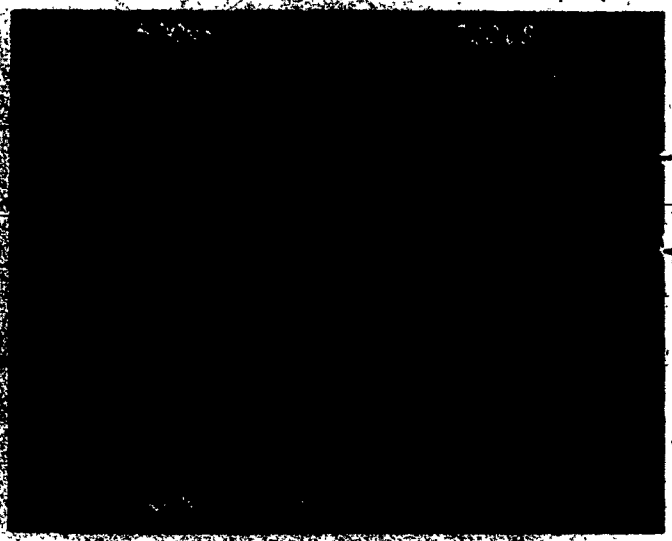

INTEGRATOR OUTPUT, $\hat{x}(t)$

ENCODER INPUT, X(t)
(800 Hz, 0 dBm0)

SAMPLING FREQUENCY, f_s

OUTPUT CODE, q(t)

FIGURE 5.2. DIDM SYSTEM AT SLOPE OVERLOAD
(f_s = 20 kHz)

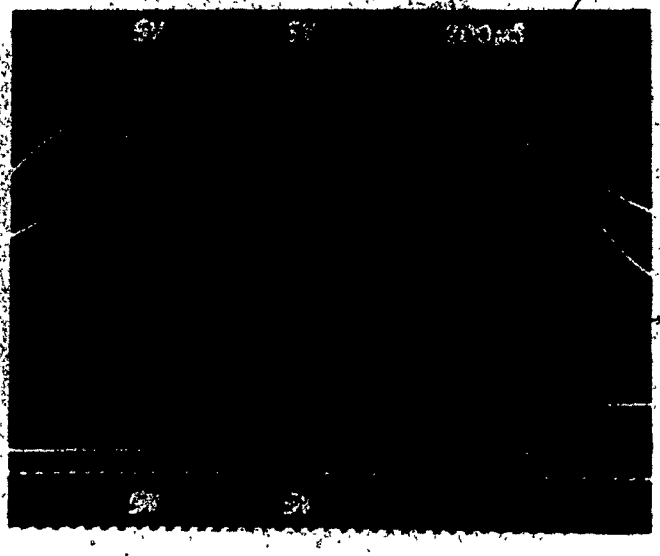

$\hat{x}(t)$

INPUT, X(t)

CODE, q(t)

f_s

FIGURE 5.3. SIDM SYSTEM AT GROSS OVERLOAD

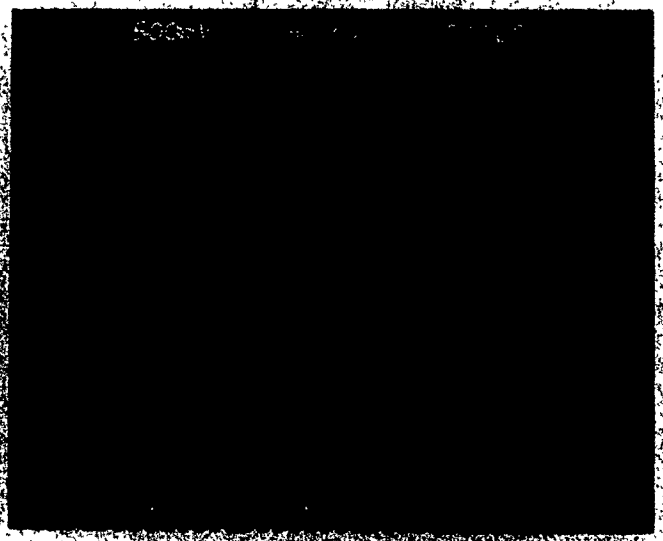

$\hat{x}(t)$

INPUT, X(t)

CODE, q(t)

f_s

FIGURE 5.4. SIDM SYSTEM BEHAVIOUR AT LOW INPUTS

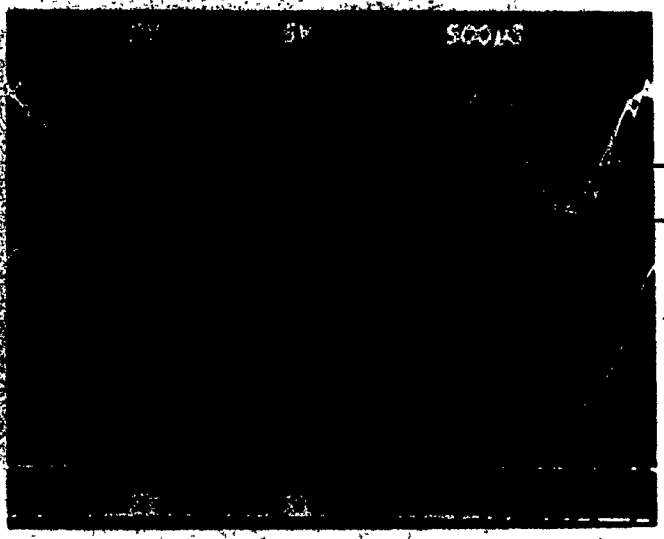

ENCODER INPUT, X(t)
(800 Hz, 0 dBm0)

$\hat{x}(t)$

DECODER OUTPUT, y(t)

OUTPUT CODE, q(t)

FIGURE 5.5. SIDM SYSTEM CODING WAVEFORMS
(f_s = 20 kHz)

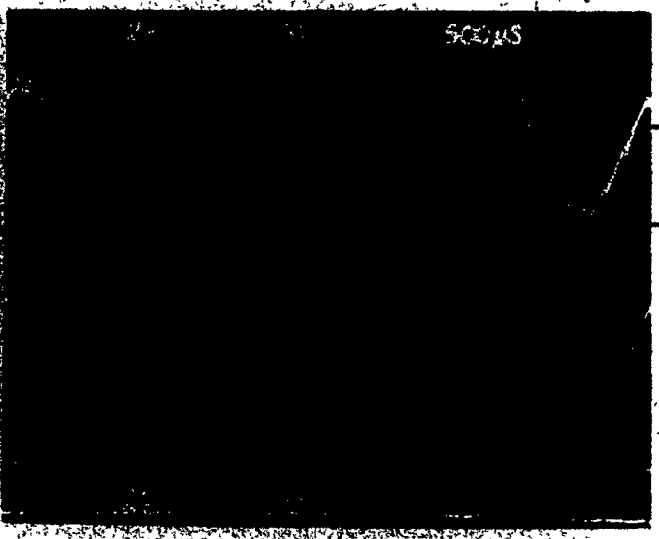

ENCODER INPUT, X(t)
(800 Hz, 0 dBm0)

$\hat{x}(t)$

DECODER OUTPUT, y(t)

OUTPUT CODE, q(t)

FIGURE 5.6. SIDM SYSTEM CODING WAVEFORMS
(f_s = 40 kHz)

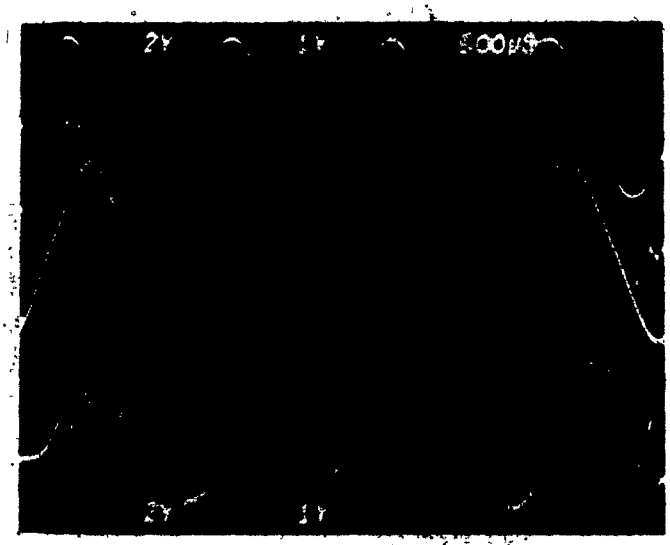

ENCODER INPUT, X(t)
(800 Hz, 0 dBm0)

INTEGRATOR OUTPUT, $\hat{x}(t)$

DECODER OUTPUT, y(t)

QUANTIZING ERROR, e(t)

FIGURE 5.7. QUANTIZING ERROR (SIDM)
(f_s = 20 kHz)

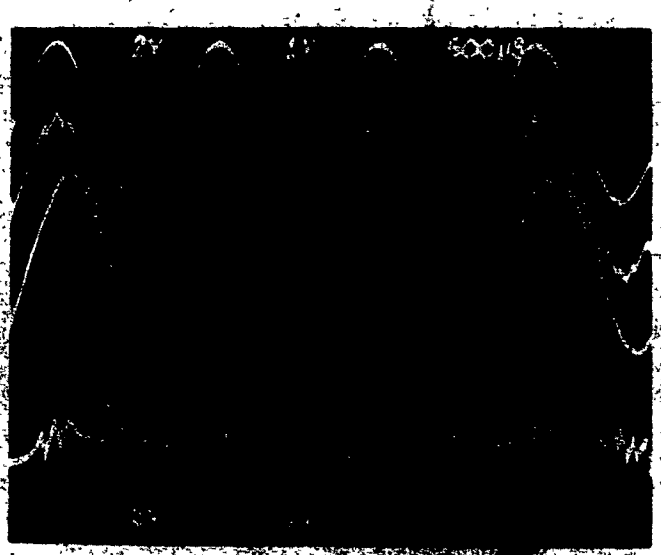

ENCODER INPUT, X(t)
(800 Hz, 0 dBm0)

INTEGRATOR OUTPUT, $\hat{x}(t)$

DECODER OUTPUT, y(t)

QUANTIZING ERROR, e(t)

FIGURE 5.8. QUANTIZING ERROR (SIDM)
(f_s = 20 kHz)

Figures 5.9., 5.10., 5.11., and 5.12. show the waveforms of a SIDM and a DIDM system at various points in the circuit. The Decoder output waveform y(t) has a 150 μsec delay with respect to the encoder input X(t). This is mainly due to the delay introduced by the filter and by the encoding-decoding process.

Figure 5.13. shows the idle waveform of both SIDM and DIDM systems. A DIDM system produces an idle waveform (Δ) considerably smaller than that of a SIDM system.

Figure 5.14. shows a SIDM system with some idle noise caused by an 160 mV offset artificially introduced in the quantizer circuit. As a result, an in-band tone of 600 Hz was measured at the decoder output.

Figure 5.15. shows the SIDM system frequency response at different input levels. The slope of 6 dB/octave is due to the integrator characteristics of Figure 4.2.

Figures 5.16., 5.17. and 5.18. show the measured signal-to-quantizing noise ratio for the experimental system. It is observed that the measured curves show a slightly lower value than the theoretical ones (dotted line) specially at the slope overload point.

The phenomena can be explained considering that when the signal level approaches the overload point, the granular noise is supplemented by further noise, due to the onset of the slope overload condition as described in Section 3.3.1.

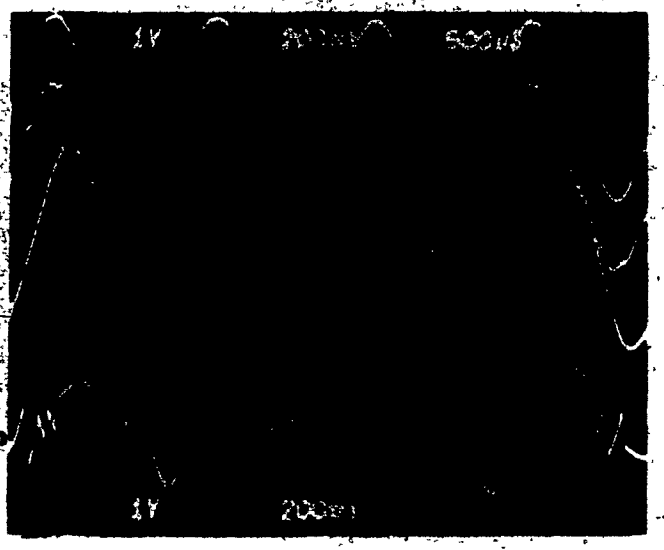

ENCODER INPUT, X(t)
(800 Hz, 0 dBm0)

INTEGRATOR OUTPUT, $\hat{x}(t)$

DECODER OUTPUT, y(t)

390 mVpp

QUANTIZING ERROR, e(t)

FIGURE 5.9. QUANTIZING ERROR (SIDM)
(f_s = 20 kHz)

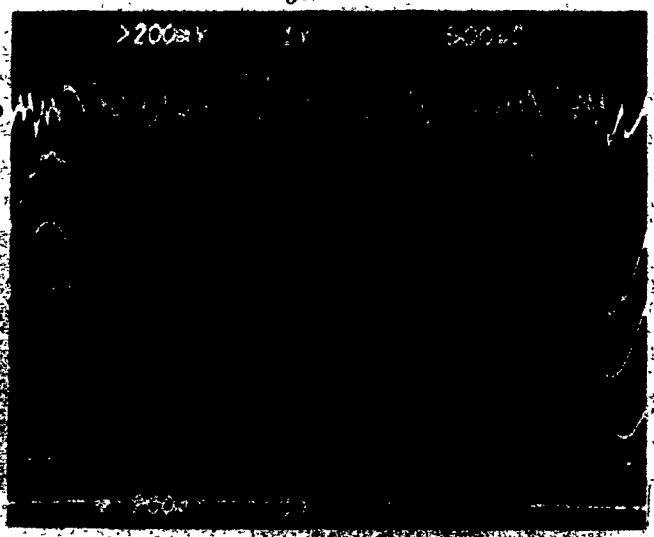

250 mVpp

QUANTIZING ERROR, e(t)

INTEGRATOR OUTPUT, $\hat{x}(t)$

ENCODER INPUT, X(t)
(800 Hz, 0 dBm0)

DECODER OUTPUT, y(t)

OUTPUT CODE, q(t)

FIGURE 5.10. QUANTIZING ERROR (SIDM)
(f_s = 20 kHz)

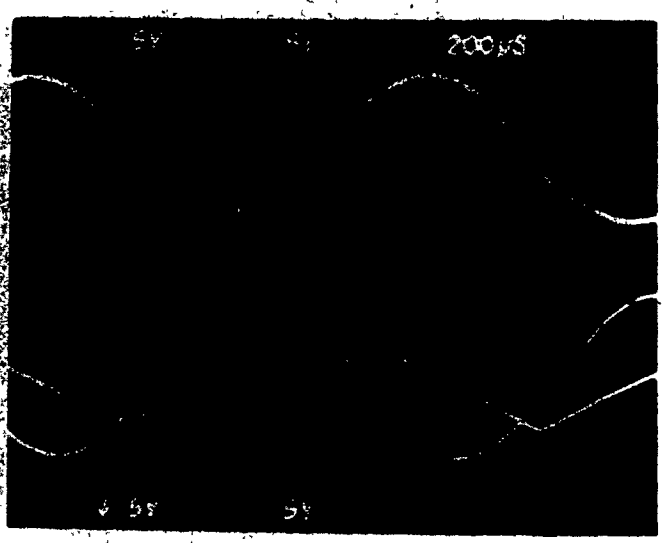

QUANTIZING ERROR, e(t)

INPUT, X(t)
(800 Hz, +10 dBm0)

$\hat{x}(t)$

FIGURE 5.11. QUANTIZING ERROR AT OVERLOAD (SIDM)
(f_s = 20 kHz)

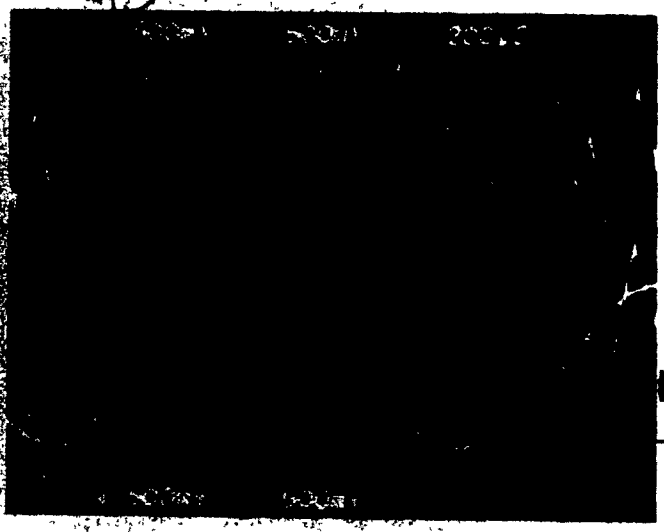

QUANTIZING ERROR, e(t)

INPUT, X(t)
(800 Hz, -10 dBm0)

$\hat{x}(t)$

FIGURE 5.12. QUANTIZING ERROR AT LOW INPUT (SIDM)
(f_s = 20 kHz)

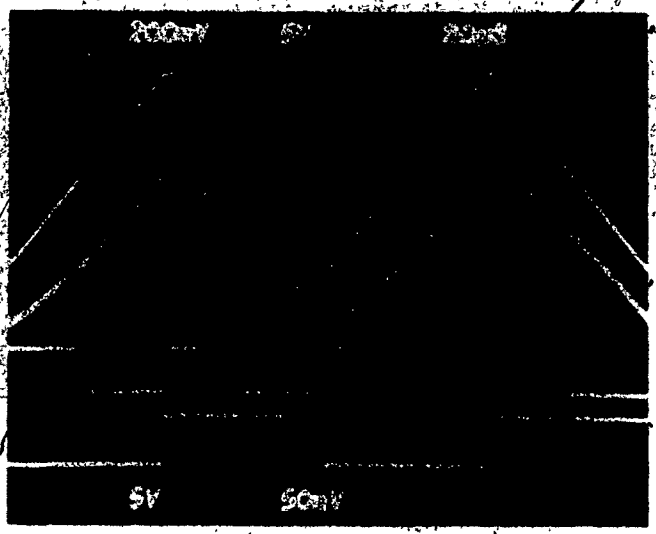

IDLE WAVEFORM FOR SIDM

IDLE WAVEFORM FOR DIDM

SAMPLING FREQUENCY, 20 kHz

IDLE CODE --1010--

FIGURE 5.13. SIDM & DIDM IDLE WAVEFORMS

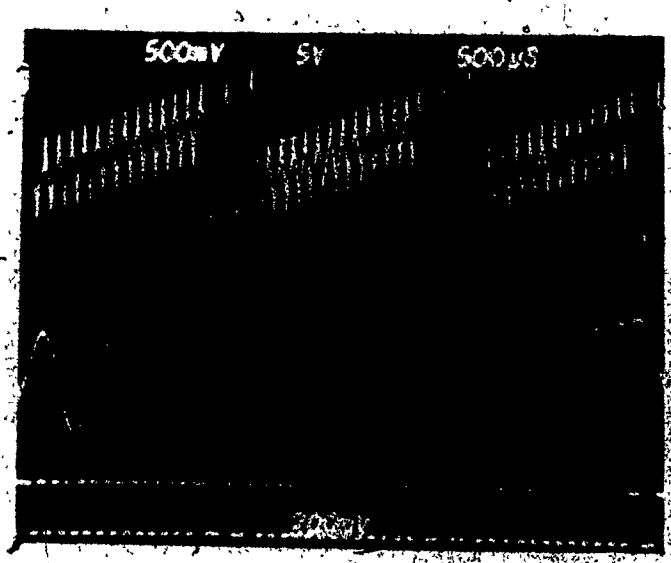

IDLE SIGNAL AT THE INTEGRATOR OUTPUT, $\hat{x}(t)$

IDLE NOISE AT THE DECODER OUTPUT $y(t)$

OUTPUT CODE

FIGURE 5.14. SIDM IDLE NOISE WAVEFORMS

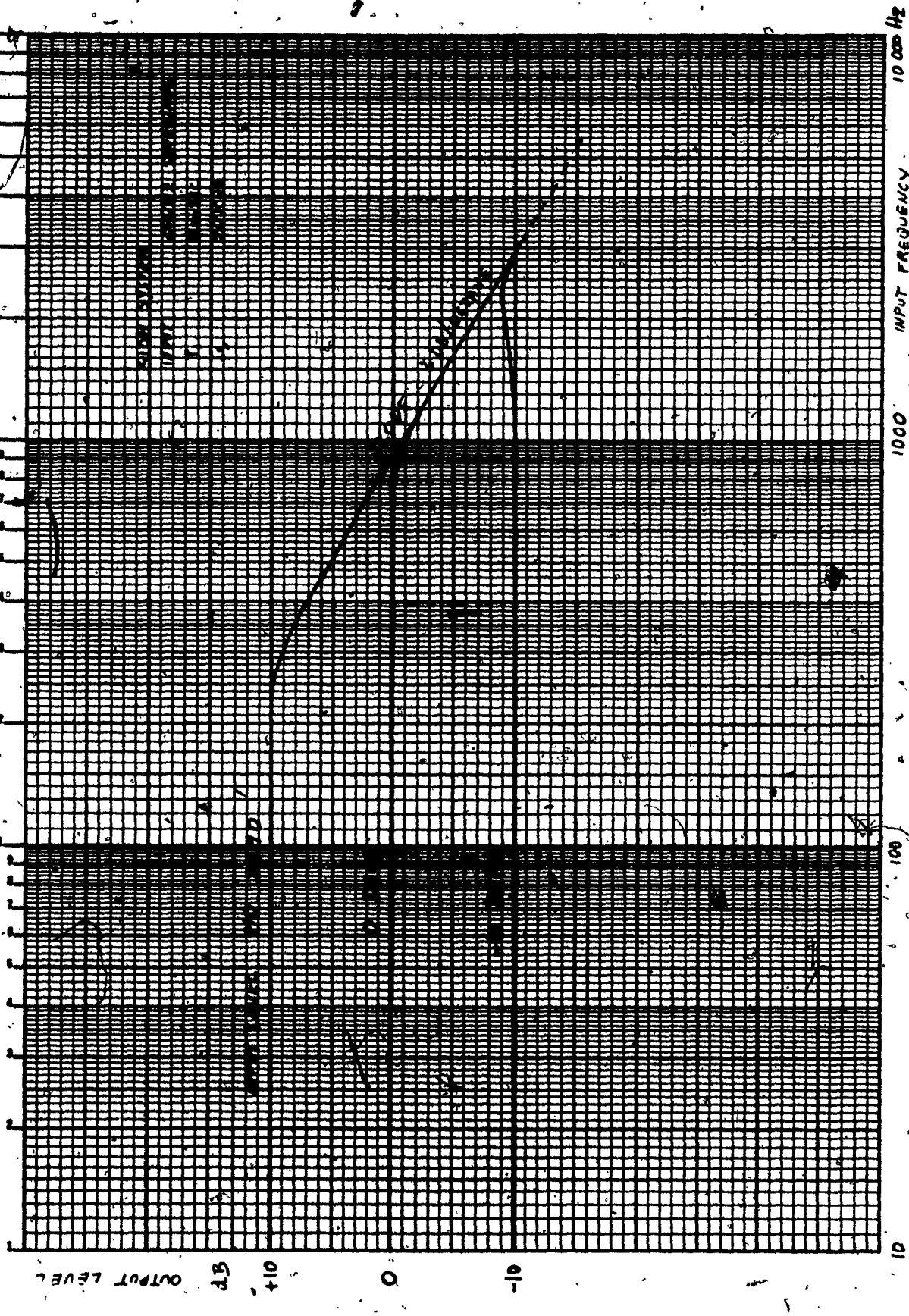

FIGURE 5.15.

EXPERIMENTAL SIDN SYSTEM FREQUENCY RESPONSE

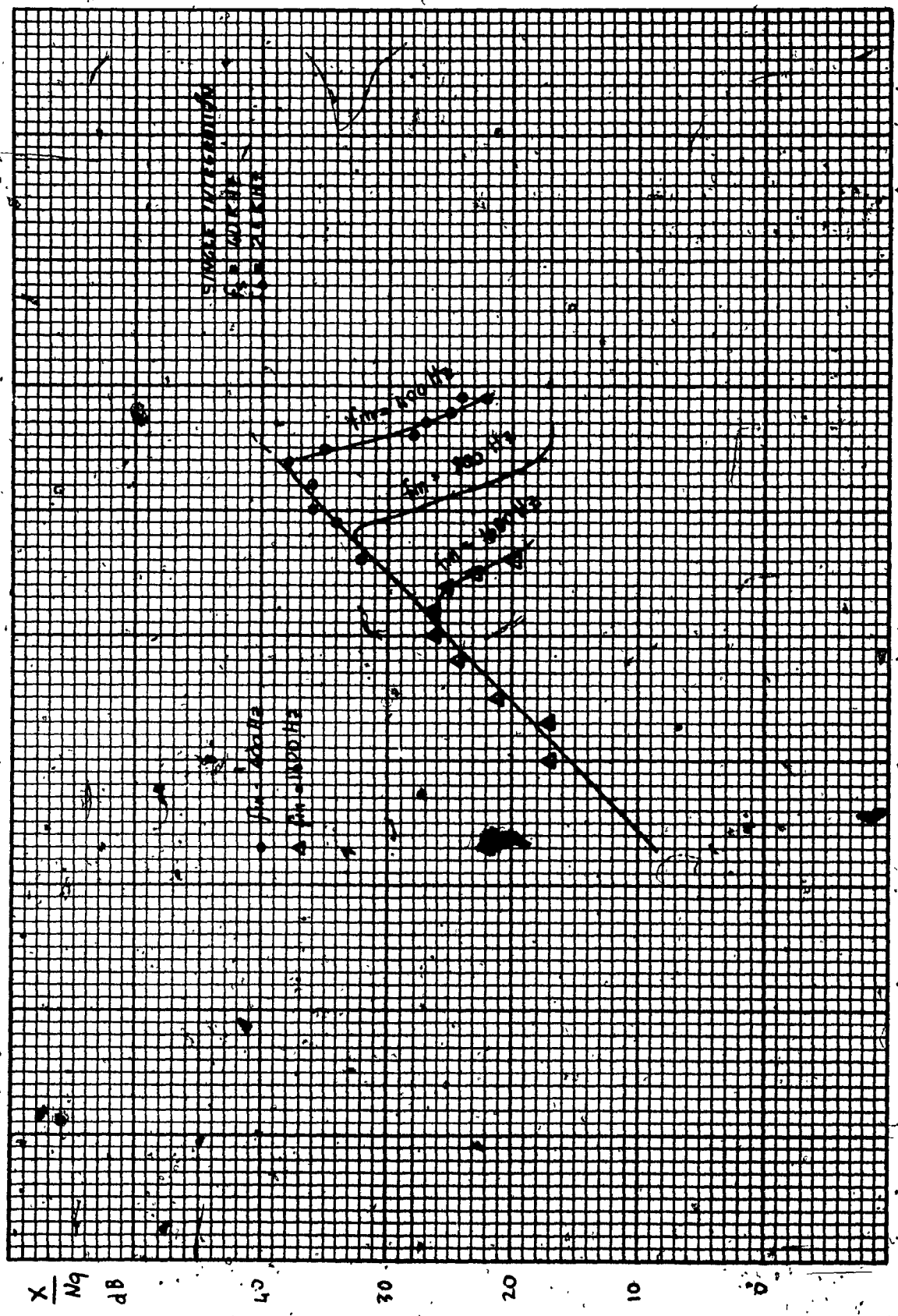

FIGURE 5.16.

SIGNAL-TO-QUANTIZING-NOISE RATIO (SIDM)

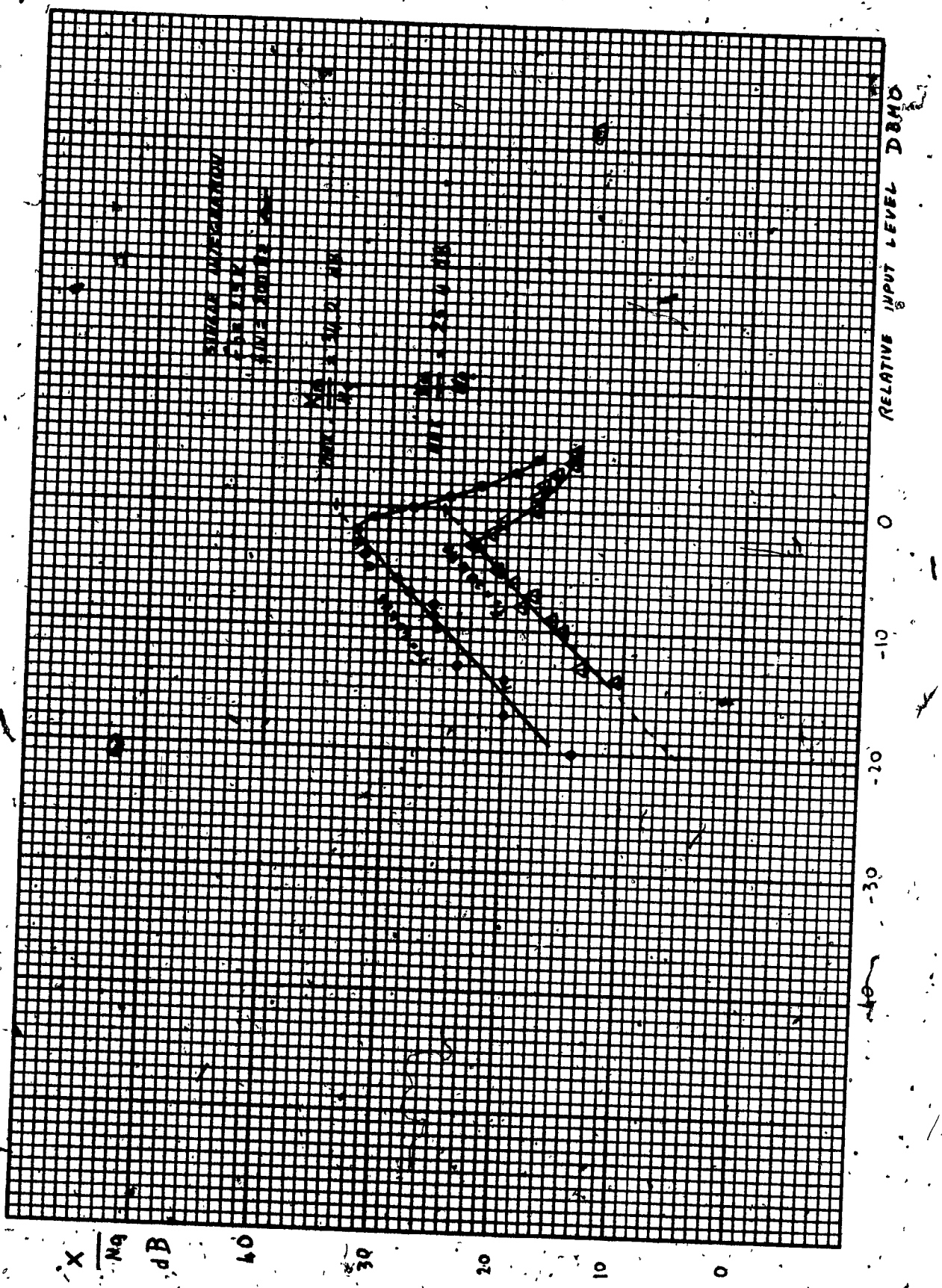

FIGURE 5.18:

SIGNAL-TO-QUANTIZING-NOISE RATIO (SIDN)

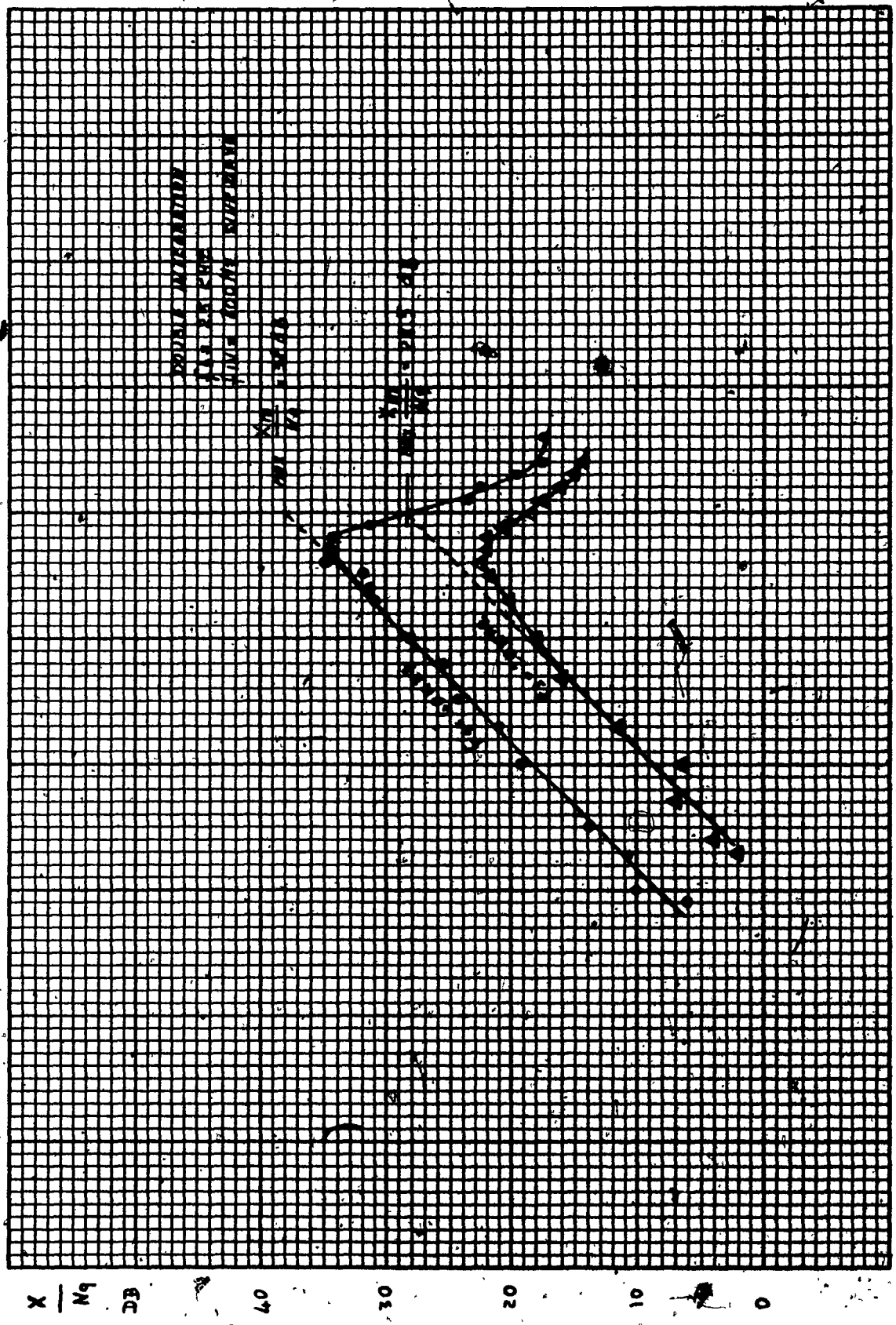

FIGURE 5.18.

SIGNAL-TO-QUANTIZING-NOISE RATIO (DIDM)

Figure 5.19. shows the power spectrum of a SIDM system output code when an 800 Hz sinewave is applied at the input. It can be observed that no dc component is contained in the code spectrum and, hence, this property is useful for cable-transmission in which low frequency cut-off is inevitable.

The absence of a dc component means that the code is well balanced. That is, the occurrence probability is 1's and 0's in the code and is equal to one-half. An 800 Hz component due to the input signal is also observed.

Figure 5.20. shows the power spectrum of $\hat{x}(t)$ when the input signal is an 800 Hz sinewave.

The quantizing noise is random with periodicity f_s and its power spectral distribution has a $\left(\frac{\sin x}{x}\right)^2$ shape with the first null at f_s.

As assumed in Section 3.3.2., the quantizing noise power spectral distribution is almost flat in the audio range (Figure 5.21.).

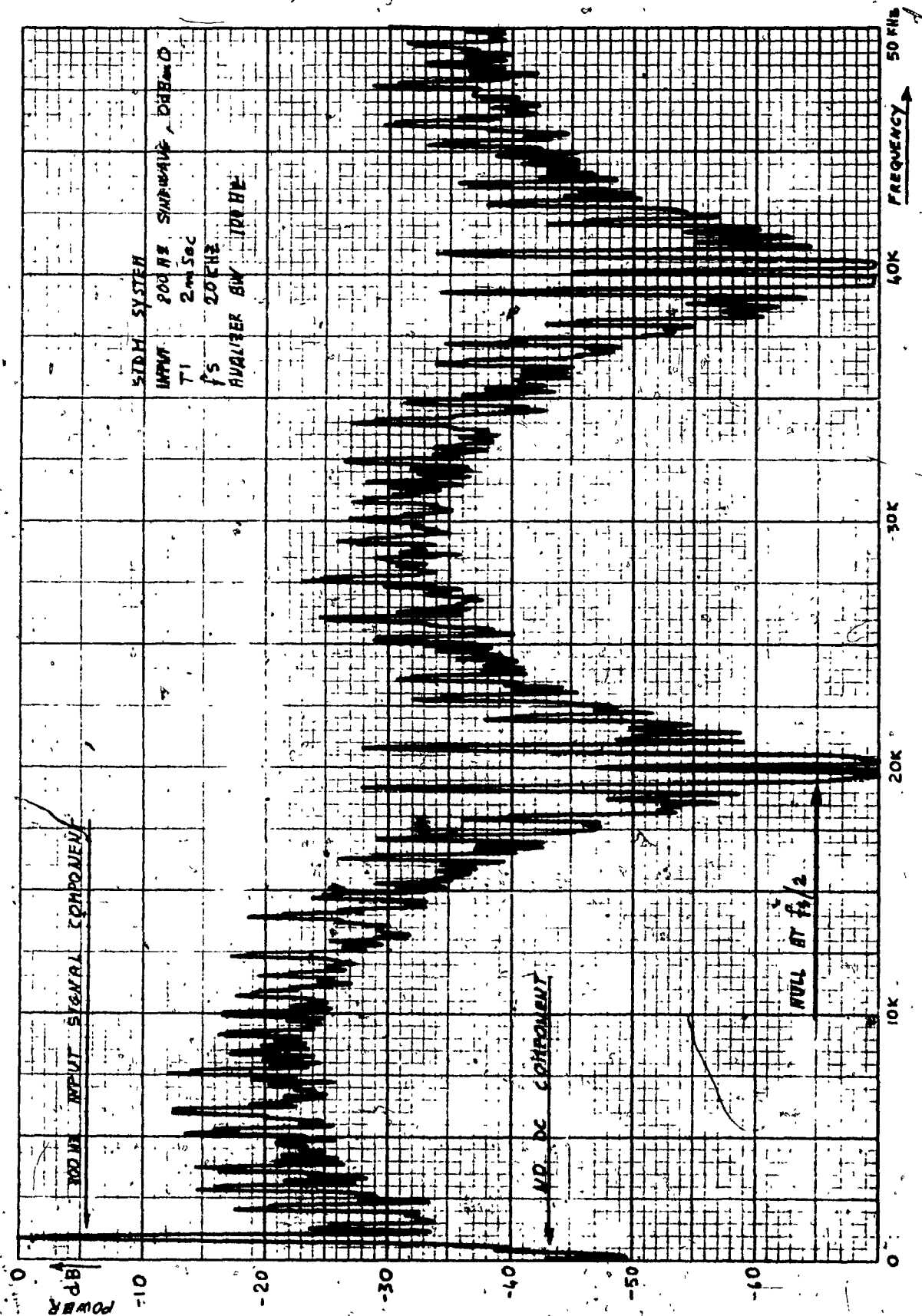

FIGURE 5.19.

OUTPUT CODE POWER FREQUENCY SPECTRUM

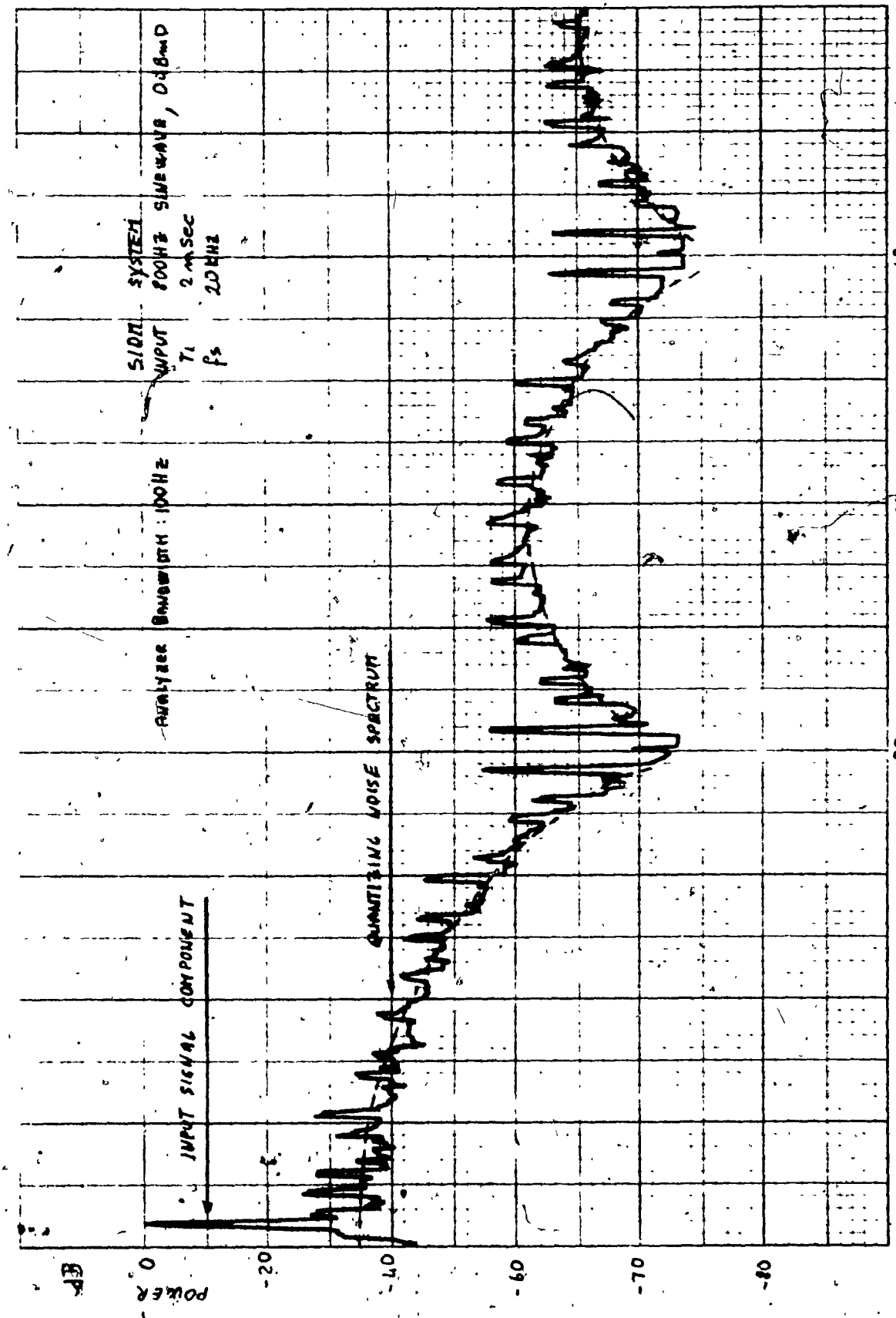

FIGURE 5.20.

x(t) POWER SPECTRUM IN THE AUDIO BAND

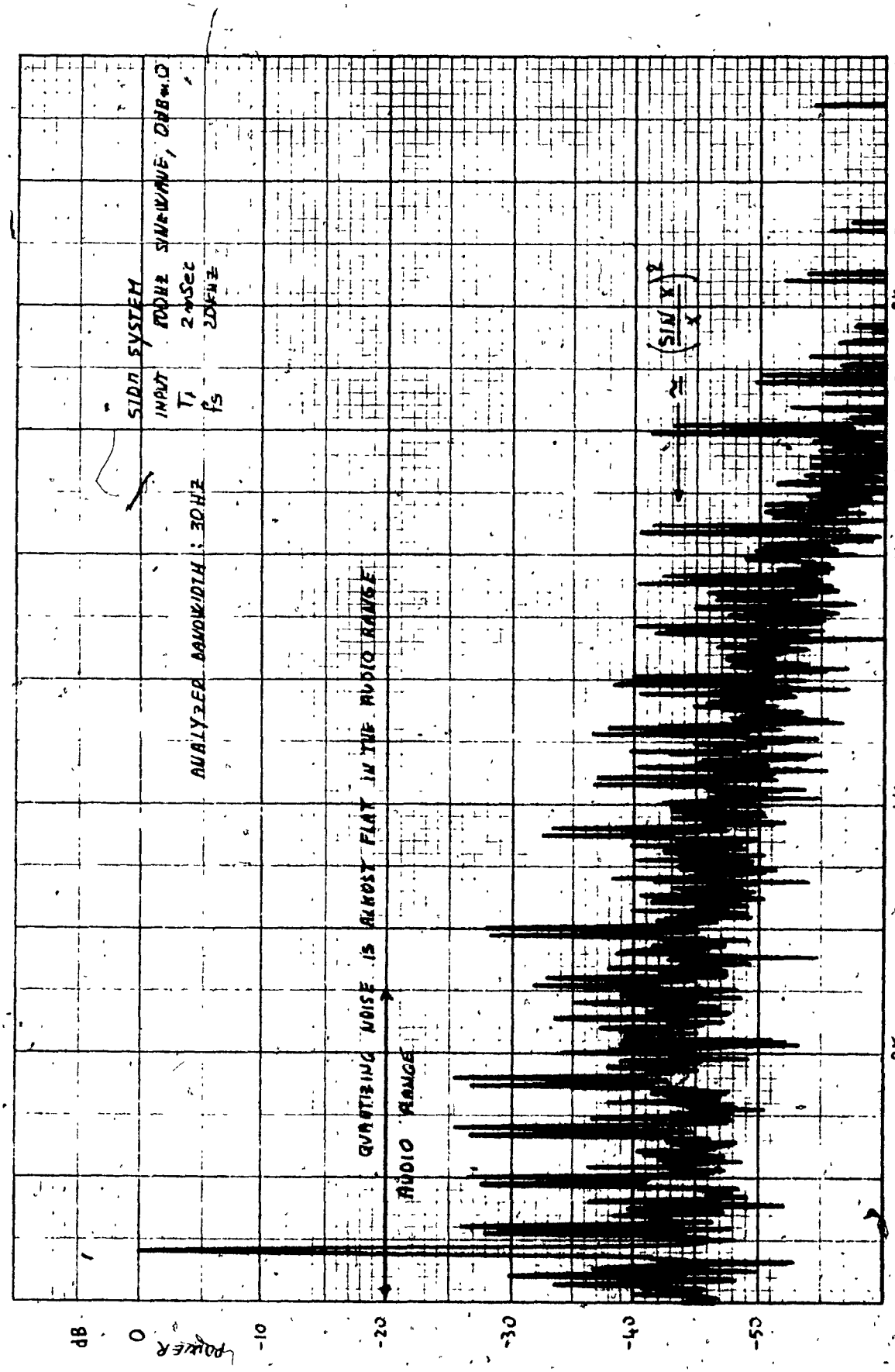

FIGURE 5.21.

$\hat{x}(t)$ OVERALL POWER SPECTRUM

CHAPTER 6

COMPANDED DELTA MODULATION

6.1. Introduction

Simple Delta Modulation can encode faithfully only signals within a small range of amplitudes. Large signal encoding suffers from slope overload distortion and small signal encoding from excessive quantizing noise. This limitation can be overcomed by adapting the quantizer output to avoid system overload distortion.

(Usually adaptation is derived dynamically from certain overload criterion of the encoder output code).

The first companded Delta Modulator was described by M.R. Winkler [4] in 1963. His method consists in doubling the quantizer output whenever two identical consecutive pulses appear at the code output.

The quantizer output is halved after each change of value of the output code.

6.2. High Information Delta Modulation System

Companded Delta Modulators are also called High Information Delta Modulation (HIDM) systems, because they contain more information per pulse. An HIDM system block diagram is shown in Figure 6.1.

The circuit is essentially identical to the one of a simple Delta Modulator with the exception that an auxiliary feedback

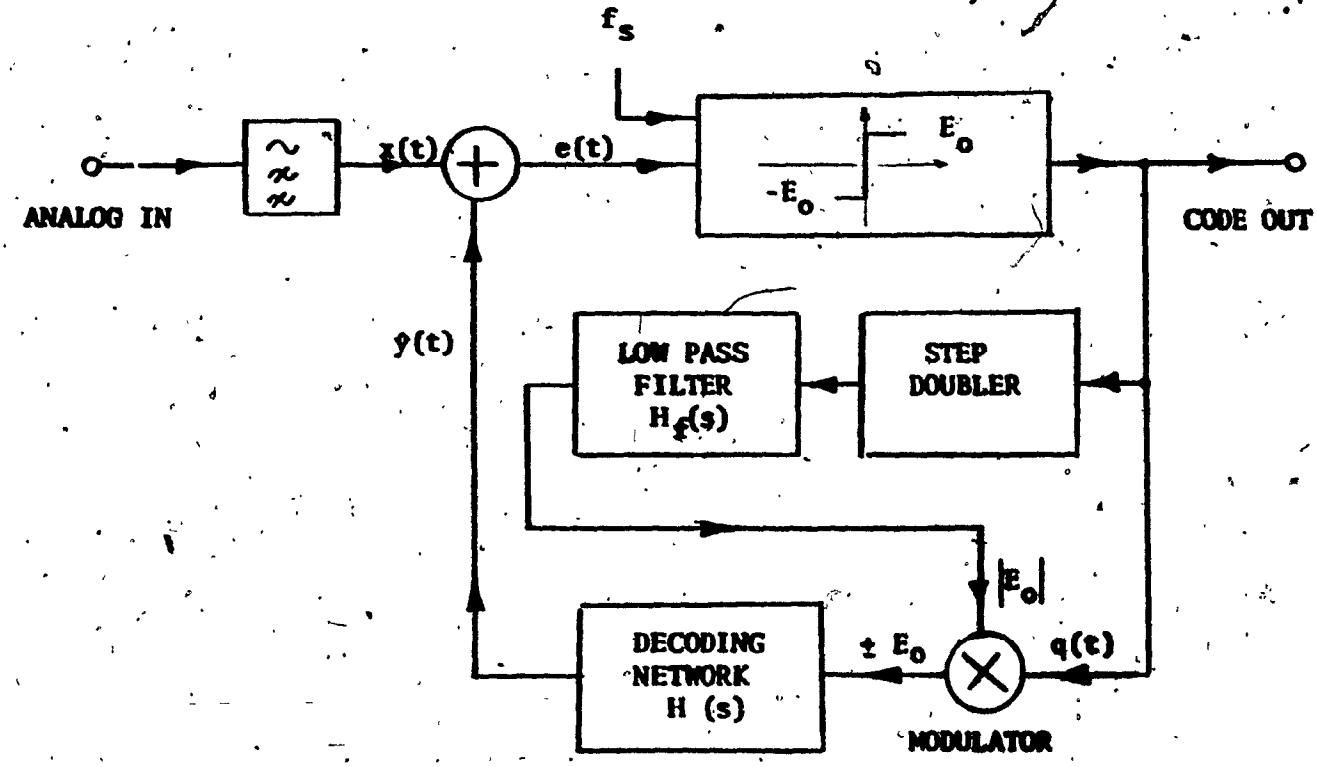

HIDM ENCODER

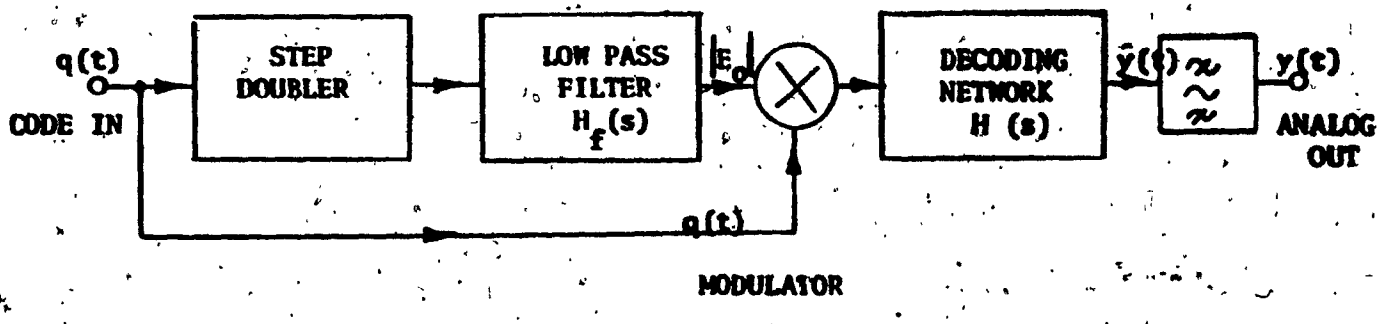

HIDM DECODER

FIGURE 6.1.

HIDM SYSTEM BLOCK DIAGRAM

loop provides a continuous adaptation of the quantizer output according to the rule shown in Table 6.1.

The algorithm of Table 6.1. takes advantage of the fact that a Delta Modulator tending to be overloaded produces a code of consecutive equal digits, while when the input signal is too small to be encoded, a code rich in idle sequences (1010) is generated. As a consequence, when the system tends to overload, the quantizer output is increased and the slope of the step size $\hat{x}(t)$ is doubled to better approximate the input signal slope. To the contrary when the output code has 01 or 10 transitions, indicating that the input signal is too small to be encoded, the quantizer output is halved and the slope of $\hat{x}(t)$ is also halved to closely match the input signal.

From Figure 6.1., we noticed that the step doubler is followed by a low pass filter which is an integrator with a cut-off frequency of 15 Hz.

Effectively this network produces an average slow varying $\pm E_0$ output to the decoding network H(s).

Therefore, the companded Delta Modulation system behaviour can be calculated from the equation of a SIDM system as described in Section 3.

6.3. The Experimental HIDM

An experimental HIDM was developed and tested. The

CURRENT DIGIT	PREVIOUS DIGIT	QUANTIZER OUTPUT
0	0	DOUBLE
0	1	HALF
1	0	HALF
1	1	DOUBLE

TABLE 6.1.

HIDM ALGORITHM

block diagram is shown in Figures 6.2. and 6.3. The transfer function of the local decoder is shown in Figure 6.4.

6.4. HIDM Experimental Results

Figure 6.5. shows the signal to quantization noise of the experimental HIDM . The signal-to-noise ratio is held almost constant over a range of more than 40 dB by the encoder companding law.

Figure 6.6. displays the system input-output characteristics at different input levels. The bandwidth at system reference level is approximately 2.5 kHz. As shown in Figure 6.6., the input signal level of -50 dBm0 are still encoded and decoded with excellent tracking.

Figure 6.7. shows how the quantizer output "adapts" to different input levels and frequencies.

The almost linear relationship between input level and quantizer output level, keeps the HIDM system always near to the overload point providing the maximum signal-to-noise ratio.

Figure 6.8. shows the compression characteristics of the modem. The input signal component presented in the output code, is held constant over the range of the companding network which is 48.2 dB.

Figure 6.9. shows the performance of a HIDM system with instantaneous companding. ($H_2(s)$ low pass network removed). The system

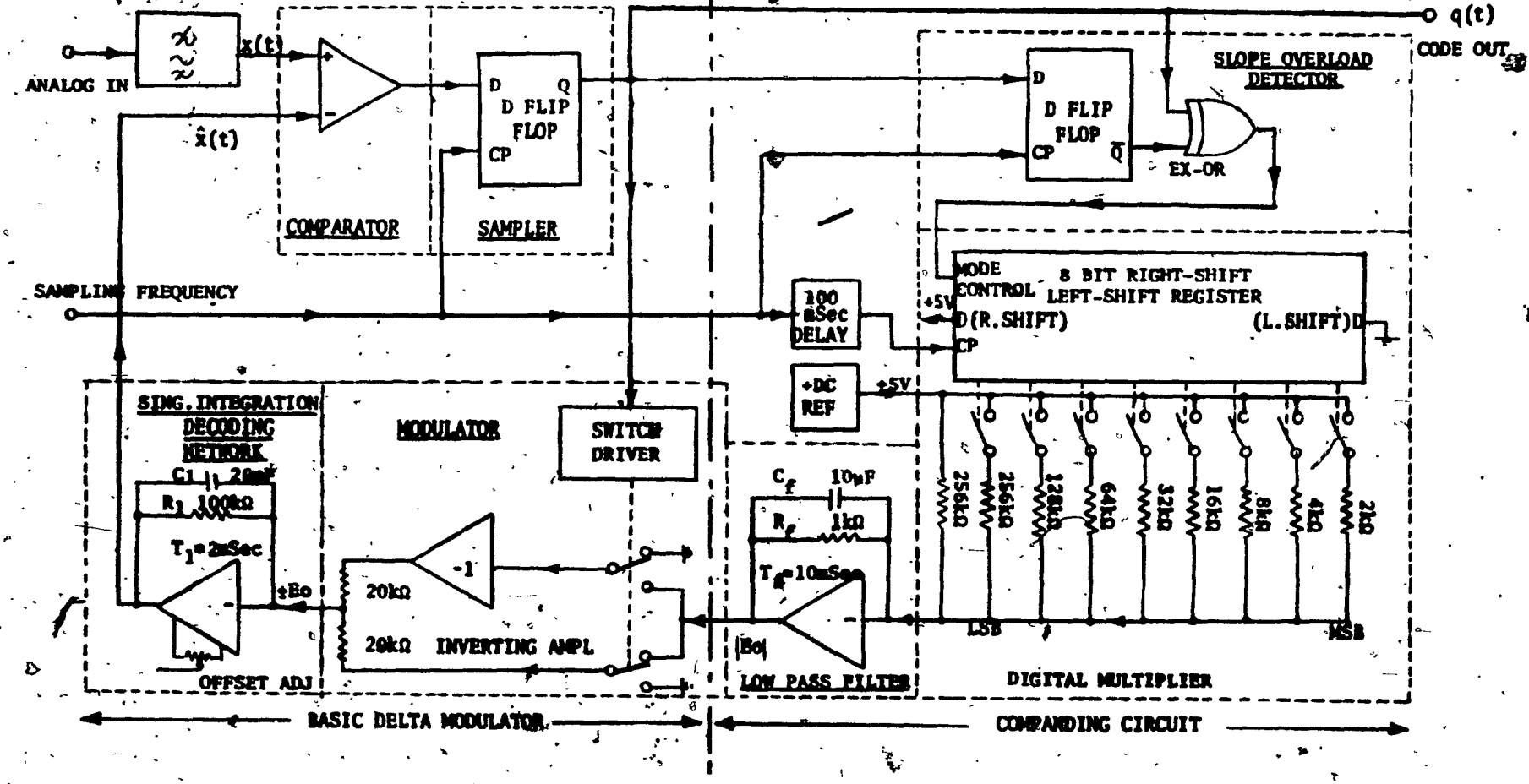

FIGURE 6.2. HIGH ENCODER BLOCK DIAGRAM.

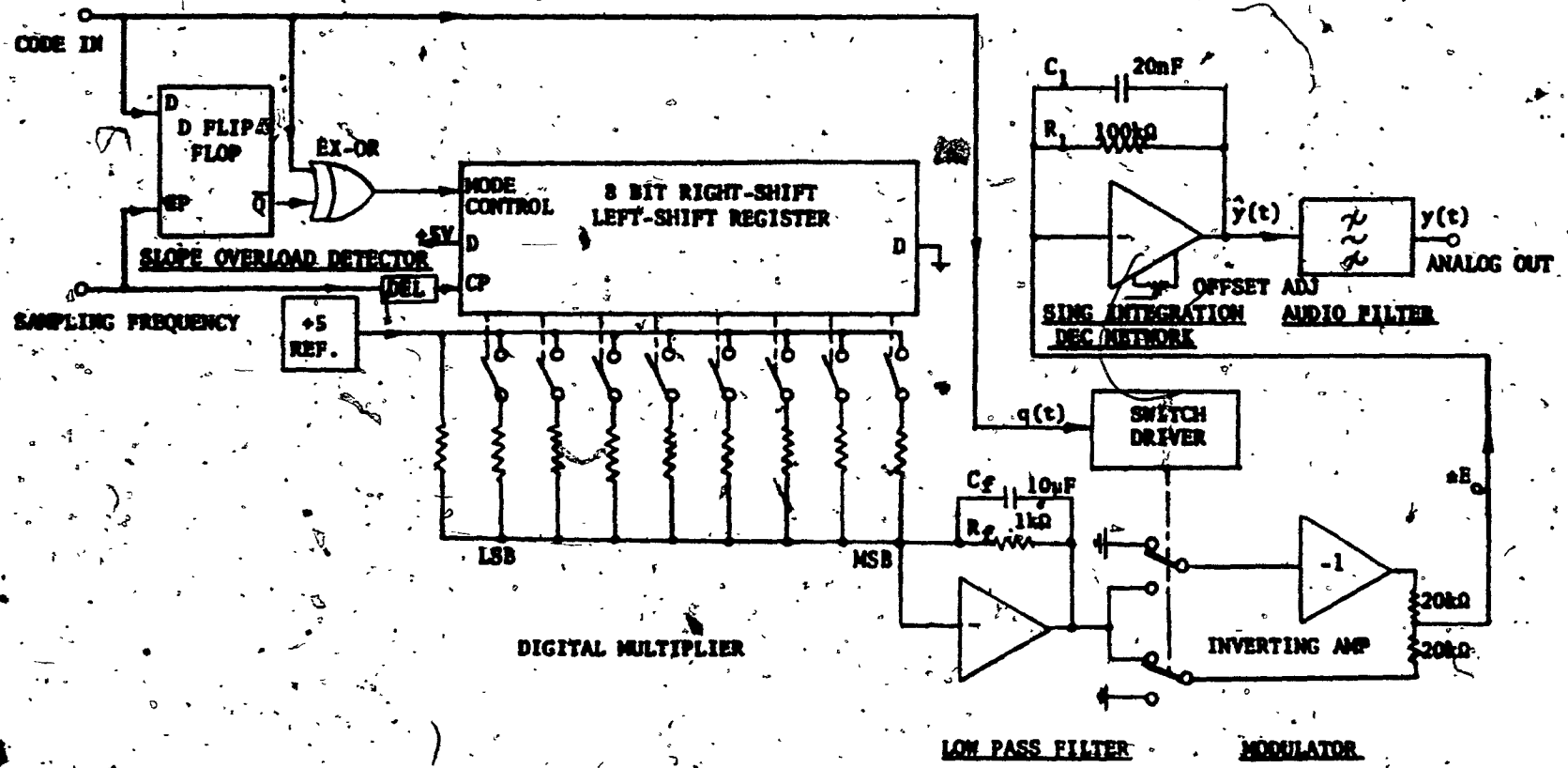

FIGURE 6.3 HIGH ORDER BLOCK DIAGRAM

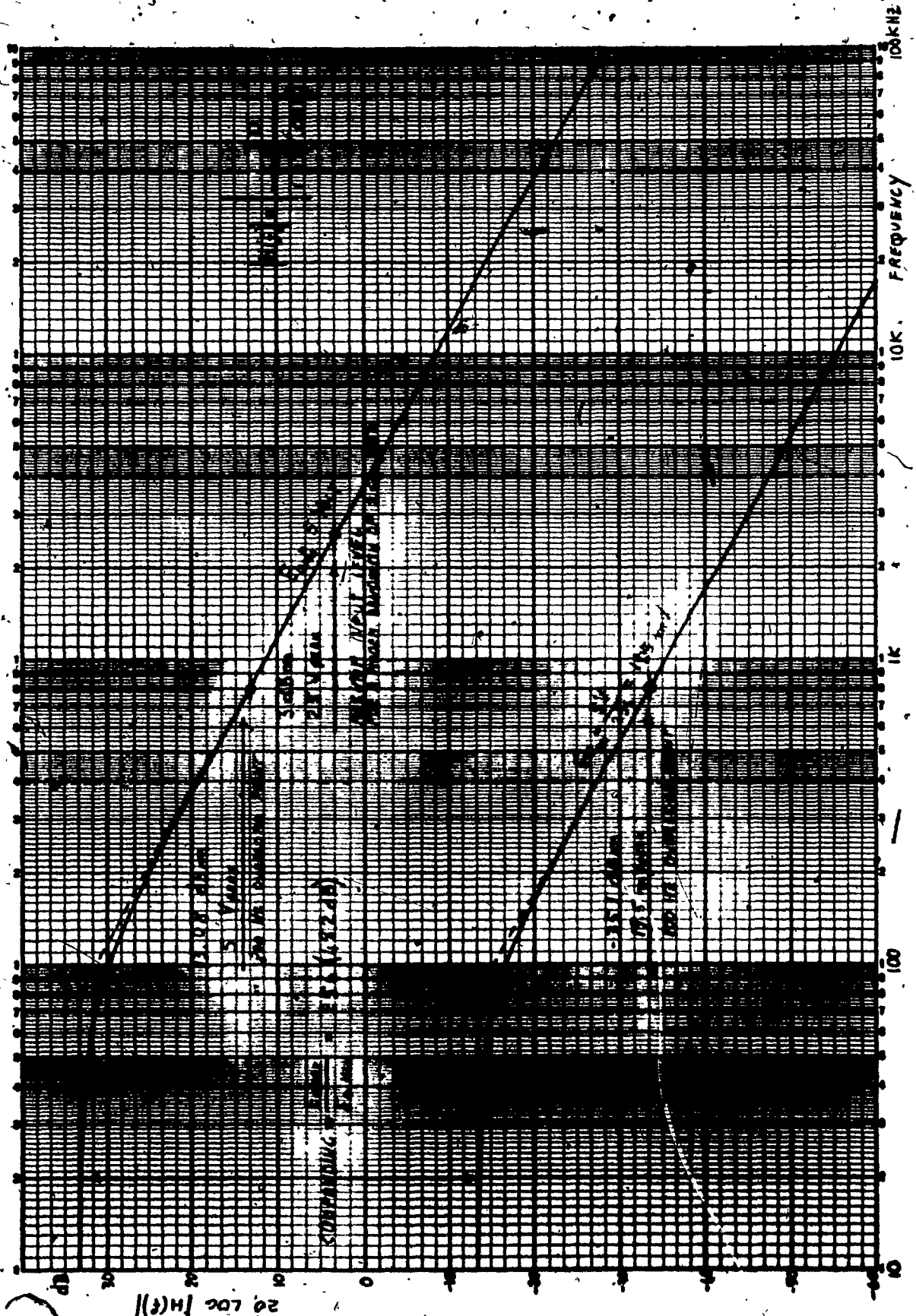

FIGURE 6.4.

FREQUENCY RESPONSE OF THE LOCAL DECODING NETWORK

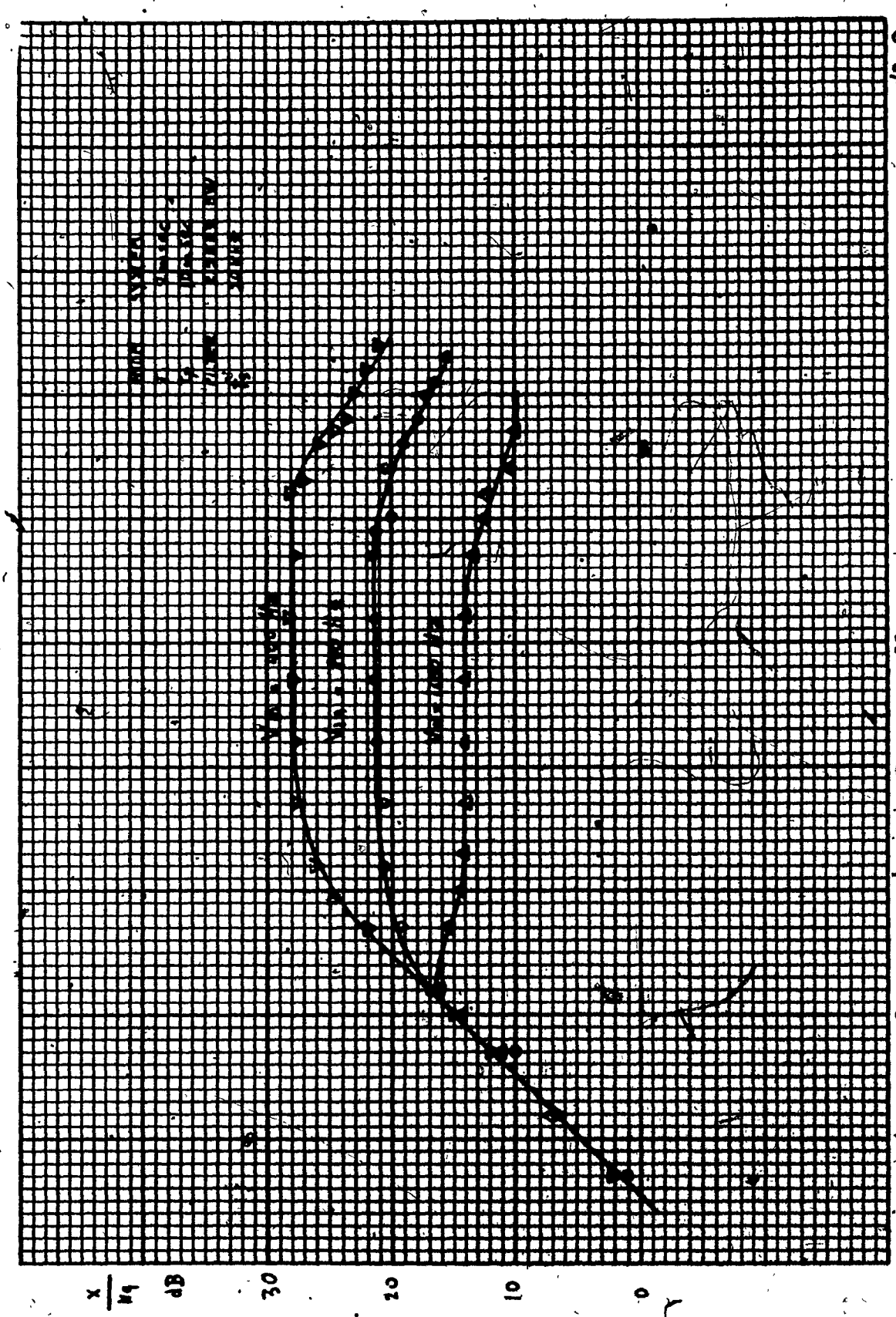

FIGURE 6.5.

SIGNAL-TO-QUANTIZING-NOISE RATIO

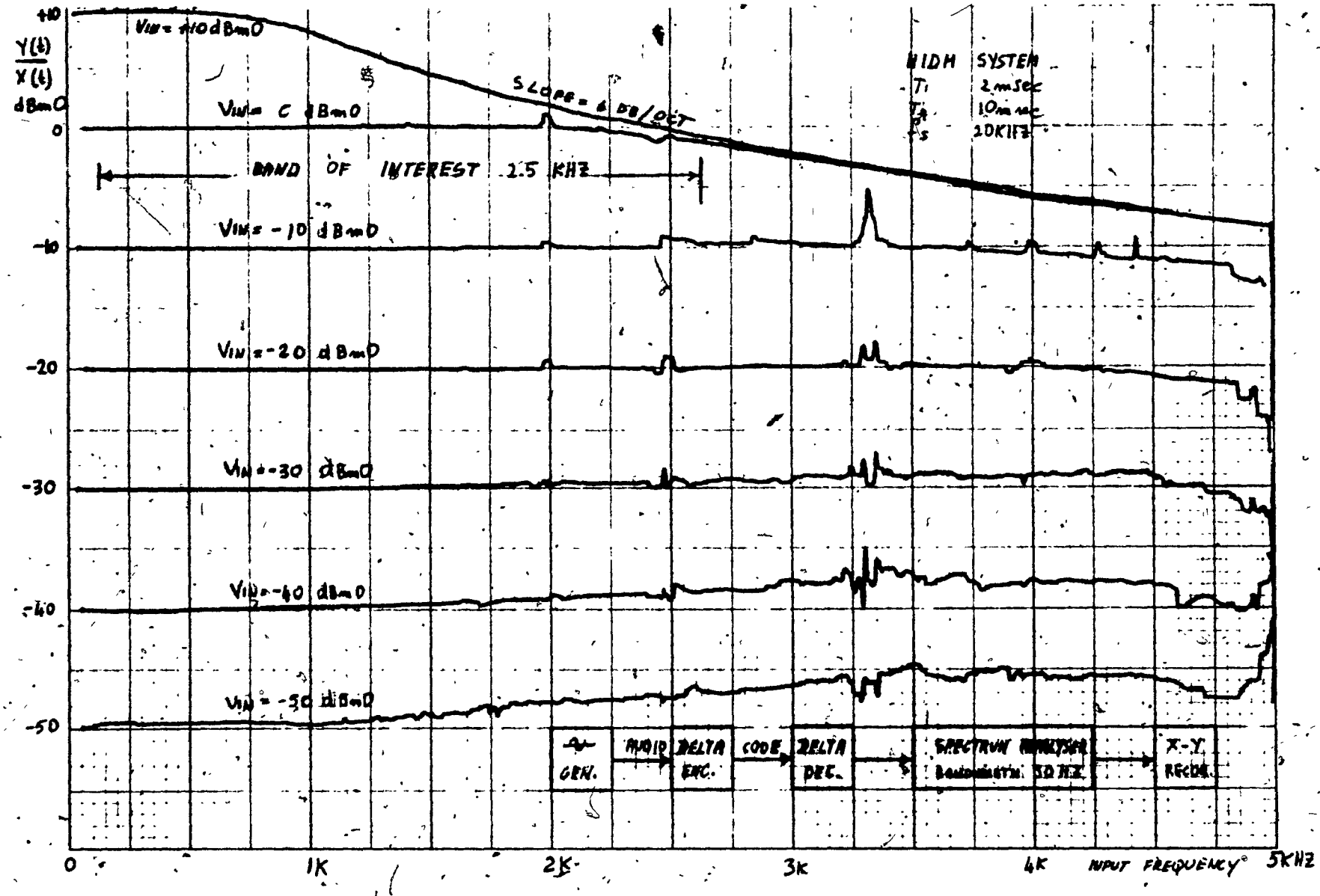

FIGURE 6.6

OVERALL TRANSMISSION CHARACTERISTICS

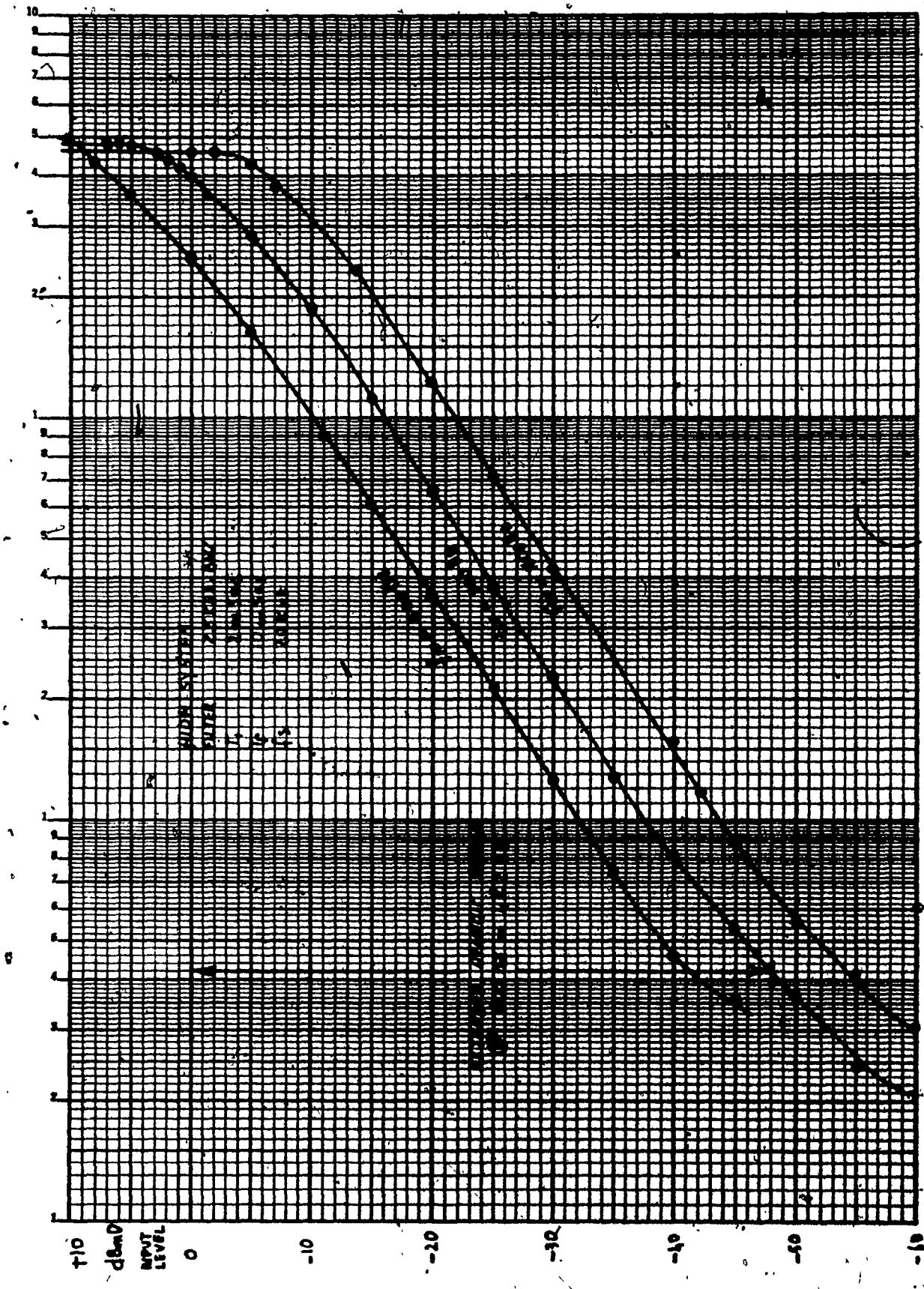

FIGURE 6.7.

INPUT SIGNAL-QUANTIZER OUTPUT CHARACTERISTIC

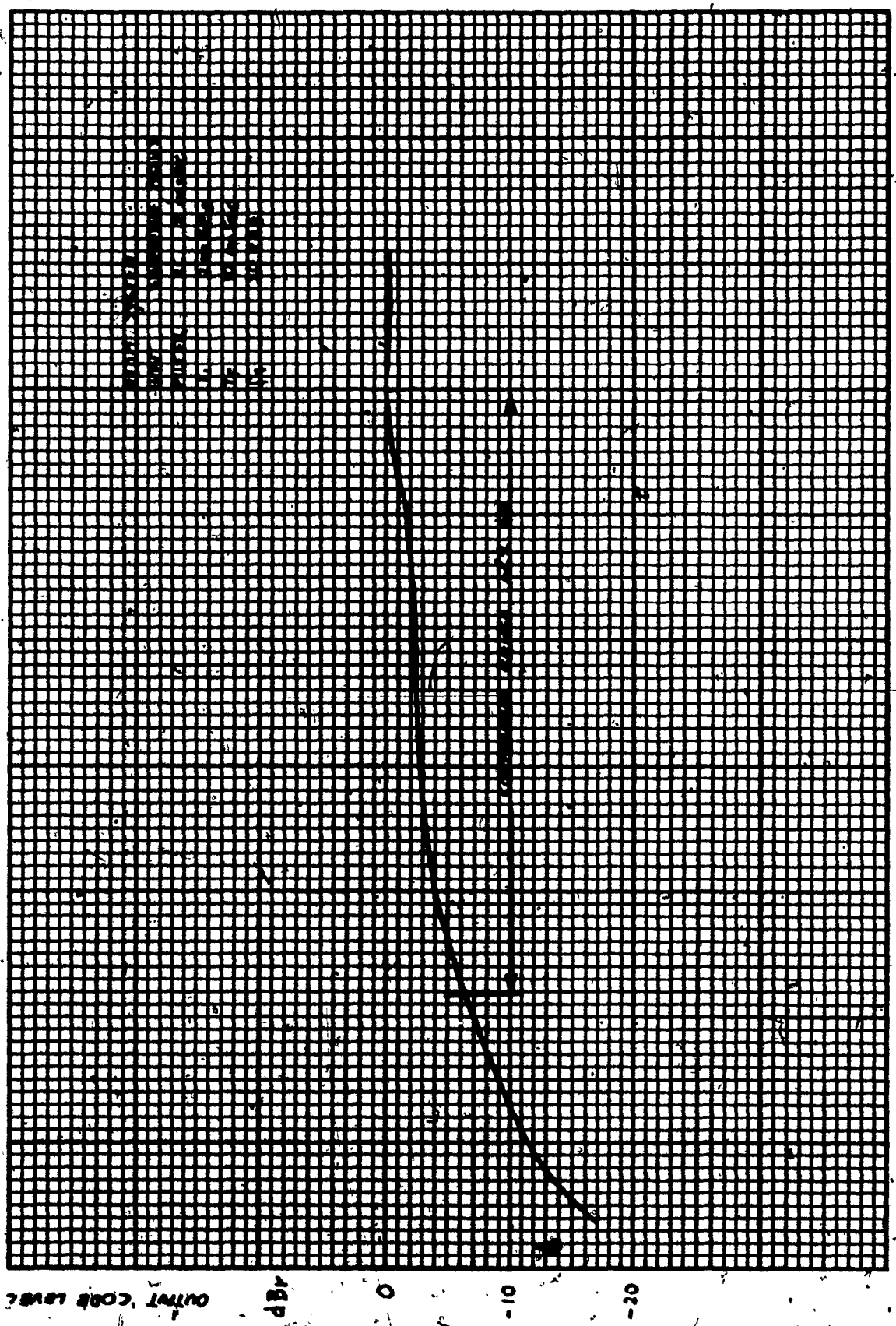

FIGURE 6.8.

ENCODER COMPRESSION CHARACTERISTICS

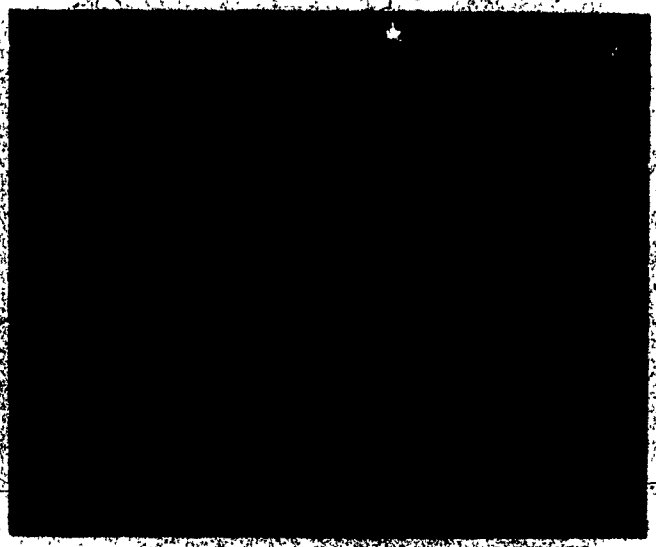

INPUT, $X(t)$

$\hat{x}(t)$

OUTPUT CODE, $q(t)$

QUANTIZING ERROR, $e(t)$.

FIGURE 6.9.

HIDN WITH INSTANTANEOUS COMPANDING

has a faster response to the input signal but the quantizing error is increased.

Figure 6.10. shows the performance of a HIDM with syllabicus companding [$H_2(s)$ low pass filter has a time constant T_2 = 10 msec]. The quantizing error is reduced and a better signal-to-quantizing-noise ratio is achieved.

Figure 6.11. shows the system response to a speech signal (the 'e' of bed).

Figures 6.12. and 6.13. show the system performance throughout the all dynamic range. It can be noticed that the step size always adapts itself to the different input amplitude.

Figure 6.12. top waveform shows the system at gross overload, whereas Figure 6.13. bottom waveform shows the system when idling.

Figures 6.14., 6.15. and 6.16. show the power spectrum of the output code of the HIDM system. This is essentially the same as the simple Delta system of Section 5.

Figures 6.17. to 6.23. show the power spectrum of the decoding network output $\hat{x}(t)$ for different input levels and frequencies. The spectrum shape does not change appreciably because the companding circuit tends to keep the system always near the overload point.

INPUT, X(t)

$\hat{x}(t)$

OUTPUT CODE, q(t)

QUANTIZING ERROR, e(t)

F I G U R E 6.10.

HIDM SYSTEM WITH SYLLABIC COMPANDING

(T_s = 10 msec)

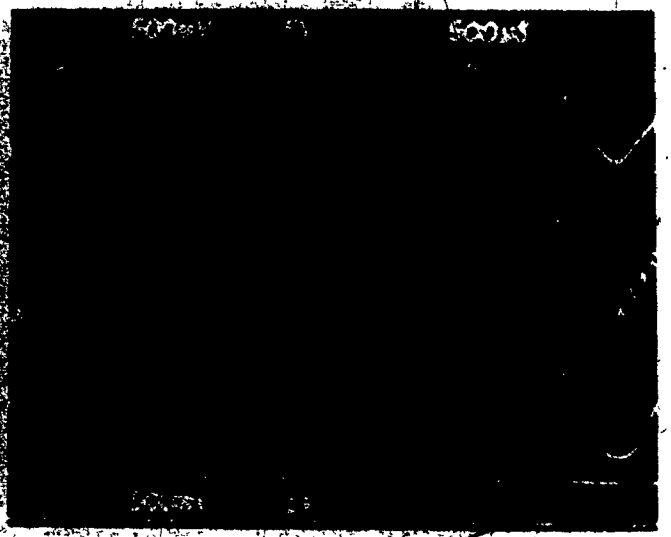

INPUT SIGNAL, X(t)

INTEGRATOR OUTPUT, $\hat{x}(t)$

DECODER OUTPUT, y(t)

CODE OUTPUT, q(t)

F I G U R E 6.11.

HIDM RESPONSE TO SPEECH SIGNALS

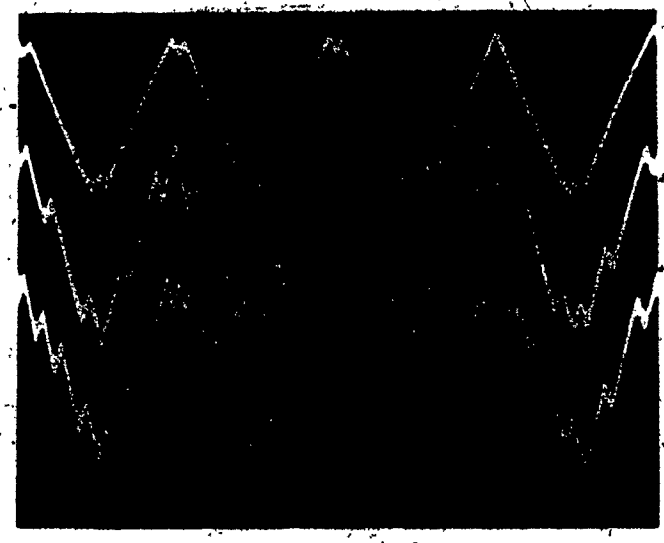

FIGURE 6.12.

SYSTEM DYNAMIC RANGE CAPABILITY

FIGURE 6.13.

SYSTEM DYNAMIC RANGE CAPABILITY

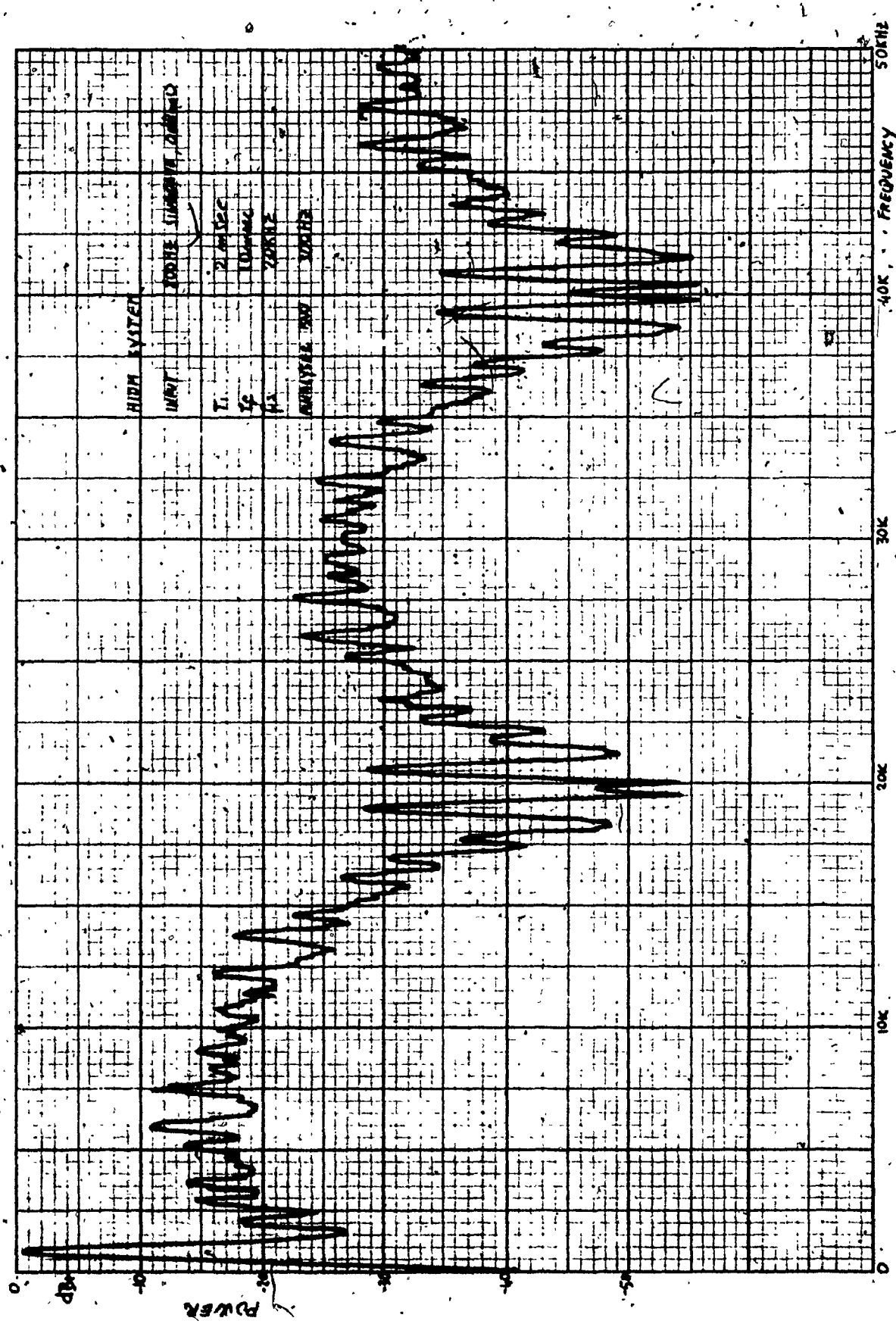

FIGURE 6.14.

OUTPUT CODE POWER FREQUENCY SPECTRUM (INPUT SIGNAL SINEWAVE 800 Hz, 0 dBmO)

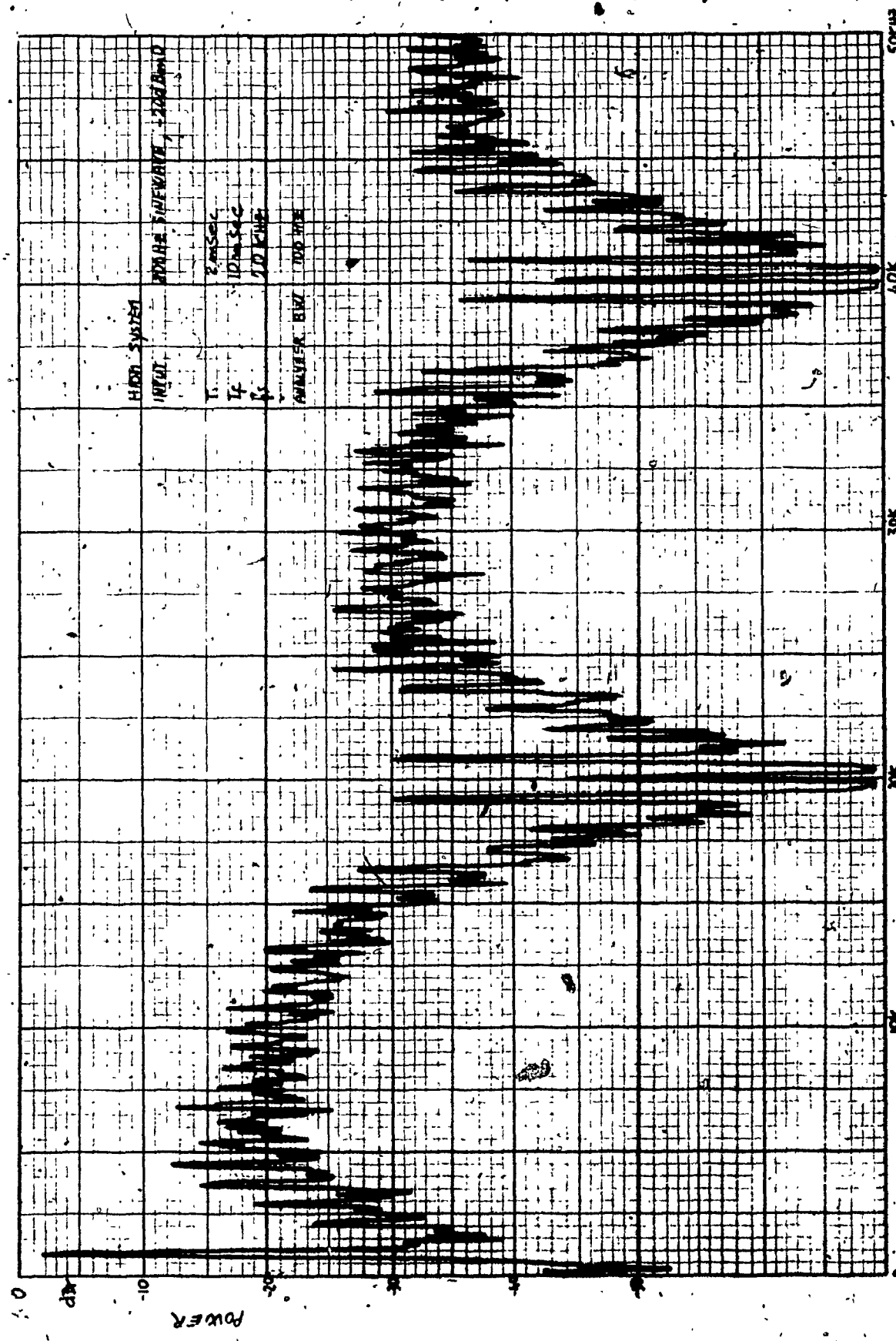

FIGURE 6.15.

OUTPUT CODE POWER FREQUENCY SPECTRUM (INPUT SIGNAL SINEWAVE 800 Hz, -20 dBm0)

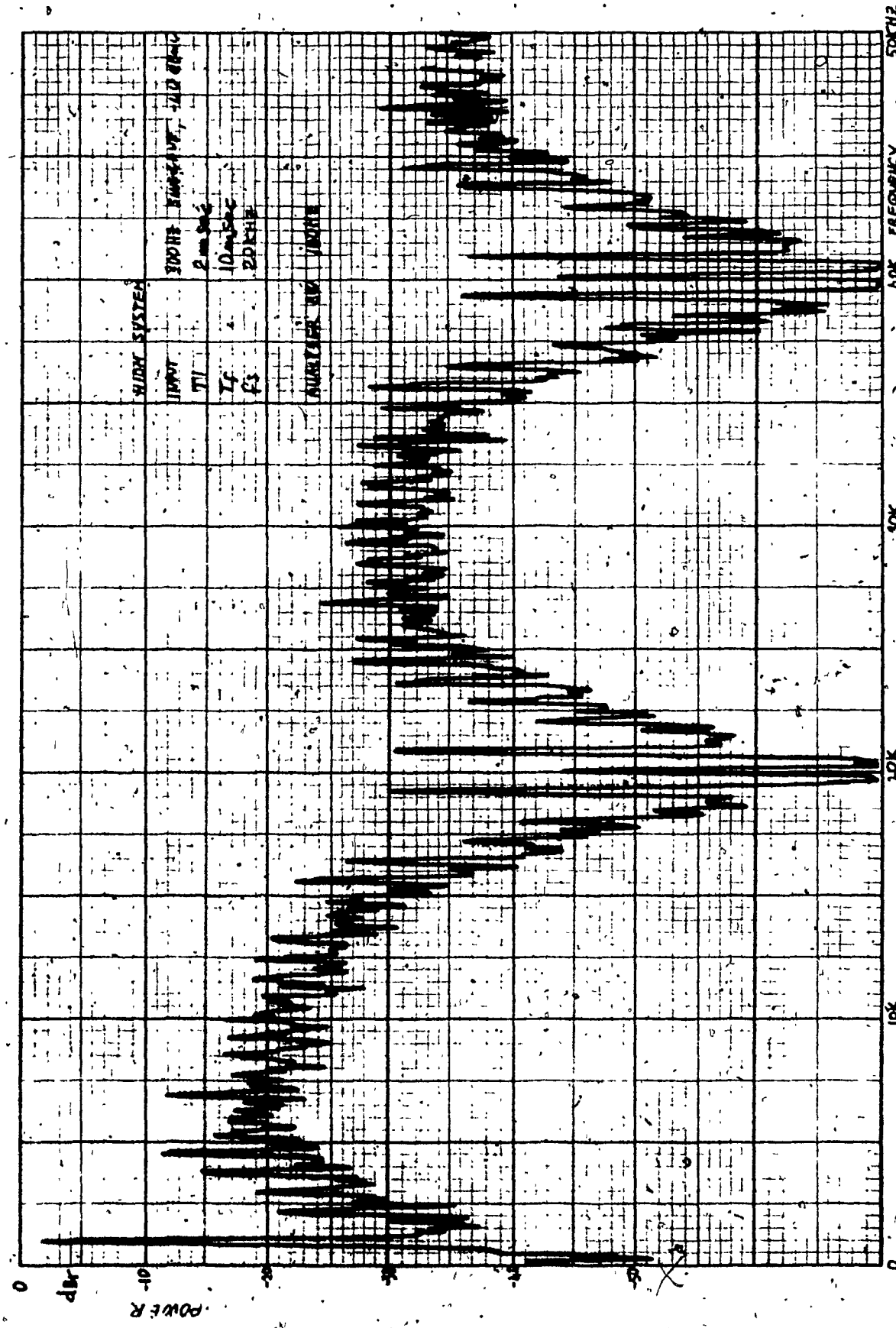

FIGURE 6.16.

OUTPUT CODE POWER FREQUENCY SPECTRUM (INPUT SIGNAL SINEWAVE 800 Hz, -40 dBmO)

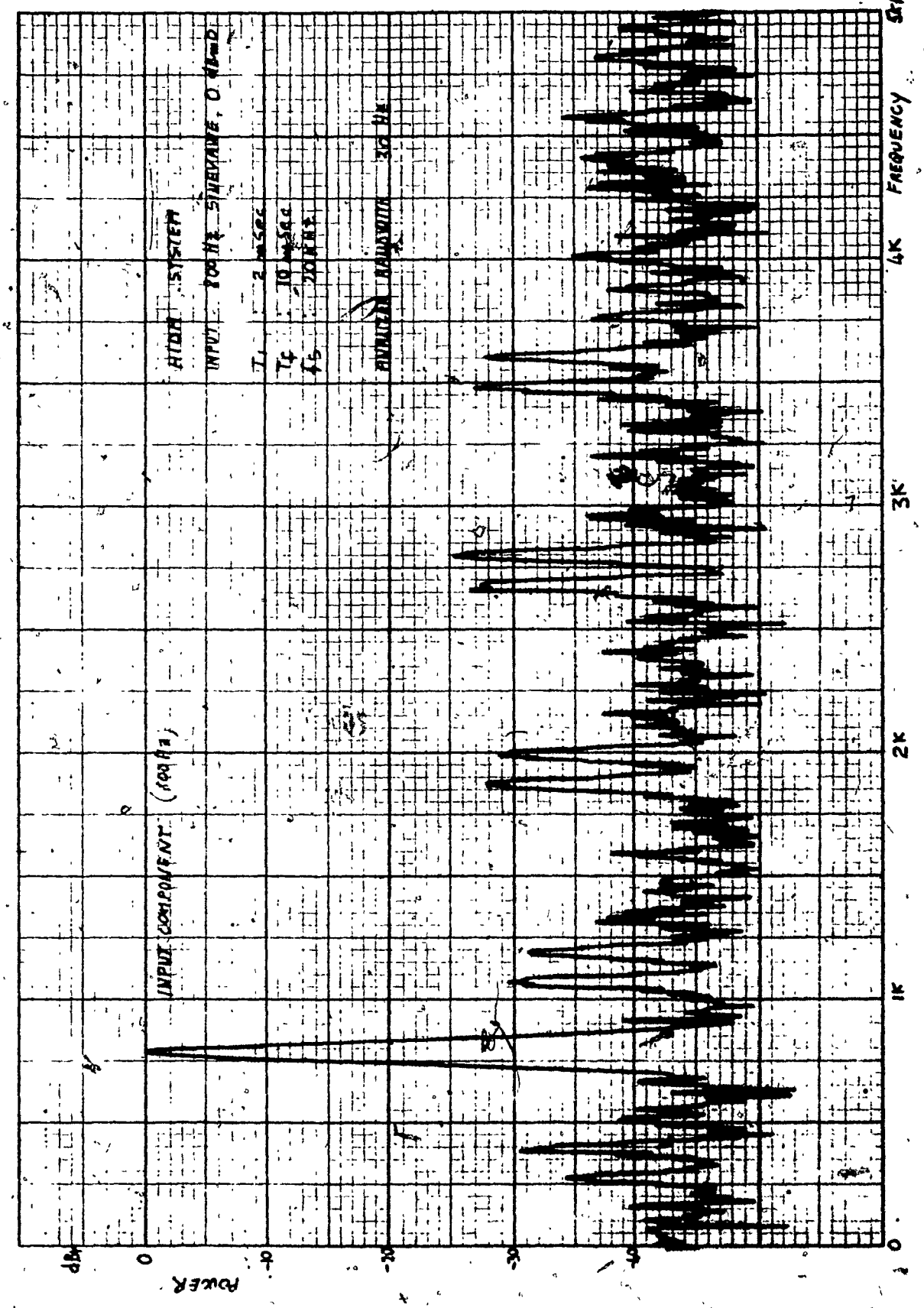

FIGURE 6.17.

INTEGRATOR OUTPUT [x(t)] POWER SPECTRUM (INPUT SIGNAL SINEWAVE 900 Hz, 0 dBmO)

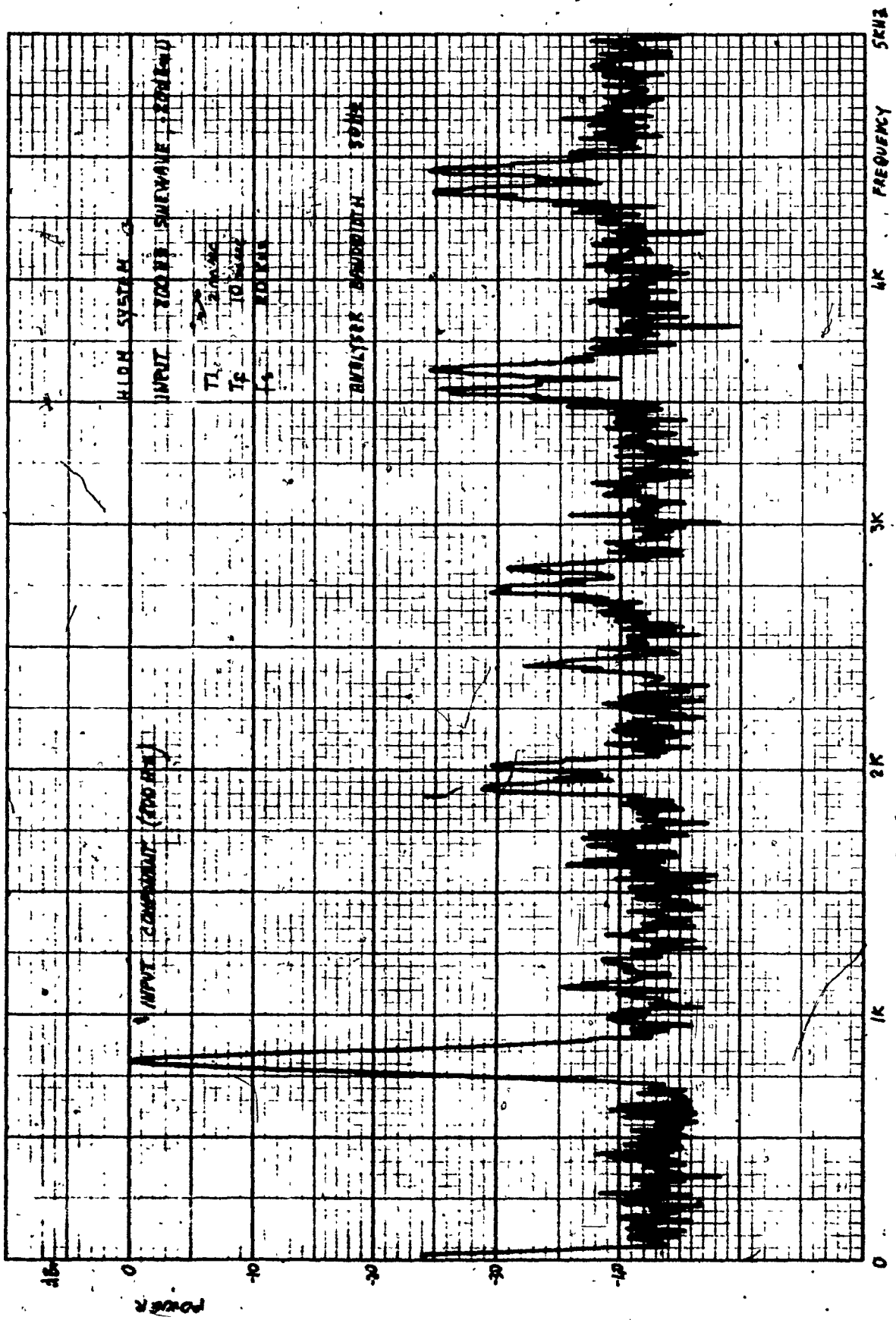

F I G U R E 6.18.

Ŝ(ε) POWER SPECTRUM (INPUT SIGNAL SINEWAVE 800 Hz, -20 dBm0)

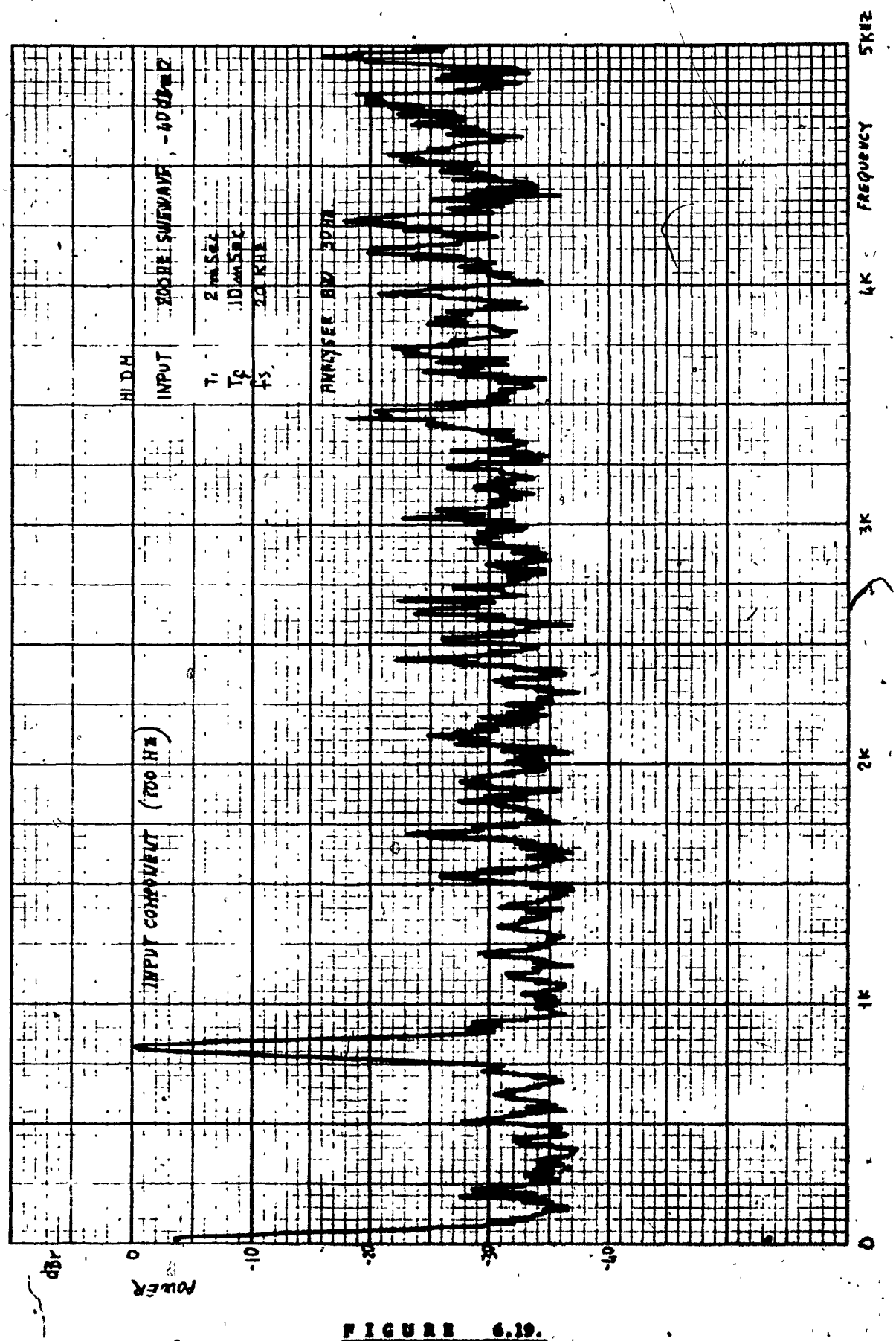

FIGURE 6.19.

x̂(t) POWER SPECTRUM (INPUT SIGNAL SINEWAVE 800 Hz, -40 dBmΩ)

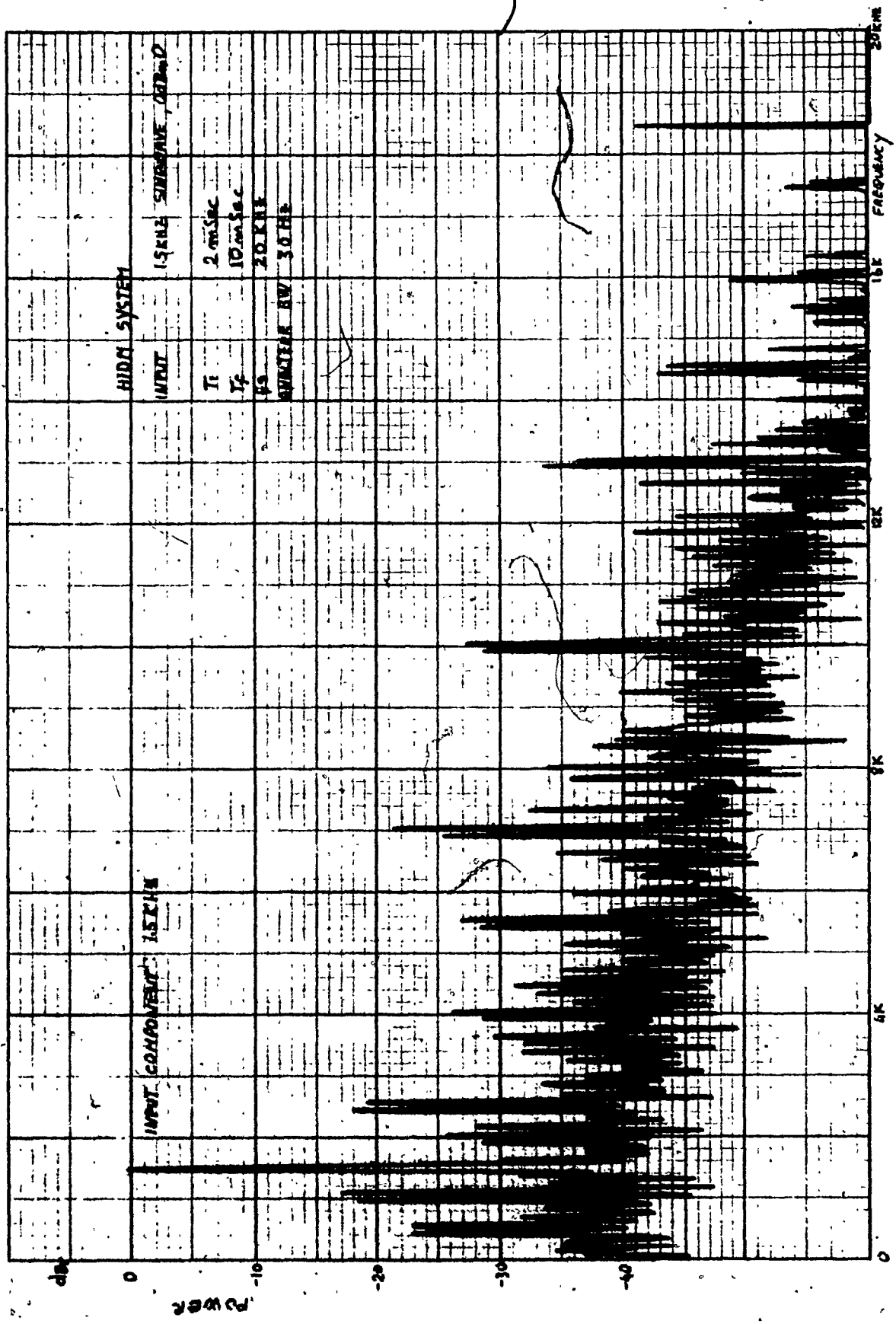

FIGURE 6.20.

$\hat{R}(\zeta)$ POWER SPECTRUM (INPUT SIGNAL SINEWAVE 1500 Hz, 0 dBmO)

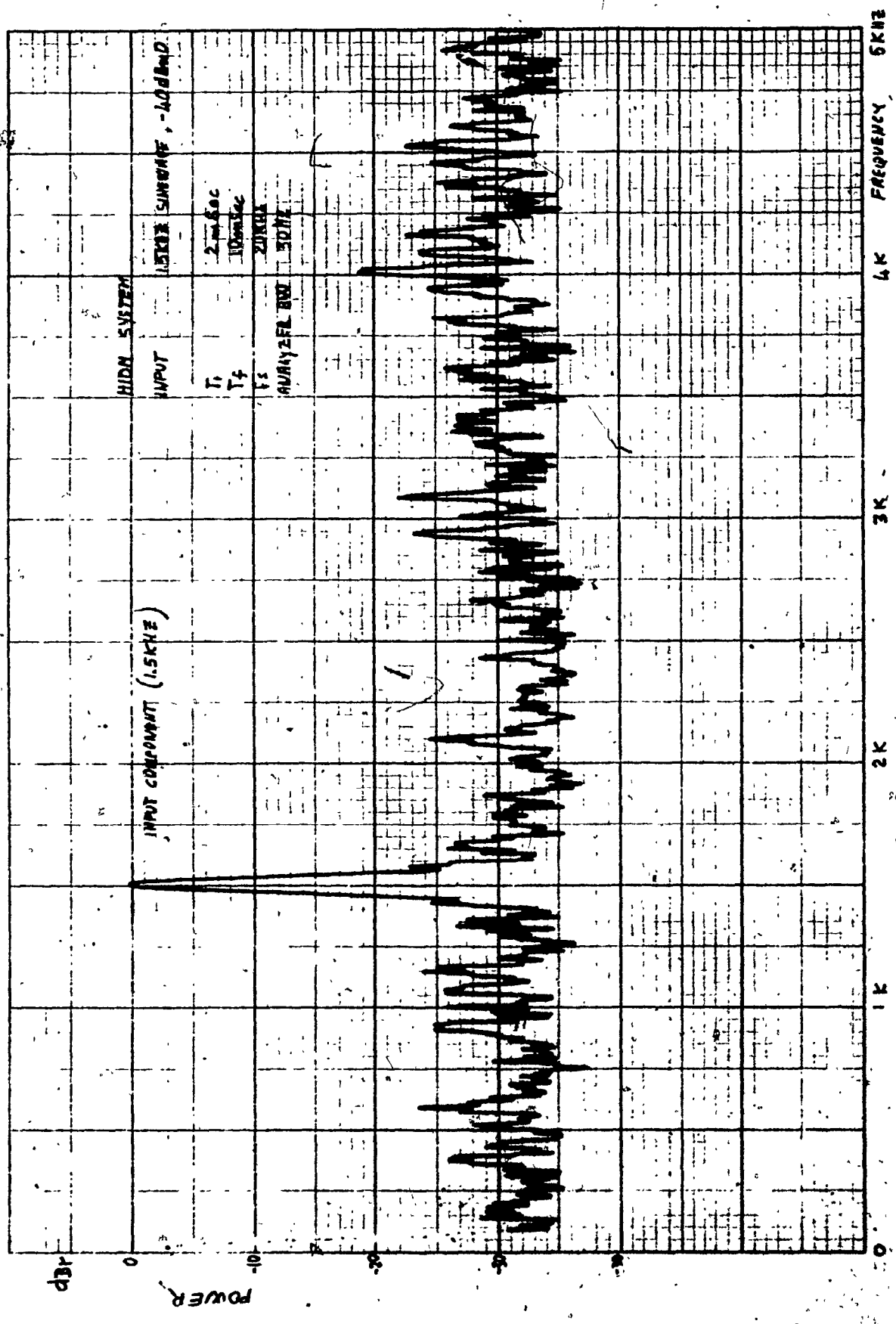

FIGURE 6.21:

$\hat{x}(\epsilon)$ POWER SPECTRUM (INPUT SIGNAL SINEWAVE 1500 Hz, 0 dBmD)

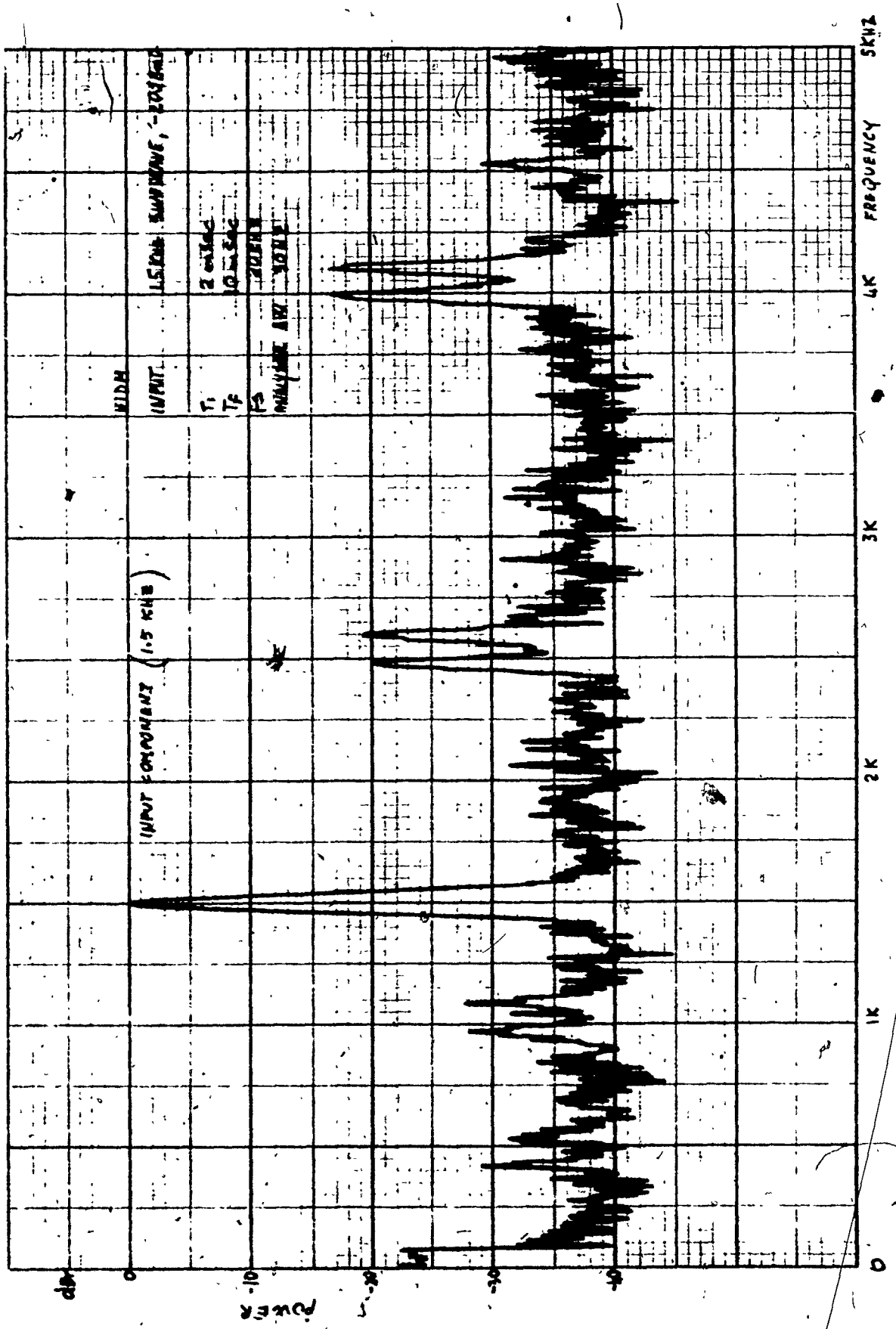

FIGURE 6.22.

3(c) POWER SPECTRUM (INPUT SIGNAL SINEWAVE 1500 Hz, -20 dBm0)

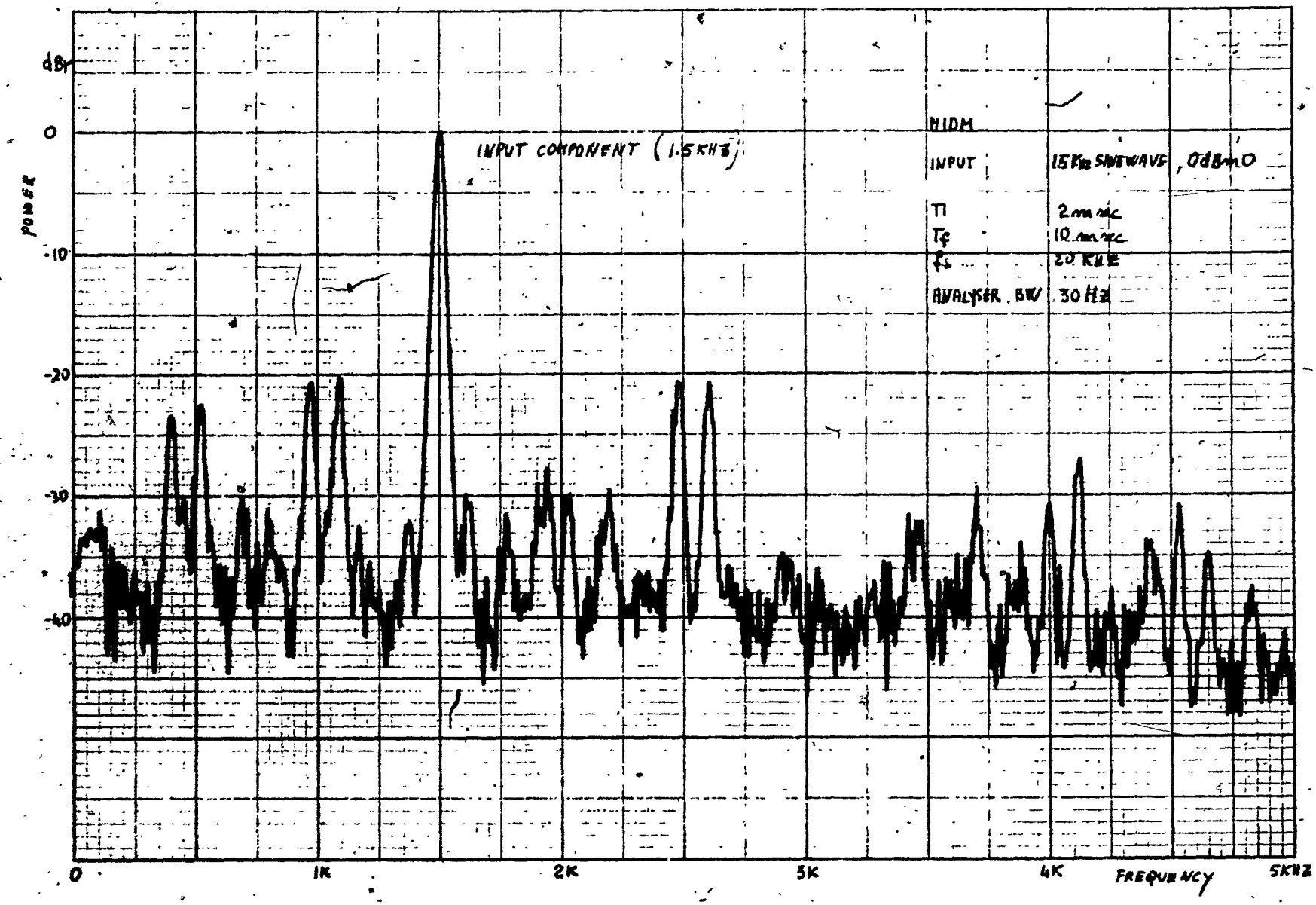

FIGURE 6.23.

3(c) POWER SPECTRUM (INPUT SIGNAL FREQUENCY 1500 Hz, -10 dBm0)

CHAPTER 7

CONCLUSIONS

In this dissertation, Single and Double Integration Delta Modulation Systems have been analyzed. It was found that a Double Integration system gives superior performance with respect to signal-to-noise ratio and idle noise reduction.

Experimental models of a SIDM and a DIDM system were designed and thoroughly tested in the laboratory. Good agreement between experimental results and the predicted theoretical values were obtained.

Although DIDM is superior to SIDM in many respects, it's dynamic range is still not sufficient to reproduce voice signals with acceptable fidelity. This problem is overcome by using a HIDM system, whereby using companding techniques, a wide dynamic range may be obtained.

A simple form of a Digitally-controlled High Information Delta Modulation system characterized by a one-bit memory and an exponential adaptation of the Quantizer output is also presented. It is shown that with the use of companding, system operation at a sampling frequency of 20 kHz is feasible.

In addition, a Dynamic Range in excess of 40 dB and an Idle Noise of -70 dBm0 has been achieved in the laboratory.

It can be seen that the experimental HIDM system as designed, using an 8-bit digital multiplier as part of the companding circuit, has many advantages over other types of Codec. These include, a nearly perfect tracking of the compressor-expandor, low cost, simplicity, low sensitivity to transmission error and a practically negligible idle noise.

Instantaneous and syllabicus companding have been experimented with and the following conclusions can be made:

i) Instantaneous companding provides fast rise-time, but, heavy distortions of the encoded signal are introduced.

ii) Syllabicus companding, to the contrary, provides smoother rise-time and better signal-to-noise ratio.

As a consequence, this type of companding must be choosen depending on the nature of the signal to be encoded. In our case, syllabicus companding was choosen because of its better performance in the presence of speech signals.

HIDM system behaviour in the presence of transmission error was also tested. Intelligible speech transmission with an error rate of 10^{-1} bit/sec is possible, whereas, error rate of 10^{-3} bit/sec or lower, produces negligible signal deteriorations.

REFERENCES

1. VAN de WEG, H.
QUANTIZING NOISE OF A SINGLE INTEGRATION DELTA MODULATION SYSTEM WITH AN n-DIGIT CODE.
Phillips Res. Rept., No. 8, pp.367-385, October 1953.

2. O'NEAL, J.B.
DELTA MODULATION QUANTIZING NOISE ANALYTICAL AND COMPUTER SIMULATION RESULTS FOR GAUSSIAN AND TELEVISION INPUT SIGNALS.
BSTJ, Vol. 45, pp.117-141, January 1966.

3. SUBBA RAO, G.V.
DELTA MODULATION
Instn. Engrs. (India) J.1967.

4. MINKLER, M.R.
HIGH INFORMATION DELTA MODULATION
IEEE International Conv. Record, pt. 8, pp.260-265, 1963.

5. DELORAINE, E.M., van MIERO, S. & DERJAVITCH, B.
METHODE ET SYSTEME DE TRANSMISSION PAR IMPULSIONS
French Patent No. 932140, August 1946.

6. de JAGER, F.
DELTA MODULATION, A METHOD OF PCM TRANSMISSION USING THE 1-UNIT CODE
Phillips Res. Rept., No. 7, pp.442-466, 1952.

7. LIBOIS, L.J.
UN NOUVEAU PROCEDE DE MODULATION CODEE LA MODULATION EN DELTA
L'Onde Electronique, vol. 32, pp.26-31, January 1952.

8. ZETTERBERG, L.H.
A COMPARISON BETWEEN DELTA AND PULSE CODE MODULATION
Ericsson Technics, vol. 11, pp.95-154, 1955.

9. INOSE, H. & YASUDA, Y.
A UNITY BIT CODING METHOD BY NEGATIVE FEEDBACK
Proc. IEEE, vol. 51, pp.1524-1535, November 1963.

10. TOMOZAWA, A. & KAKEKO, H.
COMPANDED DELTA MODULATION FOR TELEPHONE TRANSMISSION
IEEE Trans. Communication Technology, vol. COM-16, pp.149-157, February/68

11. BROLIN, S.J. & BROWN, J.H.
COMPANDED DELTA MODULATION FOR TELEPHONY
IEEE Trans. Communication Technology, vol. COM-16, pp.157-162, Feb./68

12. PROTONOTARIOS, E.N.
SLOPE OVERLOAD NOISE IN DIFFERENTIAL PULSE CODE MODULATION SYSTEMS
Bell Sys. Tech. J., vol. 46, pp.2119-61, November 1967.

13. BENNET, W.R.
SPECTRA OF QUANTIZED SIGNAL
Bell Sys. Tech. J., vol. 27, pp.446-472, July 1948.

14. WANG, P.P.
AN ABSOLUTE STABILITY CRITERIA FOR DELTA MODULATION
IEEE Trans. on Communication Technology, 16-1, pp.186-188, February/68